Exergy-Based Analysis of Aircraft Environmental Control Systems and its Integration into Model-Based Design

vorgelegt von
Diplom-Ingenieur
Daniel Bender
geb. in Nürnberg

von der Fakultät III - Prozesswissenschaften
der Technischen Universität Berlin
zur Erlangung des akademischen Grades

Doktor der Ingenieurwissenschaften
- Dr.-Ing. -

genehmigte Dissertation

Promotionsausschuss:

Vorsitzender:	Prof. Dr.-Ing. Felix Ziegler
Gutachterin:	Prof. Dr. Tetyana Morozyuk
Gutachter:	Dr. Dirk Zimmer

Tag der wissenschaftlichen Aussprache: 25. September 2018

Berlin 2019

Once you have tasted flight,
you will forever walk the earth
with your eyes turned skyward,
for there you have been, and there
you will always long to return.
– Leonardo da Vinci –

Acknowledgements

The idea for the topic of this thesis developed at the end of 2013 shortly after I started working at the DLR German Aerospace Center. Up until that time, exergy analysis had not been covered at the institute. My research on that topic then brought me to the TU Berlin. After a wonderful experience at the ELCAS2015 conference in Greece, Prof. Tsatsaronis and Prof. Morozyuk warmly welcomed us in Berlin and showed great interest in our proposal for bringing exergy and aircraft environmental control systems together. On this day, a wonderful collaboration began that hopefully will not end with this PhD thesis.

First of all, I want to express my gratitude to Prof. Tetyana Morozyuk for her personal and inspiring supervision of my PhD thesis, for the great time and discussions during my visits in Berlin and the opportunity to join the TU Berlin group for many conferences. Every time I was warmly welcomed and felt like a part of the group. I would like to express my very great appreciation to Dr. Dirk Zimmer for his unconditional support to follow the idea of this work, for getting into contact with Prof. Tsatsaronis and Prof. Morozyuk and especially for being my supervisor for this thesis as an expert in aircraft energy systems and modeling with Modelica. Further, I am particular grateful to Prof. Tsatsaronis for his support, expertise and discussions on my thesis. I would like to thank Dr.-Ing. Johann Bals and Dr.ir. Gertjan Looye who made my research visits at the TU Berlin possible and supported this collaboration.

I am grateful to the whole TU Berlin guys for welcoming me every time in Berlin or at conferences and in particular to Stefanie Tesch for supporting me with organizational issues, her expertise, giving me asylum and access to her coffee maker, and for always having a great time.

What would work be without great colleagues. Many colleagues influenced this work with discussions, inspirations, help, and support. This work would never have been completed without Alexander Pollok and Manuel Pusch. Thank you for technical and moral support.

I would like to thank my colleagues Dr. Alexander Pollok, Dr. Frans van der Linden and Lâle Evrim Briese for proofreading this thesis.

I am grateful to my family, my brother Philipp Bender and my mother Nicola Bender, for their moral support and almost unconditional understanding for not seeing me in the last couple of months. I love you. Lastly I want to thank Maika Nies for her curious proof-reading of many papers, for all the little things that made my days, and her unconditional support throughout this thesis.

Oberpfaffenhofen, Juli 2018
Daniel Bender

Abstract

Aircraft environmental control systems are complex energy intensive systems and the most important non-propellant consumer of energy among all aircraft systems. The intense pressure on airlines to remain competitive on the global market demands more efficient aircraft greater than ever. Meaningful analysis methods for the evaluation of architectural designs and effective modeling and simulation tools are crucial for the development of modern aircraft environmental control systems. This thesis contributes to both aspects: exergy-based methods as a powerful tool for the analysis of aircraft environmental control systems and its integration into a model-based design environment.

Aircraft environmental control systems (ECSs) operate in highly varying environments. Exergy analysis, by its nature, is performed with respect to a reference environment. Requirements coming from the particular boundary conditions for aircraft are identified and applied to exergy-based methods. Based on these findings, formulations of the exergy balances are provided on the component as well as the system level. A particular focus is put on splitting the individual exergy stream into thermal, mechanical and chemical parts. The definition of the reference environment is still an open issue in the scientific world. A comprehensive discussion on how to define the reference environment for the analysis of aircraft ECS is presented and concluded with a recommendation how to solve this issue.

In modern aircraft design, the industry uses design parameters such as fuel weight penalties and gross take-off weight for the evaluation of aircraft ECS. The conventional exergy-based method locates the thermodynamic inefficiencies within a system and evaluates the components regarding exergetic efficiency. Exergy analyses have been applied to environmental control systems for more than 20 years. This thesis presents a methodology for combining the aircraft fuel weight penalties with the conventional exergy analysis. Further, an approach was developed to apply advanced exergy methods to aircraft ECS and split the exergy destruction in avoidable and unavoidable parts. The combination of these methods locates the thermodynamic inefficiencies, identifies the avoidable part of the exergy destruction and measures its impact on aircraft level in terms of fuel consumption. Using this tool chain, an assessment can be made of the real potential for optimization.

Two example ECS architectures are used to apply the developed methodologies. The conventional bleed air driven pack and electric driven vapor cycle pack architectures are modeled with the object-oriented, equation-based modeling language Modelica. An exergy library was developed with the capability to integrate the exergy analysis into thermo-fluid systems. The exergy balances are provided within sensor models that can be implemented into the component models of the thermo-fluid system. The exergy analysis is then performed during simulation for each component and on system level.

The developed methods are applied to both example pack architectures to demonstrate the applicability in general and the advantage of the integration into the model-based design environment. The results clearly show the added value of the combination of the traditional aircraft design parameters and exergy-based methods.

Kurzfassung

Flugzeugklimaanlagen sind komplexe hoch energetische Systeme und nach dem Vortrieb der größte Verbraucher von Treibstoff unter allen Flugzeugsystemen. Die Nachfrage nach effizienteren Flugzeugen ist durch den enormen Wettbewerbsdruck für Airlines stärker denn je. Aussagekräftige Analysemethoden zur Bewertung von Architekturentwürfen und mächtige Modellierungs- und Simulationswerkzeuge sind ein wesentlicher Bestandteil der Entwicklung moderner Flugzeugklimaanlagen. Diese Arbeit leistet einen Beitrag zu beiden Aspekten. Exergiebasierte Methoden als mächtiges Werkzeug für die Analyse von Flugzeugklimmaanlagen auf der einen Seite, und die Integration dieser Methoden in eine modellbasierte Entwicklungsumgebung auf der anderen Seite.

Flugzeugklimaanlagen (ECS) arbeiten in stark variierenden Umgebungsbedingungen. Exergieanalyse wird von Natur aus gegenüber einer Referenzumgebung angewendet. Aus den luftfahrtbezogenen Randbedingungen werden Anforderungen für die Exergyanalyse abgeleitet und auf diese angewandt. Basierend auf diesen Randbedingungen werden Formulierungen für die Exergieblanzen auf Komponenten- und Systemebene vorgestellt. Es wird hierbei besonders auf die Aufteilung des Exergiestroms in seine thermalen, mechanischen und chemischen Teile eingegangen. Die Platzierung der Referenzumgebung ist in der wissenschaftlichen Welt noch nicht abschließend geklärt. Die Definition der Referenzumgebung wird umfassend diskutiert und abschließend wird eine Empfehlung gegeben, wie eine geeignete Definition für die Anwendung der exergiebasierten Methoden auf Flugzeugklimaanlagen aussehen könnte.

Heutzutage werden für den Flugzeugentwurf Auslegungsparameter wie der spezifische Treibstoffverbrauch und das brutto Abfluggewicht für die Bewertung von Flugzeug ECS verwendet. Mithilfe der konventionellen Exergiemethode kann genau identifiziert werden, wo thermodynamische Ineffizienzen auftreten und die Effizienz der entsprechenden Komponenten bewertet werden. Exergiebasierte Methoden werden nunmehr schon seit 20 Jahren für die Bewertung von Flugzeugklimaanlagen verwendet. Diese Arbeit stellt eine Methodik vor, mit der die Auslegungparameter aus dem Flugzeugentwurf mit exergiebasierten Methoden verknüpft werden können. Diese Kombination lokalisiert die Orte der thermodynamischen Ineffizienzen, identifiziert den vermeidbaren und nicht vermeidbaren Anteil und berechnet deren Auswirkung auf den Treibstoffverbrauch auf Flugzeugebene. Mithilfe dieser Werkzeuge kann nun das reale Optimierungspotential abgeschätzt werden.

Im Rahmen dieser Arbeit wurden die entwickelten Methoden auf zwei Beispielarchitekturen angewendet. Eine Zapfluftklimaanlage und eine elektrisch betriebene Vapor Cycle Klimaanlage wurden in der objektorientierten, gleichungsbasierten Modellierungssprache

Modelica modelliert. Eine Exergiebibliothek wurde entwickelt um die exergiebasierten Methoden für die Integration in Thermofluid Systeme bereitzustellen. Die Exergiebilanzen sind in Sensormodellen integriert, die in die Komponentenmodelle des Thermofluid Systems implementiert werden können. Auf diesem Weg wird die Exergieanalyse auf Komponenten- und Systemebene im Rahmen der Simulation ausgeführt.

Die Anwendbarkeit der entwickelten Methoden wurde anhand beider Beispielarchitekturen gezeigt und die Vorteile der Integration in eine modellbasierte Entwicklungsumgebung herausgearbeitet. Die Resultate zeigen einen klaren Mehrwert durch die Kombination der klassischen Auslegungsparameter des Flugzeugentwurfs und exergiebasierter Methoden für die Bewertung von Flugzeugklimaanlagen.

Contents

Nomenclature

Latin Symbols

Symbol	Unit	Description
A	m^2	area
c_p	J/kgK	specific heat capacity
D	N	drag
$\dot{E}$	W	exergy rate
e	J/kg	specific exergy
$\bar{e}$	J/mol	specific molar exergy
g	m/s^2	gravitational accelaration
h	J/kg	specific enthalpy
k	$-$	power law coefficient
L	N	lift
m	$-$	power law exponent
$\dot{m}$	kg/s	mass flow rate
M	mol	molar mass
p	bar	pressure
P	W	power
R	J/kg K	ideal gas constant
s	J/kg K	specific entropy
$SFC_{\mathbf{P}}$	lb/hp h	power specific fuel consumption
$SFC_{\mathbf{th}}$	lb/h lbf	thrust specific fuel consumption
T	K	temperature
$\dot{W}$	W	work
y	%	exergy destruction ratio
$y*$	%	exergy destruction share
X	kg/kg	water content
x	mol/mol	molar fraction

Greek Symbols

ϵ	%	exergetic efficiency

ζ	$-$	resistance coefficient
η	%	efficiency, effectiveness
φ	%	relative humidity
ρ	kg/m^3	density
ω	kg/kg	humidity ratio

Subscripts

0	reference environment
bleed	bleed
D	exergy destruction
El	electrical
evap	evaporated
F	fuel
F	fuel consumption
g	gaseous
i	i-th fluid stream / substance
is	isentropic
k	k-th component
l	l-th constituent
(l)	liquid
L	losses, liquid
L	saturated state
F	product
ram	ram
ref	reference
sat	saturation
t	total (exergy)
tot	total (with respect to system)

Superscripts

AV	avoidable
Ch	chemical
EN	endogenous
EX	exogenous
Ph	physical
T	thermal
M	mechanical
UN	unavoidable

Abreviations

ACARE	Advisory Council for Aviation Research and Innovation in Europe
ACM	air cycle machine
APU	auxiliary power unit
BCMP	base compressor
CMP	compressor
CON	condenser
CPCS	cabin pressure control system
dP	fan bypass valve
EBAS	engine bleed air system
ECS	environmental control system
eVCP	electric driven vapor cycle pack
FAA	Federal Aviation Administration
GTW	gross take-off weight
IN	(water) injector
ISA	international standard atmosphere
MHX	main heat exchanger
MSL	Modelica Standard Library
NASA	National Aeronautics and Space Administration
PHX	primary heat exchanger
RAC	ram air channel
REH	reheater
SFC	specific fuel consumption
TCV	temperature control valve
TRB	turbine
VaC	vapor cycle (controller)
VOC	volatile organic compounds
WE	water extractor
WIP	wing ice protection

List of Figures

List of Tables

Chapter 1
Introduction

1.1 Motivation

The intense pressure on airlines to remain competitive on the global market demands more efficient aircraft greater than ever. Besides the reduction of weight and fuel consumption, particular emphasis is put on environmental issues. The Advisory Council for Aviation Research and Innovation in Europe (ACARE) defined within its FlightPath 2050 five main goals to be achieved by the year 2050 [1]. One of these objectives addresses the protection of the environment and the energy supply. Future aircraft technologies and procedures are needed to enable major reduction in noise, CO_2 and NO_x emissions*. On conventional aircraft, the only significant energy source is fuel. Most of this energy is used for thrust generation. The engines produce electrical, hydraulic and pneumatic power that is required to operate all the systems such as flight controls, avionics, flight deck systems, cabin entertainment and the environmental control system (ECS). The primary task of environmental control systems is to ensure an environment to fulfill the physiological needs and comfort demands of passengers and crew. This includes temperature and humidity control as well as cabin pressure regulation. Furthermore, de- or anti-icing capabilities and sufficient ventilation, fresh air supply and the removal of pollutants are provided [2]. ECS on board of today's civil aircraft are highly elaborate constructions since they have to provide optimal climatic conditions for a large variety of atmospheric conditions, while being lightweight, small in volume and reliable in operation. With exception of the propulsion, the ECS is the largest non-propellant consumer of energy among all systems on board of conventional civil aircraft. About $3-5\,\%$ [3, 4, 5] of the total energy consumption can be attributed to the ECS. Hence, there is a need to design these systems highly efficient in order to reduce fuel burn, save cost in operation and reduce emissions.

The industry trend towards a more-electric-aircraft [6, 7, 8, 9] leads also to new architectures for the ECS, combining conventional pneumatically driven air-cycle systems with electrically driven vapor cycle systems. This adds further complexity to the design task at hand. On the architectural level, this highly complex design task is currently performed using model-based design methods and a multitude of numerical optimization methods [10, 11, 12]. With rising complexity and high optimization goals, the current approach is reaching its limits. A deeper system understanding is needed to achieve better results. In

*Relative to the capabilities of typical new aircraft in 2000, the emissions of CO_2 shall be reduced by 75 % per passenger kilometer, NO_x shall be reduced by 90 % and noise emissions of flying aircraft by 65 %.[1]

particular, it is important to understand how efficiency gains in one component affect the performance of other system parts. Also, it is important to identify which sub-parts of the system offer the largest optimization potential. A new methodology is needed to acquire this system understanding in a systematic way [13].

In modern aircraft design, the main design drivers are the minimization of fuel consumption and maximization of weight to be transported [14]. The so-called "traditional" design parameters include weight, power consumption and drag. Basic calculations such as trade-off analyses rule most optimization studies. They rely on rules-of-thumb, individual experience and non-integrated, non-interdisciplinary approaches [14, 15]. Cost-benefit studies among various options are performed on different basis and thus may lead to sub-optimal solutions [14].

Today, model-based design methods can be regarded as the tool of choice for the design of modern aircraft environmental control systems. It allows fast assessments of different architectures in an early design stage and investigation of design cases for component sizing and identification of performance limitations. The provided data, such as electrical power demand, drag, size and weight makes up the basis for an architecture assessment, further improvement as well as optimization. At this point, exergy-based methods can provide valuable additional information and lead to a noticeable benefit for both the component and system level evaluation.

Exergy-based methods are a well established tool for the analysis of complex and highly integrative energy conversion systems. These methods give not only information about the real thermodynamic value of an energy stream but also identify the location of the inefficiencies within a system [16]. Two decades ago, first attempts have been performed to apply exergy-based methods to aircraft ECS [17] and compare them to traditional design parameters. Exergy, by its nature, is always determined with respect to a defined reference environment. Most terrestrial applications, such as power plants, operate at stationary, hardly changing operation points. Power generation systems, for example, usually operate above ambient conditions and allow an explicit formulation of the exergy-based equations. However, aircraft operate in highly varying conditions and the same applies to the environmental control system. The processes within the ECS takes place at different temperature, pressure and humidity levels which vary among the different flight phases. This is the linchpin of the whole exergy analysis as its application requires a comprehensive formulation considering each possible combination of operation point and environment condition [18].

At the moment, exergy-based methods are not yet well established in industrial design processes. Possible causes are the lack of knowledge about exergy-based methods and their currently rather academic reputation. Associated with these drawbacks, there is no comprehensive description of the exergy methodology that fully satisfies the needs of aircraft ECS design within a model-based design environment. This thesis intends to bridge the gap between academic methods and industrial application.

1.2 Contribution

This thesis contains two main contributions. The first part deals with the adaptation of the exergy-based methods to aircraft ECS, while the second part of this thesis targets the integration of the exergy-based methods into a model-based design environment.

For the adaptation of exergy-based methods to aircraft environmental control systems, requirements were derived from the particular boundary conditions ECSs operate in. This thesis contributes here with a formulation of the exergy balances on component and system level that fulfills the identified requirements. Particular focus was put on the splitting of the exergy stream into thermal, mechanical and chemical parts. A formulation of the chemical exergy of moist air was developed with respect to any possible reference environment that allows both the working fluid and reference environment being in unsaturated, saturated or fog region. An additional contribution of this work is a recommendation about the definition of the reference environment based on the results of simulation studies and the definitions of the exergy balances for the electric driven vapor cycle pack.

A methodology was developed to combine the traditional aircraft design parameters with the exergy-based analysis. This allows the assessment of the exergetic performance of the ECS on aircraft level by measuring the impact on the fuel consumption cause by the environmental control system. A further contribution is a methodology to apply advanced exergy analysis to aircraft ECSs. An approach was developed that allows the splitting of the exergy destruction into avoidable and unavoidable parts. This achievement can identify the avoidable share of the fuel consumption caused by the ECS and thus gives information about the real potential for optimization.

The second main contribution of this thesis is the integration of exergy analysis to a model-based design environment. An exergy library was developed based on the object-oriented, equation-based modeling language Modelica. This library provides the capability to integrate exergy analysis to thermo-fluid systems. The library contains already the exergy balances on component level for typical components of an aircraft ECS. The exergy analysis can be performed during the simulation on component and system level. All contribution of this thesis are implemented in the library.

A conventional bleed air driven pack and an electric driven vapor cycle pack architecture were chosen to show the applicability of the developed methods within the model-based environment of Modelica.

1.3 Thesis Overview

This thesis is structured in seven chapters. The following paragraphs give an overview about the chapters.

Chapter 2 gives a review about state-of-the-art aircraft ECSs, traditional evaluation and optimization criteria in modern industry, and an overview about exergy-based methodology for aircraft ECS. An example illustrates the strengths and limitations of each method.

Chapter 3 introduces the two example pack architectures. A conventional bleed air driven pack architecture and an electric driven vapor cycle pack architecture are modeled in Modelica and used for testing the exergy-based methodologies addressed and developed within this thesis.

Chapter 4 is devoted to the methodology of exergy-based analysis. An introduction to conventional exergy-based methods is given followed by a detailed discussion about the splitting into physical and chemical exergy of the fluid stream of moist air. Exergy balances are formulated on component and system level under consideration of the particular situation for aircraft ECS with changing environments and varying operation conditions. A discussion about the definition of the reference environment complements the conventional exergy analysis. Further, the traditional design parameters, i.e. fuel weight penalties, are combined with exergy factors to extend the exergy analysis to aircraft level in terms of exergy of fuel consumption. The exergy destruction of the components are split into avoidable and unavoidable parts by applying the advanced exergy method and evaluate in this way the potential for optimization.

Chapter 5 deals with modeling and simulation. The modeling and simulation environment that is used for this work is introduced. The exergy library developed within this thesis is further presented.

In Chapter 6, the adapted methods are finally applied to the two example pack architectures. Based on the results, the significance of the methodologies are discussed.

Chapter 7 concludes this work with a summary of the achievements of this thesis and gives an outline about the benefits for future aircraft ECS in the frame of model-based design and a short outlook on suggestions for future work.

Chapter 2

State of the Art

2.1 Aircraft Environmental Control Systems

The primary task of the ECS is to ensure an environment that fulfills the physiological needs and comfort demands of passengers and crew. These tasks require functionalities such as temperature and humidity control as well as regulation of cabin pressurization. De- or anti-icing capabilities and sufficient ventilation, fresh air supply and the removal of pollutants are furthermore provided by the ECS [2].

Figure 2.1 shows an overview of a conventional environmental control system. It consists of several subsystems: Air conditioning system, temperature control system, ventilation control system, air distribution system, and cabin pressure control system (CPCS). Systems such as combined ozone/VOC converters, humidification systems, or dry air generation systems can optionally be installed on an ECS [2]. The key part of the ECS is the air generation unit (also called air conditioning pack, or pack). The pack conditions

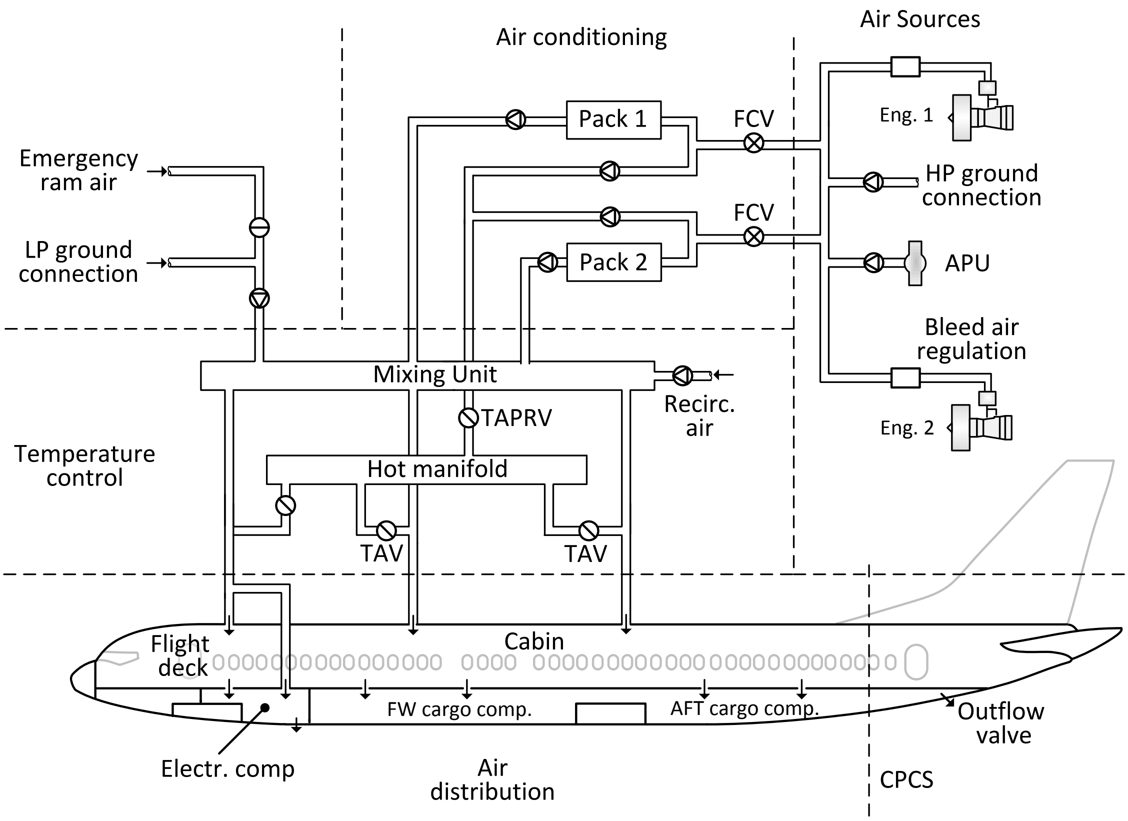

Figure 2.1: Environmental control system of a conventional aircraft. (adopted from [2])

the air flow in terms of temperature, pressure and humidity. Usually there are two packs installed in an aircraft. Conventional systems use engine bleed air as their power source. The bleed air is drawn from the compressor stages upstream the combustion chamber and passes some valves and a precooler before it enters the pack [19]. Provided at high temperature ($\sim$ 220°C) and high pressure ($\sim$ 2.5 bar), the air must be conditioned before it is distributed into the cabin. First, the air flow is lead to the pack where it is cooled and dehumidified. It passes several heat exchangers, a compressor, a turbine and valves before the flow reaches the right condition to be lead to the mixing unit. Now, it merges with recirculated, filtered air from the cabin. From there, the air is moved to the flight deck and different compartments of the cabin. A single isle aircraft contains about three different temperature controlled zones. These can increase up to eight zones for long range aircraft. A new ventilation concept allows even a higher number of zones [20].

Unconventional ECS follow the more electric aircraft approach by avoiding the inefficient bleed air extraction from the engines [21]. The fresh air is not taken from the compressor stage of the engines but enters the system through air inlets installed at the fuselage. Contrary to the conventional system, the energy for the pack is not provided in form of pneumatic power (such as air at high temperature and pressure conditions). The ambient air must be heated and compressed by electrically driven machines. Therefore, the electrical power is gained through generators mounted on the engine shaft or from the auxiliary power unit (APU). The unconventional ECS concept typically includes a vapor compression cycle to additionally cool the recirculated, filtered air from the cabin before it meets the fresh air from the air cycle in the mixing unit [22, 23] and ensures dehumidification capabilities for the outside air during ground operations.

Air Cycles

Within the environmental control system, the air conditioning pack is the central part. The thermodynamic cycle of this unit is derived from the reverse Joule cycle for open systems. Air is compressed, heat is then rejected at high temperature and finally the air is expanded to be cooled below ambient conditions. Figure 2.2 shows four typical air cycles that are installed in conventional ECS architectures using bleed air. The cycle on the very left is the simplest of the four cycles and compared to the others it is quite inefficient. It is part of the

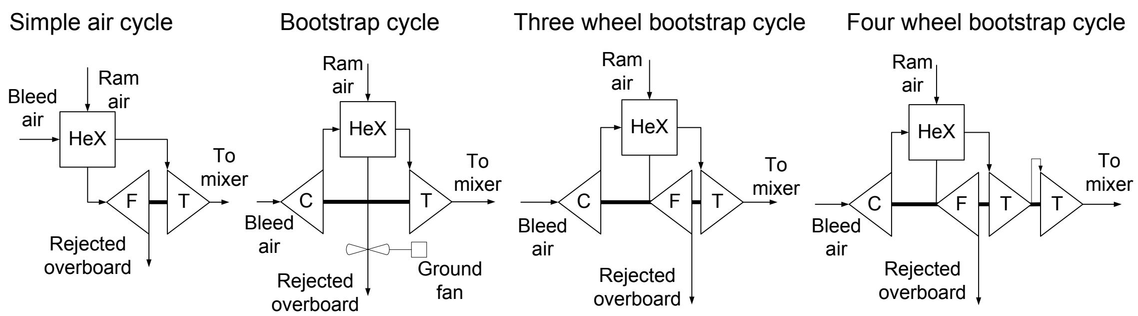

Figure 2.2: Typical air cycles used aboard commercial aircraft. (adopted from [2])

ECS aboard the Fokker 100, for example. The next one is the bootstrap cycle. Contrary to the simple approach, the bleed air is first compressed before entering the heat exchanger where it is cooled against ram air. The higher inlet temperature at the hot side makes the process more efficient. Inside the turbine the air flow is expanded below ambient temperature. On ground the ram air flow is provided by the ground fan which is usually driven electrically (i.e. Boeing 727) or pneumatically (i.e. Boeing 737 Classic).

The three wheel bootstrap cycle has a slightly lower efficiency compared to the classic bootstrap cycle as the fan (F) is mounted on the same shaft as the compressor (C) and the turbine (T). This arrangement has the advantage of being self-contained and does not depend on other power sources.

In the beginning of this section, humidity control was mentioned as one of the main tasks of the ECS. As cooling is mostly involved during the conditioning process of the air, the temperature can sink below the saturation point. Condensation and free water in the moist air flow would be the consequence. As this could theoretically happen in any component of the ECS (resulting in formation of ice) or the cabin (fogging), humidity control is crucial for the reliable operation of the ECS and thus the aircraft. To prevent the air flow from reaching the saturation point, water extractors are implemented to the system. Two concepts can be distinguished: The lowest temperature occurs downstream of the turbine and free water can be found there. The approach to place a water separator at this point is called low pressure water separation. In the case of condensation, ice build-up cannot be prevented by other means than limiting the expansion process of the turbine to a minimum exit temperature of 0°C [4]. This results in strong restrictions concerning the pack design and its cooling capacity. The alternative is the positioning of the water separator upstream the turbine. This concept is called the high pressure water separation.

Coming back to the three wheel bootstrap cycle, two designs concerning water separation are used in ECS architectures. In the early version of the Boeing 747 the low pressure design was used. Using the high pressure water separation, the three wheel bootstrap cycle is probably the most common pack configuration today (used in the Airbus A320 and A330/A340 families, Boeing 757, Boeing 737NG, later version of the Boeing 747 and early versions of the Boeing 767). [2]

The four wheel bootstrap cycle resembles the three wheel bootstrap cycle and differs mainly by an additional turbine stage on the shaft. The different requirements concerning humidity control for ground cases and cruising conditions at high altitude can be achieved by this architecture. Whether the three or four wheel bootstrap cycle is used seems to be a matter of philosophy. It must be decided on a case to case basis. The latter cycle is used in today's versions of the Airbus A380, Boeing 777 and later version of 767, and the Embraer EMB 170/190 family. [24]

Figure 2.3 shows the electrical ECS architecture of the Boeing 787. Outside air enters the ECS through dedicated cabin air inlets and is compressed in cabin pressurization compressors. Afterwards, the fresh air enters the low-pressure air-conditioning packs. The air inflow can be adjusted in accordance with the number of airplane occupants. Contrary to bleed air driven architectures, this is possible thanks to the adjustable speed of the electrical motors driving the pack compressors. The electrical power demanded by the turbo-machinery is supplied by engine-driven and auxiliary power unit (APU)-driven generators. Besides the fresh air supply, bleed air is used in conventional architectures for wing ice protection (WIP). Here, the WIP is realized by using an electro-thermal ice protection scheme. Up to now, the Boeing 787 is the only commercial aircraft having a no-bleed ECS installed aboard. [21]

Looking at the total fuel burn due to the ECS, the share caused by the bleed air is more than 80 % [4]. The amount of fresh air is mostly fixed due to ventilation requirements for crew and passengers. A further reduction in fuel consumption while using bleed air systems cannot be expected for future air conditioning systems. This is the reason why industrial research focuses on bleed-less architectures where a reduction in ECS fuel consumption of about 20 % is expected [4]. Boeing expects an improvement in fuel consumption on aircraft level of about $1 - 2\,\%$ during cruise condition due to the no-bleed system of the 787 [21].

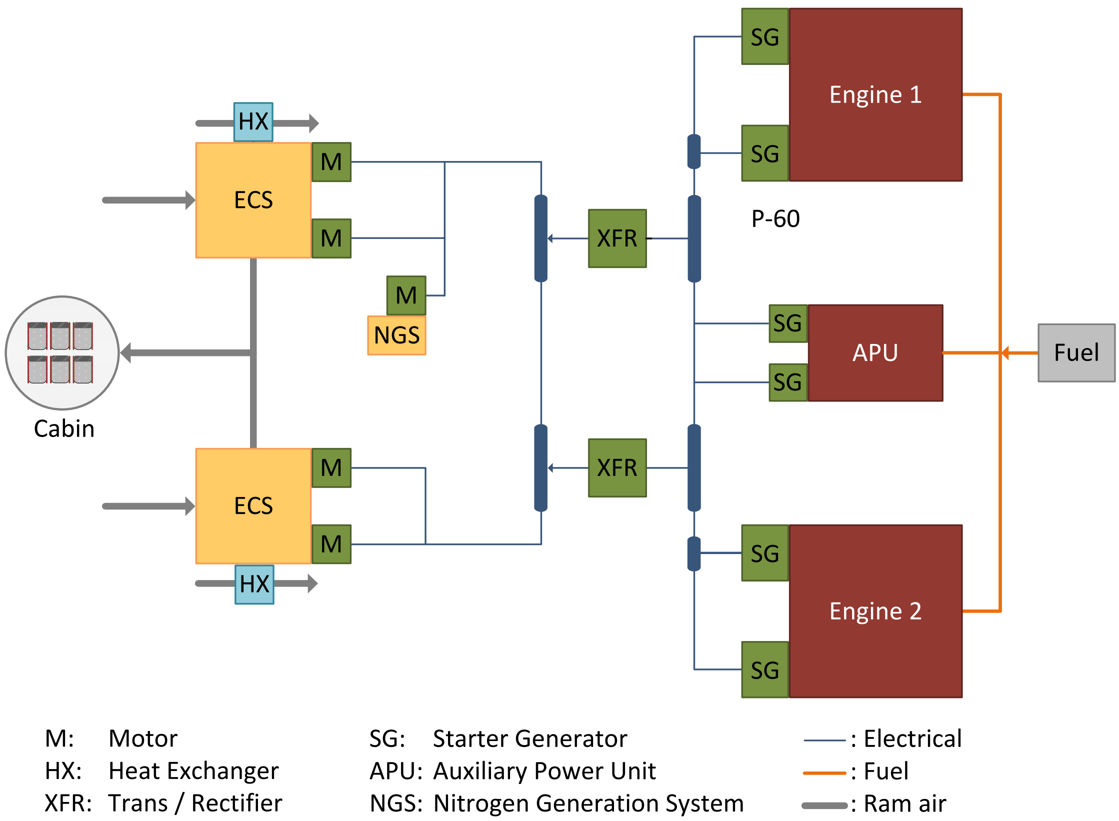

Figure 2.3: 787 No-Bleed ECS architecture. (adopted from [21])

2.2 Model-Based Design of Aircraft ECS

Model-based design methods have become well established methods for numerical simulations of complex thermo-fluid systems. This comprises the simulation of single components and large scale systems with large time scales. Much effort has been put into the modeling of energy intensive systems for different fields of applications. Ranging from basic thermo-fluid modeling [25] to automotive refrigeration systems [26], superconducting [27], large buildings simulation [28] and environmental control systems of aircraft [2, 29].

The modeling and simulation process as part of a design process usually comes along with subsequent evaluation and optimization tasks of the system of interest. Optimization capabilities for different kinds of applications are provided by specific modeling libraries [30, 31]. The evaluation of energy conversion systems is performed in most cases using evaluation criteria based on the first law of thermodynamics. Energy balances are formulated and the efficiency of a conversion process is measured by comparing the supplied energy with the desired output of the process. The difference of the supplied energy and output represents the waste energy, in other words the losses of the process. Most component models of energy conversion processes, such as turbo components or heat exchangers are either described by thermodynamic efficiencies based on the first law of thermodynamics or are equipped with such.

The optimization of an unconventional ECS architecture is described in [23] . A combined architecture and performance optimization approach embedded in a model-based environment, based on [2], is presented. The selected problem characteristics, i.e. efficiency and weight were available in the component models and the aircraft level metrics, such as mission fuel burn were introduced manually. Hence, an additional library or tool was not necessary. Unfortunately, this does not apply for analysis that ask for extended questions. Environmental or economical issues are usually not mandatory for the simulation of the energy conversion process and are influenced by additional factors such as costs and system specific aspects linked to their field of application. [32] present the simulation and optimization of a complex industrial energy system with respect to economic benefits. The analysis was performed using an applied simulation tool based on Modelica. A physical domain independent library was developed by [33]. Economic models are provided for the implementation into Modelica and allow energy management tasks.

Exergy analysis can be seen as an extended thermodynamic analysis that requires a different view of the energy conversion process. The exergy equations need only basic math and are usually performed subsequent of the simulation process. When it comes to exergy analysis of dynamic systems, a subsequent analysis needs more effort as the number of operation points increases significantly. [34] developed a Modelica-based tool to provide a dynamic exergy analysis for buildings simulation. The exergy equations are formulated on a basic level that does not meet the requirements for the application to aircraft environmental control systems.

It can be concluded that there are no tools or libraries available that satisfy the needs for an integration of a comprehensive exergy-based analysis into model-based environments for the design of ECS.

2.3 Traditional Evaluation and Optimization Criteria

In the last 60 years, aircraft fuel effiency has improved significantly. Figure 2.4 illustrates this trend. The energy intensity has been reduced by a factor of about 4.5 since 1960 [35]. Energy intensity measures the energy that has to be supplied to transport one passenger for one kilometer. The trend predicts a further decrease in energy intensity for the future. As the environmental control systems causes about $3 - 5\,\%$ of the total fuel consumption, it has an important role in the challenge for increasing fuel efficiency.

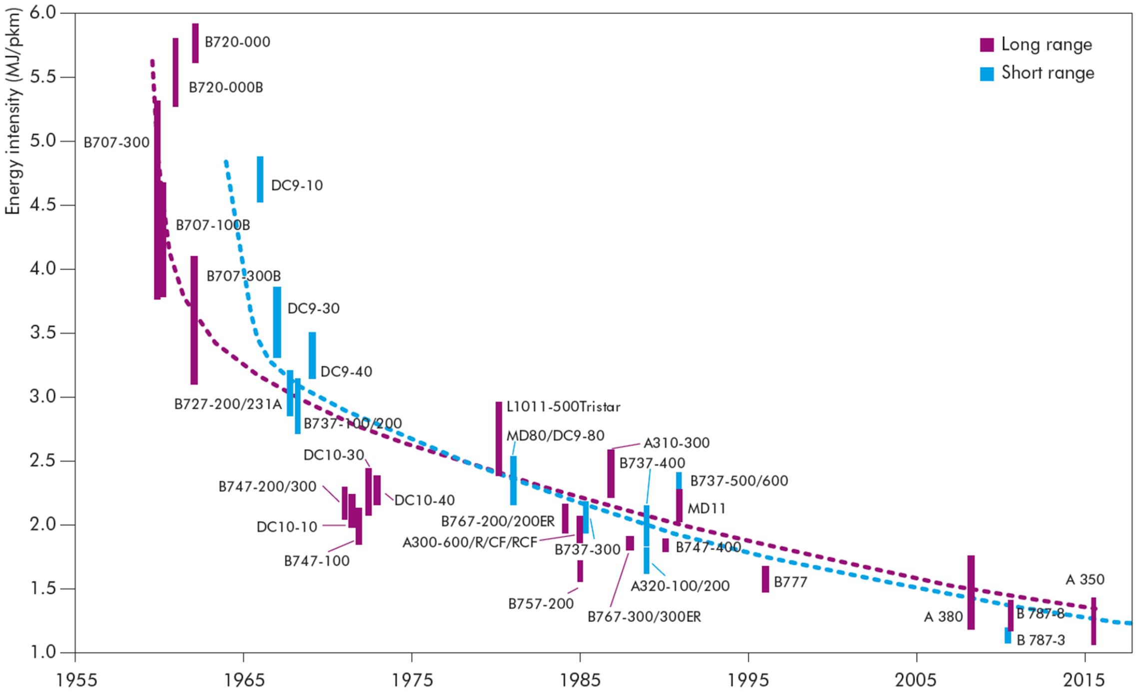

Figure 2.4: Trends of aircraft fuel efficiency. [35]

2.3.1 Traditional Design Parameters

In modern aircraft design, the main design drivers, besides reliability, can be reduced to the so-called traditional design parameters [36] fuel burn, specific fuel consumption (SFC) and gross take-off weight (GTW). The environmental control system mainly consists of thermodynamic cycles. Fuel burn, SFC and GTW are based on the first law of thermodynamics and are used in industry for analysis of integrated thermal systems [37]. By weighting system performance and components weight, specific fuel penalties or GTW can be determined for each component of the system. Penalties are defined for factors that influence the flight performance of an aircraft. They are expressed in terms of weight, external and momentum drags, and changes in power plant performance due to bleed air or shaft power extraction, or both. These penalties provide a common denominator for the comparison of systems in the preliminary design phase and thus support the choice of system to be used. The optimization process is then performed by calculating specific penalty numbers for system fixed weight, variable weight, power consumption, ram air, and bleed air consumption, in terms of take-off weight and selecting the system that results in greater payload or range [38]. The fuel weight penalties mentioned here are explained in detail in Section 4.2.

2.3.2 Optimization and Evaluation

Two levels for the optimization of aircraft ECS can be considered. On the architecture level, geometrical parameters of the components are regarded. The second level assesses the performance of the system in terms of energy flows, i.e. mass flows of the working fluids or operation conditions. Early works focused on the optimization of components in isolation. Heat exchangers have been addressed quite often for thermodynamically optimization by themselves [39, 40, 41, 42, 43]. The heat exchangers were analyzed in isolation regarding their heat and mass transfer and optimized for efficiency improvement. For the evaluation of ECS, this approach was not sufficient as the remaining part of the system and boundary restrictions were not considered. Vargas and Bejan [44] recognized this issue and illustrated the geometric optimization of a heat exchanger embedded in the ECS of a contemporary aircraft. They moved away from thermodynamic isolation towards optimizing the global system performance by varying the geometric features of one component. In [45], the same authors presented an integrated approach of finding the optimum solution on aircraft level by minimizing the thermodynamic losses within the ECS. This was achieved by optimizing the heat exchanger geometry which was identified as the dominating component.

The impact of the integration of a high-performance spray-cooled avionics chassis into the environmental control system on aircraft level was analyzed and evaluated by [17]. A detailed analysis on a component-by-component basis was performed to determine system performance and component weights. The overall system was optimized for a minimum GTW. Besides the traditional methods, such as GTW, an introductory entropy generation analysis was performed. Using a model-based environment, [46] presented a method for the optimization of ECS architectures on aircraft level with respect to fuel consumption and/or weight. Here, the link is illustrated between the global aircraft level optimization and local system optimization by using exchange rates, i.e. fuel weight penalties. These exchange rates allow a local system optimization without the need of a global aircraft level model. The same approach was applied short after to the optimization of an unconventional environmental control system [23]. For both applications, the optimal design of the overall system can be found by varying different parameters such as heat exchanger effectiveness and size, compressor and turbine performance or ECS coolant flow rates in order to minimize the total SFC or GTW [23, 46]. The resulting optimal design

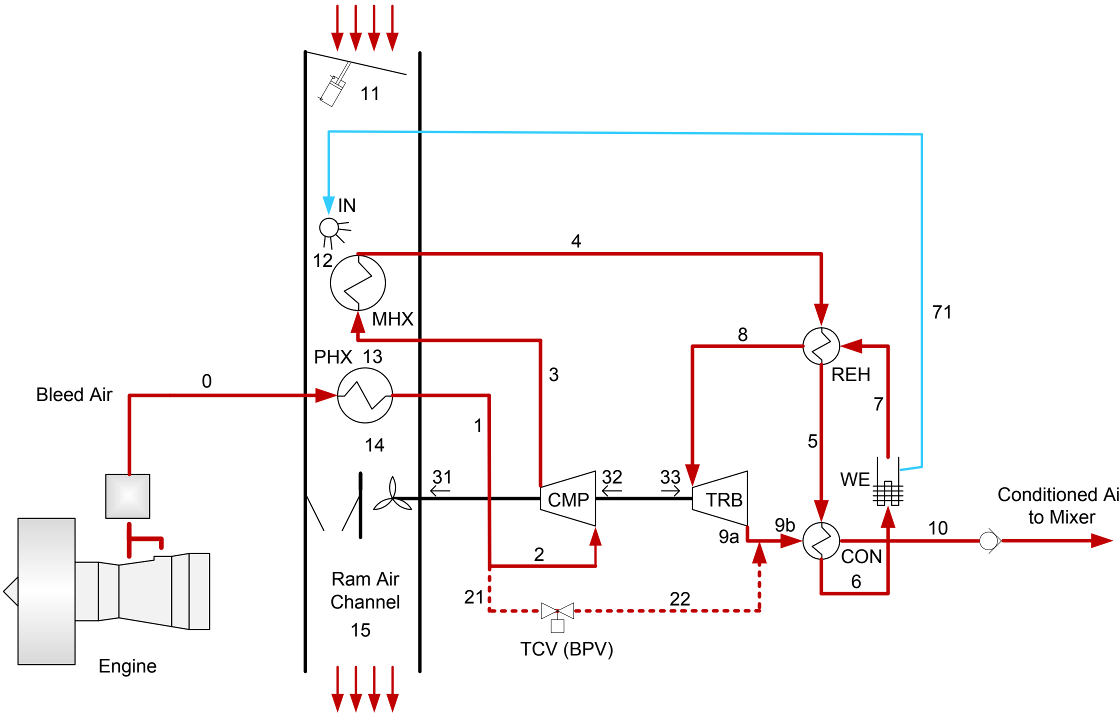

Figure 2.5: Schematic diagram of a three wheel bootstrap cycle pack.

has to undergo a performance analysis to proof its satisfaction for all operating conditions of the aircraft.

The advantage of these traditional exchange rates, respectively fuel penalty factors is the simple application to any environmental control system and the standardized aircraft level results gained for trade-off analysis of different system designs.

2.3.3 Application Example

The core part of this thesis is the modification and combination of the presented state of the art methods for the analysis and evaluation of aircraft ECS. The presentation of the existing methods and work in literature usually remains factual and hard to follow for non-experts of this field. An illustrative example shall convey a better understanding for the reader. The presented state of the art methodologies are applied to the example with the aim to outline the strengths and limitations. The example architecture is a three wheel bootstrap cycle pack with a high pressure water separation loop. Figure 2.5 shows the flow schematic of the pack architecture. A description of the system is dispensed with at this point, but can be found in Chapter 3.

For applying the traditional trade factors, i.e. fuel weight penalties, to the system, a cruise flight phase was chosen with a length of 1.5 h. Table 2.1 lists the boundary conditions for the flight phase. For using the fuel weight penalty correlations of [38], some aircraft and engine specific data are required. These contain the system weight, thrust specific fuel consumption, lift-to-drag ratio and turbine inlet temperature. Unfortunately, numbers about system weights are highly confidential information of the aircraft manufacturers and

Table 2.1: Flight conditions for the cruise case.

Mission Phase	Cruise
Cruise Time	1.5 h
Altitude	37000 ft
Flight Speed	0.77 Ma
Env. Pressure	0.22 bar
Env. Temperature	−56.3 °C
Humidity	60.0 %

hardly available in literature. For this example, data from [24] were taken and adjusted with a technology factor based on aircraft fuel efficiency trends of Figure 2.4. In [24], the major component weight for a three wheel bootstrap cycle system is given with 400 lbs. The paper was published in 1993. Using the trend line in Figure 2.4, an energy intensity of 2 MJ/pkm was state of the art back in that time. Today, a number of 1.3 MJ/pkm can be read, which means a reduction by a factor of 0.65. Applied to the weight given in literature, a system weight of

$$W_{\text{system}} = 0.65 \cdot 400\,\text{lb} = 260\,\text{lb} \approx 118\,\text{kg}$$

can be assumed with today's technology. The specific fuel consumption and lift-to-drag ratio are calculated using models from the Base of Aircraft Data (BADA) [47]. An Airbus A320 with V2500 engines was chosen as aircraft type. The turbine inlet temperature T_{tb} is taken from [48]. The conventional bleed pack is not supplied with any additional power taken from the engine shaft. Therefore the shaft power P_{shaft} is zero. Table 2.2 lists the performance and aircraft data for the considered cruise case.

Table 2.2: ECS performance and aircraft data for the cruise case.

$\dot{m}_{\text{bleed}}$	0.5 kg/s
$\dot{m}_{\text{ram}}$	0.48 kg/s
W_{system}	118 kg
P_{shaft}	0.0 W
SFC_{th}	0.514 lb/h.lbf
L/D	15.32
T_{tb}	932 °C

The pack model of Figure 2.5 was then simulated in the Modelica-based modeling and simulation environment Dymola [49]. The model was built from the library presented in [2]. The environment conditions correspond to the one listed in Table 2.1. The fuel weight penalties were implemented to the simulation model and calculated during the simulation. The results of the fuel weight penalties show an increase of 117.17 kg fuel due to the air conditioning system. Figure 2.6 shows the distribution of the fuel weight penalties. The conventional pack does not consume any electrical or external mechanical power. Therefore this share does not exist. The share caused by ram air drag and system weight is in the range of $6 - 8\,\%$. The bleed air is the main consumer of additional fuel

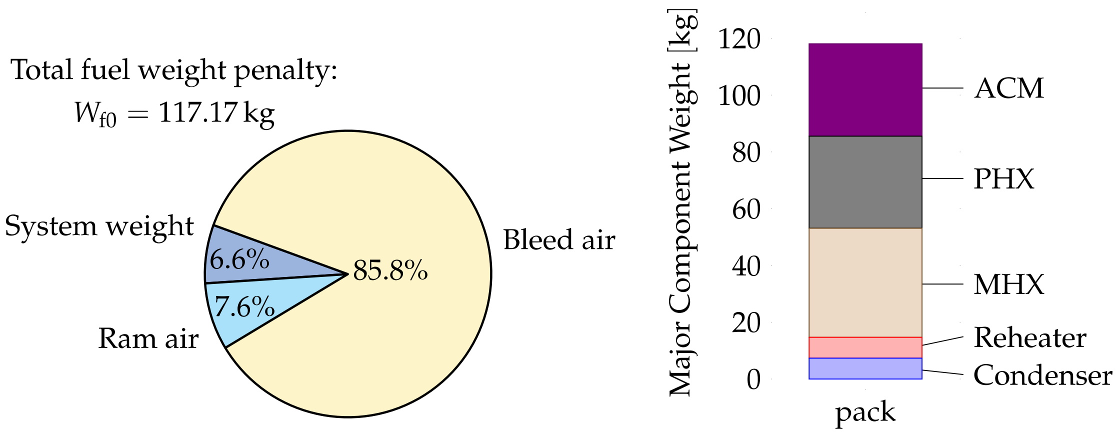

Figure 2.6: Fuel weight penalties and major component weights of the conventional bleed pack.

required for the air conditioning pack. The right side of Figure 2.6 shows the weight of the major pack components. The ACM includes the turbine, compressor, fan and shaft.

The results show that the bleed air causes the major penalty. The mass flow of the bleed air can hardly be optimized as it is determined by federal regulations for the fresh air supply [50]. The bleed air enters the pack at high temperature and high pressure. It leaves the engine's compressor stages at even higher energetic conditions. For bleed air driven ECS, a significant improvement on aircraft level is not expected. This is the main reason why industry focuses on bleed-less architectures for future aircraft environmental control systems [4].

A possible next step would now be to use the simulation model and perform an optimization to minimize fuel weight penalties. Similar to [46], [23] and [51], the objective function could be the improvement of component efficiencies and the reduction of weight.

2.3.4 Limitations

The traditional design parameters that are currently used in industry give meaningful information about fuel weight penalties, specific fuel consumption and GTW. With little information, it is possible to investigate the impact from ECS architecture performance and weight on aircraft level without having a model of the whole aircraft. The trade factors are well known and the aircraft manufacturers adjust them to their own needs. The fuel weight penalties split the total penalty into four parts: bleed air off-take, ram air drag, shaft power off-take and weight. Unfortunately, no information about the share of the single components on the penalties can be extracted. Sure, the thermodynamic efficiency of each component is available but it does not give any information about the share of the total losses. Further, no information about the potential for optimization can be extracted. Literature and the application example showed that for bleed air driven systems, the optimization potential on aircraft level is vanishingly small as the major share for additional fuel is the bleed air off-take itself.

Future architectures, such as electrically driven packs, will potentially contain a vapor cycle and will be driven by electrical power. Such systems have more degrees of freedom and higher interactions. The potential for optimization is much higher compared to conventional systems. Unfortunately, traditional design factors are not able to capture these effects. Other analysis methods are needed that cover the thermodynamic interactions within the system and outline potential for optimization.

2.4 Exergy-Based Methods

The second law method has already a long tradition in the aerospace sector - especially for the application on environmental control systems. Early works for ECS architecture optimization of advanced aircraft by using entropy generation analysis on system level can be found two decades ago [17]. The efforts then increased significantly in the beginning of 2000s, focusing on integrative thermodynamic optimization of environmental control systems. Single components, mostly heat exchangers, were optimized regarding their geometry parameters by minimizing entropy generation on system level [45, 44]. Contrary to previous methods using an isolated view, components were optimized regarding aircraft-level performance. Conventional energy-based and exergy-based approaches were applied by several authors [37, 52, 53] to the same highly integrated aircraft thermal systems and compared in terms of their significance. It emerged that both approaches led to similar outcomes, but are awkward for direct comparisons as they seek answers for different questions [53]. Instead of opposing the two evaluations, their combination was suggested in order to search for a pareto optimal design [51].

Exergy-based analysis is seen advantageous as a decision making tool for aircraft systems design, but a solid proof of this hypothesis is still outstanding. It is a powerful method to compare and analyze systems and their components, but also raises the question, how non-exergy related aspects can be addressed in the exergy analysis framework [14]. For the application on aircraft ECS, such aspects are evaluation criteria concerning fuel consumption and GTW on aircraft level. Several publications addressed this topic by finding coupling functions between aircraft trade factors and conventional exergy analysis [54, 55, 56, 57, 58, 59]. Later in this work, in Section 4.2, a more detailed review about this topic is given. Besides the environmental control system, various other aircraft systems were addressed with entropy and exergy-based analysis methods. Figure 2.7 illustrates the exergy flows through a modern commercial aircraft. Vargas et al. [45] describe the exergy flows by the following equation:

$$\dot{E}_{\mathrm{F}} = \dot{E}_{\mathrm{D,\,ECS}} + \dot{E}_{\mathrm{D,\,engine}} + \dot{E}_{\mathrm{D,\,misc}} + \dot{E}_{\mathrm{D,\,drag}} + \dot{E}_{\mathrm{D,\,lift}} \tag{2.1}$$

They split the exergy of fuel required for the flight of an aircraft into the different causes for destruction. The major part is destroyed within the engines due to the combustion process and other losses. The exergy needed for flight, i.e. for lift and overcoming aerodynamic drag, forms the second largest part. The environmental control system

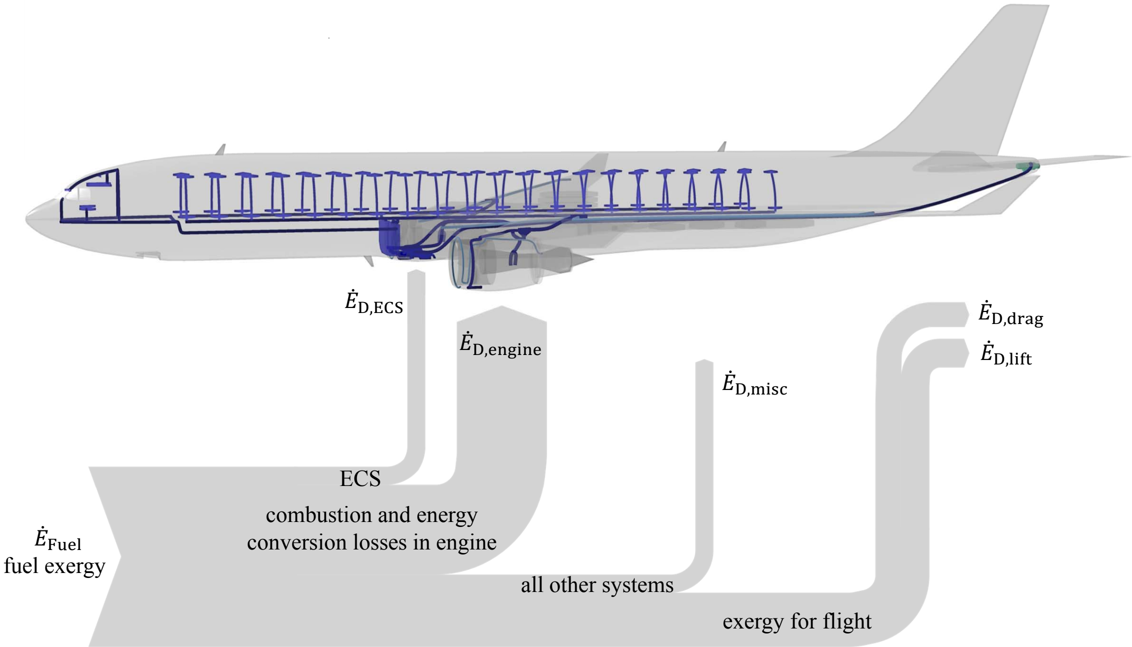

Figure 2.7: Distribution of exergy destruction on a modern civil aircraft. (adopted from [45])

causes the third largest exergy destruction compared to the total fuel exergy demanded for flying, but is the largest consumer among all aircraft systems, whereas the engines are not regarded as an aircraft system. The rest is destroyed by different applications consuming energy.

A comprehensive review about the adoption of exergy analysis for use in aerospace was published in [60]. It includes the application to propulsion systems, aerodynamic and structural optimization using exergy, multidisciplinary optimization with exergy metrics, mapping exergy over the variable flight envelope and the development of exergy methods for future aerospace applications. They conclude, inter alia, that exergy analysis provides a consistent common currency across subsystems that maps loss-producing mechanisms at system level and builds a foundation for robust and efficient optimization.

Exergy is by its nature a relative magnitude. When it comes to exergy analysis, one part is to define the reference environment. A well excepted definition of exergy was published by Prof. Tsatsaronis [61]:

Exergy of a thermodynamic system is the maximum theoretical useful work (shaft work or electrical work) obtainable as the system is brought into complete thermodynamic equilibrium with the thermodynamic environment while the system interacts with this environment only.

In literature, there is no comprehensive discussion about the selection of the reference environment. It is usually set to the ambient environment. For terrestrial applications on power plants, several studies have been performed on the influence of the reference point selection. The results of an energy and exergy analysis of a coal-fired electrical generating station were only marginally influenced by reasonable variations in reference environment properties [62]. A steam power plant in Jordan [63] and a thermal power plant in Ankara [64] were both analyzed using exergy methods and varying reference state temperatures (10 − 45 °C and 5 − 30 °C). For all temperature variations, both results spotted the boiler as the main source of irreversibility. However, the condenser showed the highest sensitivity concerning the reference state temperature variations. [65] did an exergy analysis of a dual pressure heat recovery steam generator for varying reference state temperatures and different high pressure (HP) and low pressure (LP) steam generation states in different sections of the generator. The results showed that variations in reference state temperatures lead to different variations of exergy losses and efficiencies for the LP and HP stages. The effect of varying reference state temperatures on exergy efficiency of a high-oleic methyl ester (HOME) fueled internal combustion engine was studied by [66]. It turned out that the exergy efficiency values ranged from 29.78 % to 34.93 % based on reference state temperatures between 5 °C and 30 °C. A model of an existing building was simulated [67] with the reference state described by hourly temperatures, monthly and yearly averaged. The difference of the results is small if temperature of the energy flows is far from the reference temperature and high if the temperature is close to the reference temperature.

In early 2000, [68] discussed the sensitivity of exergy efficiency to the selection of the reference environment for aerospace engines. The approaches for a varying (ambient conditions) and constant (sea level and cruise level) reference environment were presented. The influence on specific fuel exergy and rational efficiency was discussed. [69] gave a comprehensive review about exergy-based methodologies used in studies for the assessment of aircraft gas turbines. A lack of agreement on exergy analysis paradigms and assumptions is noted by the authors, in particular for the disagreement concerning the theoretical ambient (reference state) conditions for the air composition. Ambient pressure was agreed to be 101.32 kPa, whereas ambient temperature varied according to theoretical assumptions. [70] mentioned in a report based on three master theses the importance about the selection of the reference environment for the analysis of aircraft ECS without any further discussion. They presented the influence of reference point selection on the optimization of the length of a scramjet combustor. For the analysis of aircraft environmental control systems with exergy-based methods, a comprehensive discussion has never been outlined to the best knowledge of the author.

Advanced exergy analysis helps to investigate the origins of exergy destruction and the potential of minimizing inefficiencies. The exergy destruction is further split into four parts: avoidable and unavoidable exergy destruction, and endogenous and exogenous parts. This is illustrated in Table 2.3. The unavoidable part refers to the exergy destruction that cannot be further reduced due to technological limitations. The avoidable part describes the remaining exergy destruction and is an indicator for the potential of optimization. The endogenous part describes the destruction occurring in one component only because of its inefficiencies under consideration of all other components working at ideal conditions. The exogenous part is the remaining part of the exergy destruction. The four parts can be combined for more meaningful indicators. [71]

Table 2.3: Splitting of exergy destruction within a component. [71]

	endogenous	exogenous
unavoidable	cannot be reduced because of technical limitations related to the component	cannot be reduced because of limitations associated with the other components or the system structure
avoidable	can be reduced by improving the efficiency of the component	can be reduced by a structural improvement of the overall system or by improving the efficiency of the remaining components

Introduced in [72] and [73], advanced exergy methods have been applied to several fields of energy conversion systems, such as power plants [74, 75, 71], refrigeration systems [72, 76], terrestrial air conditioning [77], and regasification of LNG (liquefied natural gas) [78, 79].

Advanced exergy methods have rarely been used for aircraft applications. In literature, there are only three publications reported for aerospace applications and all of them are related to engines. [69] presents the splitting of exergy destruction into parts for an aircraft gas engine, [80] used the advanced methods for the evaluation of a military turbojet engine and [81] performed an advanced analysis of a turboprop engine. For aircraft environmental control systems, there are currently no publicized results that use advanced exergy methods.

2.4.1 Application Example

Following the approach of the previous section, an application example shall illustrate the state of the art of exergy analysis for aircraft ECS. For this aim, the same pack architecture introduced in Figure 2.5 is used. Again, the cruise phase is chosen for the analysis. The flight conditions correspond to those in Table 2.1 and the mass flows of bleed air and ram air to those in Table 2.2. The remaining performance parameters are not needed for the conventional exergy analysis. For the exergy analysis, the approach of defining exergy rates into fuel and product exergy is applied [82]. This methodology assigns the entering and exiting energy streams of a process into an exergetic fuel and product. The change of physical and chemical exergy with respect to the reference environment drives the formulation of the exergy balances. The difference between fuel and product is the destroyed exergy on component and on system level, while exergy losses are additionally considered within the balance. This approach is seen superior compared to just balancing entering and exiting energy streams [83, 84] and is explained in detail later in Section 4.1.4.

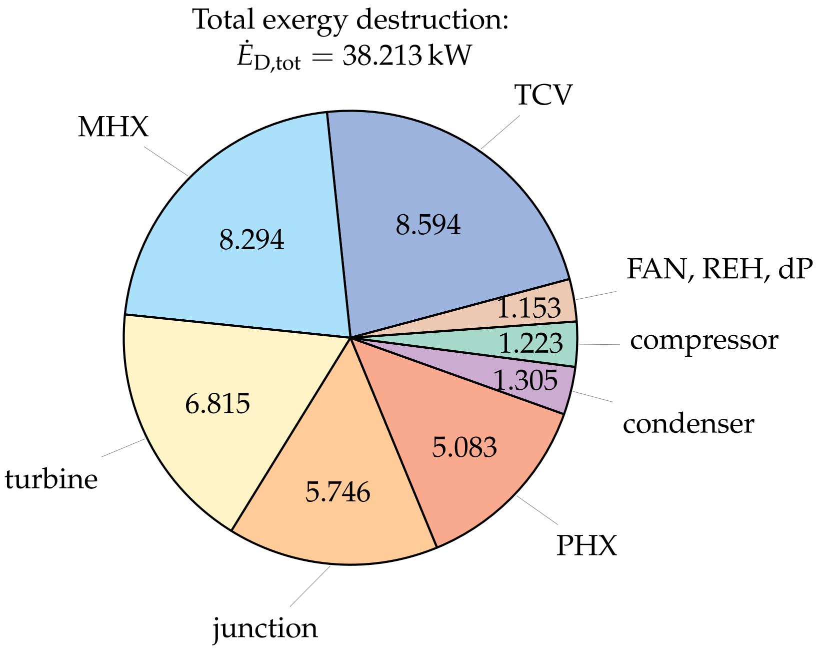

Figure 2.8: Distribution of exergy destruction during cruise for the conventional bleed pack.

The exergy analysis was applied to the same pack model of Figure 2.5 and simulated in the Modelica-based modeling and simulation environment Dymola [49]. Figure 2.8 shows the distribution of the destroyed exergy during the cruise phase. The components with the major exergy destruction are the temperature control valve (TCV), main heat exchanger (MHX), turbine, junction and primary heat exchanger (PHX). The remaining 10 % are caused by condenser, compressor, fan, reheater (REH) and fan bypass valve (dP). The TCV regulates the ACM bypass and its large destruction is caused by the high pressure drop. A valve does not have any exergetic product and is regarded as a dissipative component. The same applies for the junction where the bypass flow of the TCV (Figure 2.5, #22) meets the turbine discharge flow (#9a). For dissipative components, there is no efficiency defined and the only way to reduce the exergy destruction is to reduce the mass flow passing the TCV. The exergetic efficiency is defined as the ratio of exergy of product and the exergy of fuel supplied to the component. For productive components this value is an indicator about their exergetic performance.

The exergetic efficiencies for the productive components are displayed in Figure 2.9. The fan in the ram air channel works during cruise as resistance and is therefore regarded as a dissipative component. The results show that the compressor has the best exergy efficiency, followed by the PHX, MHX, turbine and at last the condenser. Turbo components work usually at higher efficiencies. The compressor works almost at the same conditions for all flight phases and the operation points do not deviate much from the design point.

Considering only one of the values, exergy destruction or exergy efficiency, would result to misleading conclusions. It is important to always combine them. The reheater and condenser could be a possible target for optimization as they operate at the lowest exergy efficiency. But taking into account their exergy destruction, the impact of an improvement

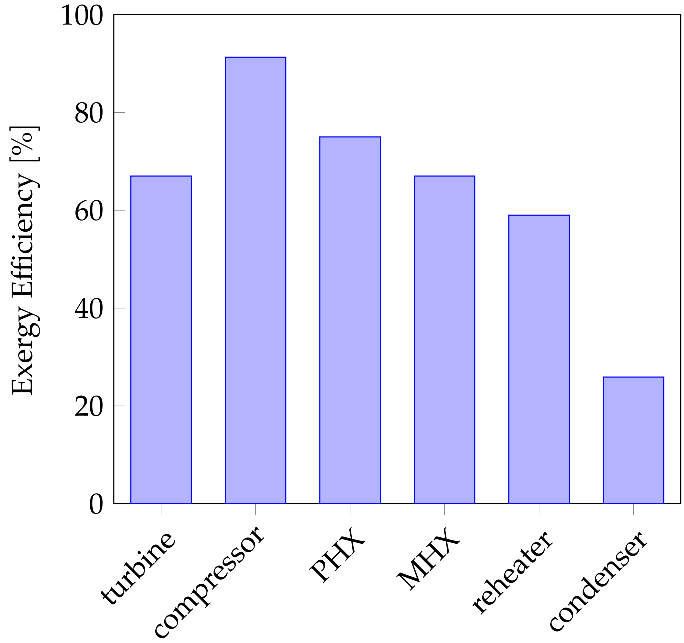

Figure 2.9: Exergy efficiencies of components during cruise for the conventional bleed pack.

would be very low and possibly not worth the effort. However, the PHX, turbine and MHX are good candidates for optimization from the results point of view. They cause the highest exergetic destruction of the productive components and the efficiencies have open space left.

It was already mentioned that the exergy analysis of the component processes is performed following the fuel and product approach. This requires the strict consideration of the reference environment. The exergy rates for fuel and product exergy depend on either the process takes place above, below or across the reference environment. The $T - s$ diagram in Figure 2.10 shows the state points of the bleed air among the pack. The numbers correspond to those in Figure 2.5. Two reference temperatures T_0 are drawn in the $T - s$ diagram. The lower one for an exemplary cruise condition and the other for an exemplary condition at sea level (both temperatures are not related to the actual example conditions). The locations of the reference temperatures lead to different definitions of the exergy balances. For example, the cooling within the MHX (#3 − #4) operates above the reference temperature for T_0 being at cruise conditions and intersects the reference temperature for the case of T_0 being set to sea level. The expansion process within the turbine (#8 − #9a) operates either below T_0 or intersects the reference temperature. Assuming a mission based analysis for a whole flight mission and setting the reference environment equal to ambient conditions, all processes could be affected. This example shows clearly that a comprehensive description of the exergy equations is mandatory for an exergy analysis of aircraft ECSs, especially within a model-based design environment.

Finally, the exergy analysis and the traditional analysis can be combined. Regarding the reheater and condenser, Figure 2.6 confirms the conclusion drawn from the exergy analysis. Derived from the results, they impact only the system weight, while being the

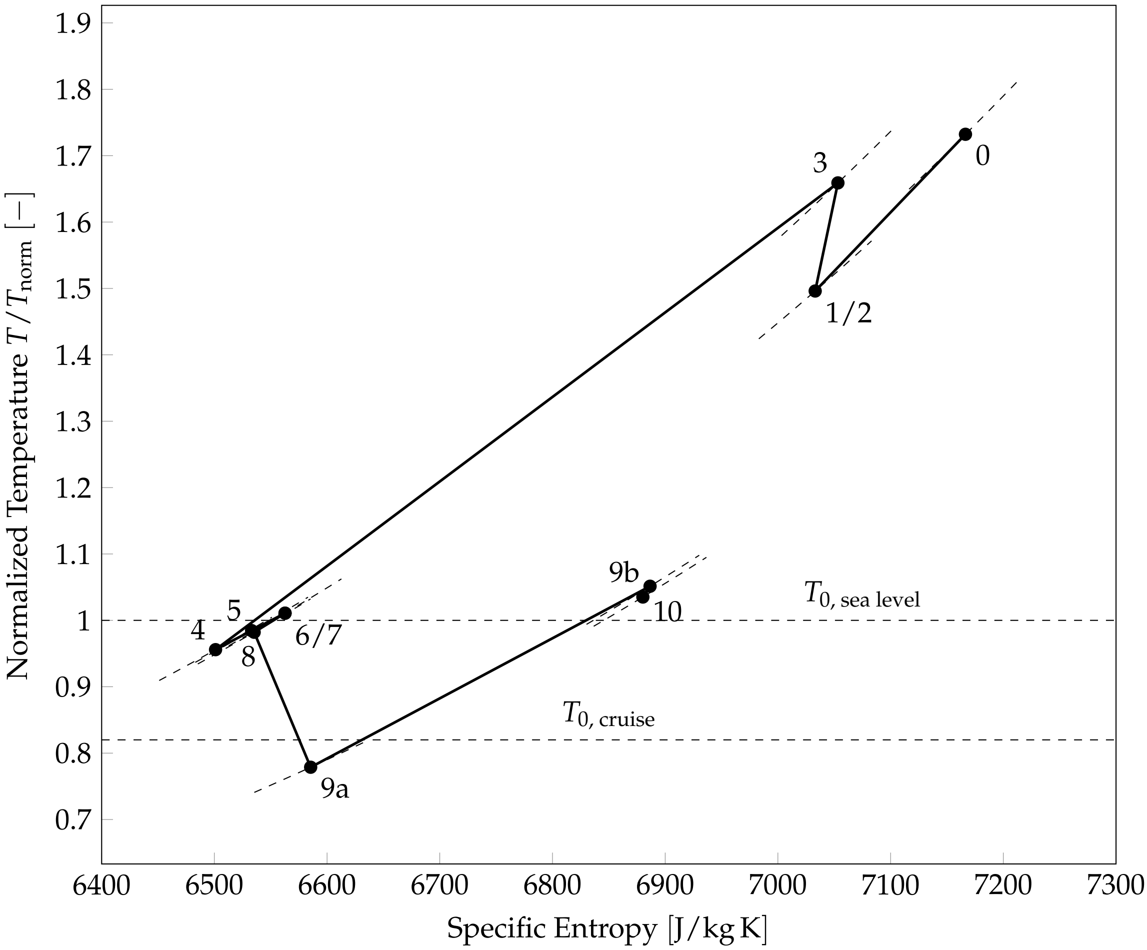

Figure 2.10: T-s diagram at cruise phase for the conventional bleed pack.

lightest components. The MHX and PHX have the major share of the weight and by improving their performance, the ram air flow may be reduced which causes less drag. However, the improvement of heat exchangers usually comes along with increasing the heat transfer area what results in higher weight. Both analyses give first assessments where to start improving the system and components.

2.4.2 Limitations

The conventional exergy analysis gives information about the total exergy destruction and the share of each component. Compared to the traditional analysis using fuel penalties, the impact of each component on system level can be measured. The exergetic efficiency shows the thermodynamic performance from an exergetic point of view considering the reference environment. Performing an exergy analysis within model-based design environments, Figure 2.10 shows the importance of a comprehensive formulation of the exergy balances considering all possible operation conditions with respect to the reference environment.

However, the conventional exergy analysis has some limitations. The exergy destruction and exergy efficiencies give information about the exergetic performance of each component and about their share of losses on system level. A poor performing component with high exergy destruction would then be the first candidate for optimization. Unfortunately, there is no information about the limitations for improvement. In other words, which amount of exergy destruction can be avoided and how much can not due to technological limitations, interactions with the system, etc. This applies especially for aircraft ECSs that operate at varying conditions and concurrently have to fulfill performance and conditioning requirements. Optimization always comes along with costs. An indicator for the potential of optimization could support the selection process for improvement and optimization, and save time for optimization effort with little prospect of success.

Chapter 3
System Description

Two different pack architectures have been selected to apply the exergy-based methods and evaluate them. Both, the significance for the evaluation of aircraft ECS and applicability within model-based design shall be considered. One system represents a conventional bleed air driven pack that has been used for many years and can be regarded as state of the art for environmental control systems of conventional commercial aircraft. The second system is an integral part of recent research for future aircraft configurations and follows the more-electric-aircraft approach.

This chapter starts with a short introduction to ventilation requirements for recent civil aircraft ECS coming from federal regulations. Afterwards both pack architectures are introduced with their equipments installed, fluid flows, operation modes and control laws.

3.1 ECS Ventilation Requirements

The ventilation of an aircraft cabin has to fulfill general requirements. The air that enters the cabin consists of filtered recirculated air and fresh air from the pack. The share of fresh air is prescribed by the number of passengers aboard. The Federal Aviation Administration (FAA) prescribes for cabin ventilation in its airworthiness standards a minimum of 0.55 lb/min ($\approx$ 0.25 kg/min) fresh air per occupant for normal operating conditions. The pressure altitude of the cabin must not exceed 8000 ft ($\approx$ 2438.4 m). The regulations of [50] include further restrictions for harmful and hazardous concentrations of CO, CO_2, O_3 and smoke. The latter are not considered in the simulations within this work and thus not further discussed. The temperature inside the cabin is usually kept within a range of 22°C − 24°C for comfort reasons. Limitations are given in [50] for the exposure time at any given temperature above 100°F ($\approx$ 38°C). [50]

3.2 Conventional Bleed Air Driven Pack

Fig. 3.1 illustrates the detailed schematic of the air generation unit that is used for the exergetic analysis in this work. It includes a conventional bleed air driven three wheel bootstrap cycle. The different flows are enumerated for a better allocation with simulation results. In principle three different flows are considered. The bleed air arises from the compressor stage at the engine, passing at first the pneumatic distribution device before entering the ozone converter. Inside the primary heat exchanger (PHX) the hot air is

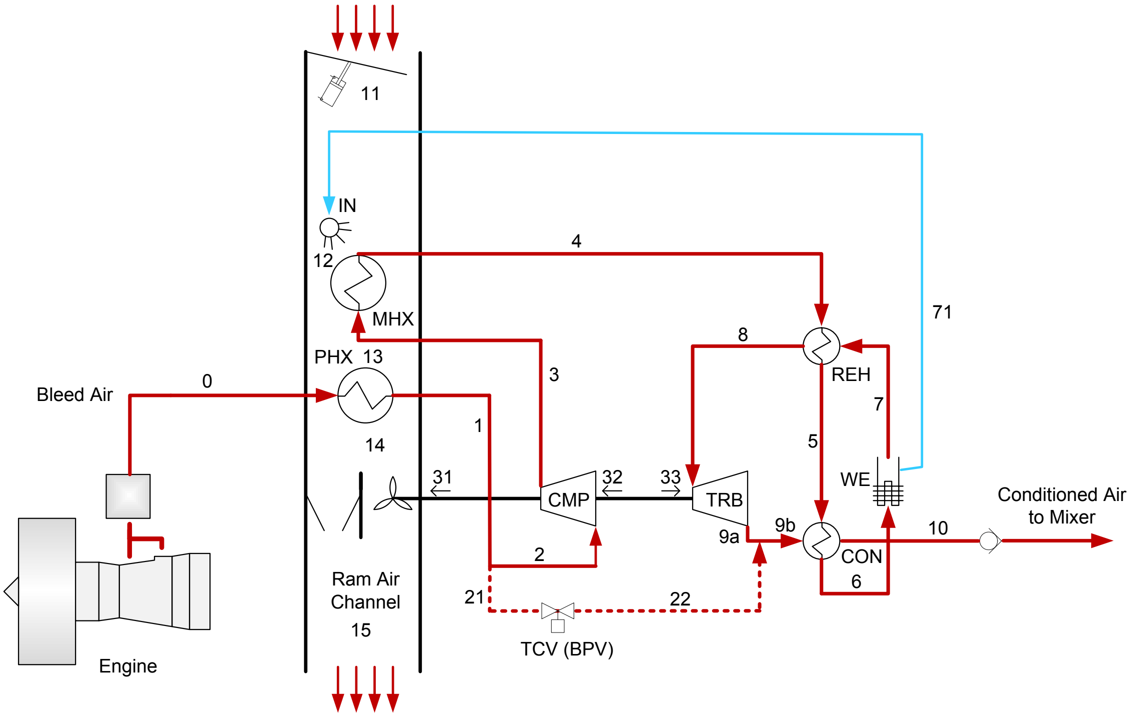

Figure 3.1: Schematic diagram of the conventional bleed air driven pack.

cooled down against the ram air flow. Before entering the compressor stage (CMP), a part of the air flow is separated and bypassed through the temperature control valve (TCV). Downstream the compressor stage the heated and compressed air is cooled down a second time inside the main heat exchanger (MHX) against the cold ram air flow. Here the most intense heat exchange takes place due to large temperature differences. The air flow now enters the hot side of the reheater (REH) and is cooled down again before its temperature is further decreased inside the condenser (CON) in order to dehumidify the air flow and prevent downstream conditions from reaching the saturation point. This configuration of the three wheel bootstrap cycle uses the concept of high pressure water separation. In case of condensation, the free water is separated in the water extractor (WE) and carried to the injector (IN) located at the beginning of the ram air channel. The dehumidified air flow now passes the reheater a second time, this time at the cold side where it is reheated against its upstream air flow. Inside the turbine (TRB) the air is expanded to a sufficient pressure level. Concurrently, the temperature decreases significantly below ambient conditions. At this point the air reaches its coldest condition. Meeting the separated air from the temperature control valve, the flow gains a higher temperature and finally is heated up inside the condenser again before it leaves the air pack to the mixing unit where it is mixed with recirculated and filtered air from the cabin. The second flow occurring is the ram air flow. It functions as a heat sink and enters the aircraft through inlets outside the aircraft's fuselage. The amount of air flow can be controlled by flaps installed at the inlet and outlet of the ram air channel.Water from the water extractor is now injected into the ram air flow where it evaporates and subsequently the temperature of the ram air flow is decreased.

The cool air passes successively the main heat exchanger and primary heat exchanger before it leaves the ram air channel to the ambient. In ground operation the ram air flow is driven by the ram air fan that is mounted on the same shaft as the compressor and turbine.

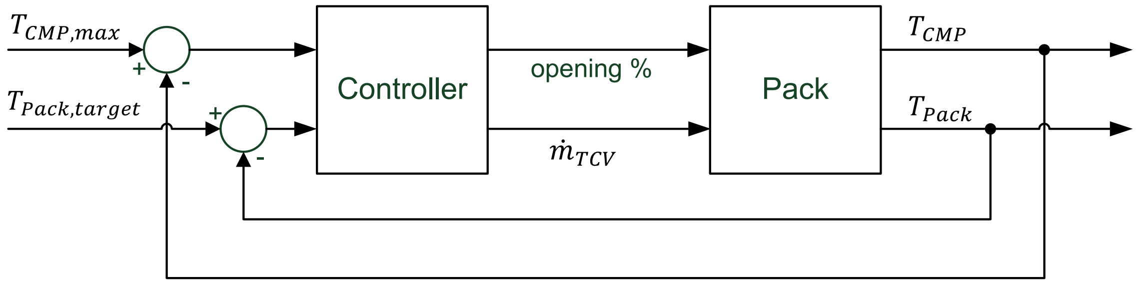

Figure 3.2: Control schematic of the conventional pack.

The correct operation of the conventional pack during flight is ensured by basic control laws. Within the pack model this is realized by a central pack controller model. The mass flow, temperature und water content at the bleed air inlet are prescribed by an air source model (Figure 3.1, #0). The schematic of the pack controller is shown in Figure 3.4. The controller is responsible for the compressor outlet temperature (Figure 3.1, #3) and the pack discharge temperature (Figure 3.1, #10). The compressor outlet temperature is kept below the critical temperature of 180°C by regulating the ram air flow. The ram air fan is mounted on one shaft with the air cycle machine and runs at constant speed. During ground operations it forces the ram air flow. During flight conditions the ram air fan keeps running and is partly bypassed. The air flow through the ram air channel is controlled by the ram air channel inlet and outlet door. The pack discharge temperature is controlled by the temperature control valve to adjust the bypass flow of the air cycle machine (ACM). The ACM comprises the turbine, compressor and fan mounted on the same shaft.

3.3 Electric Driven Vapor Cycle Pack

Figure 3.3 shows the schematic of an electric driven vapor cycle pack (eVCP) architecture. Contrary to the bleed air driven pack (Figure 3.1), fresh air enters the system through a scoop air inlet at ambient conditions. First the air is compressed in the base compressor (BCMP) and passes the primary heat exchanger installed in the ram air channel (RAC). During ground operations these two components are bypassed. The compressor of the air cycle machine further increases the pressure before the air is cooled in the reheater and meets again the ram air in the main heat exchanger. Downstream the MHX the fresh air temperature is further decreased in the evaporator of the vapor cycle (VaC) so that it reaches the saturation point during ground and low altitude operations.

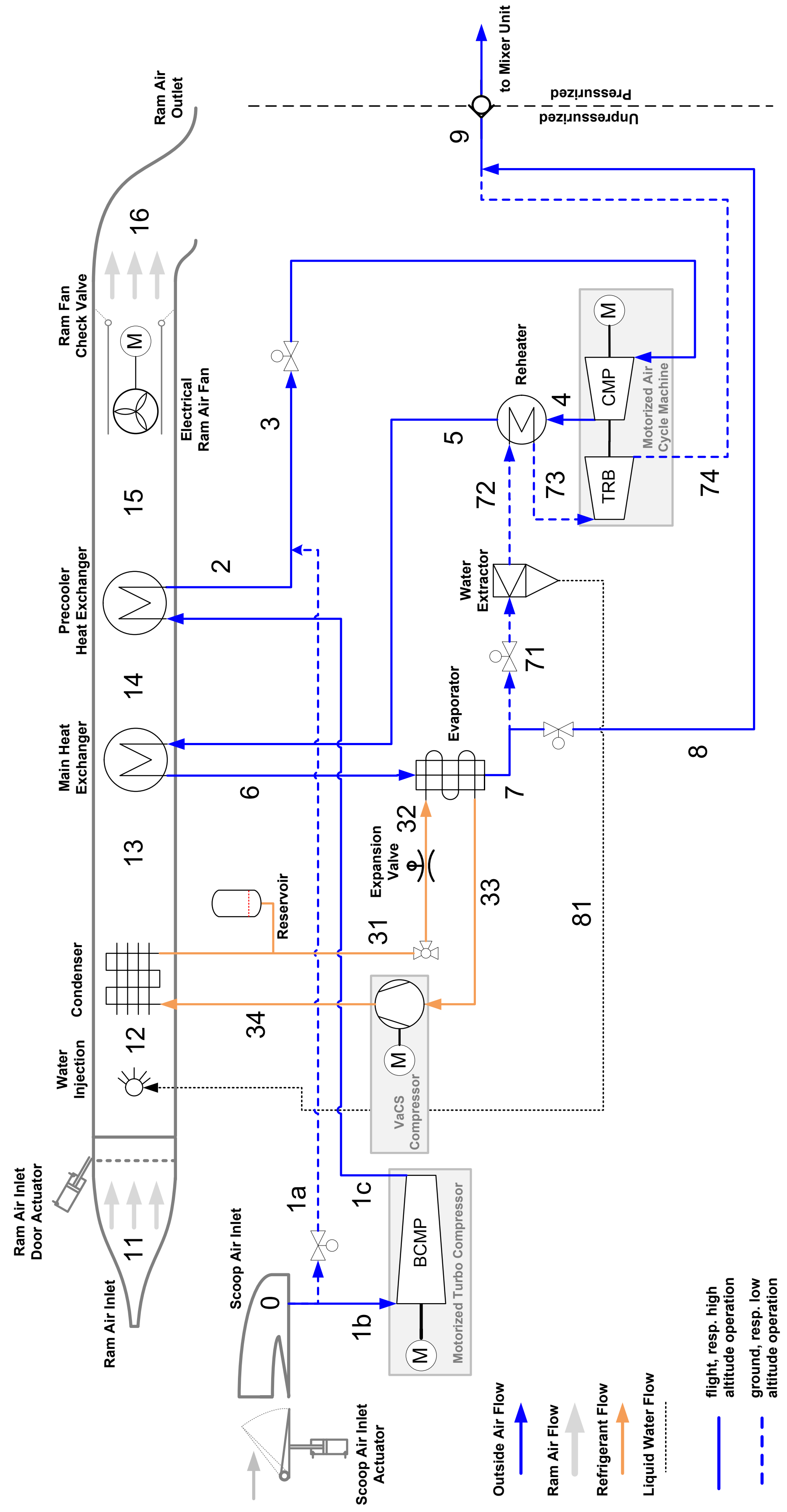

Figure 3.3: Schematic of an electric driven vapour cycle pack (eVCP) reference architecture.(adopted from [85])

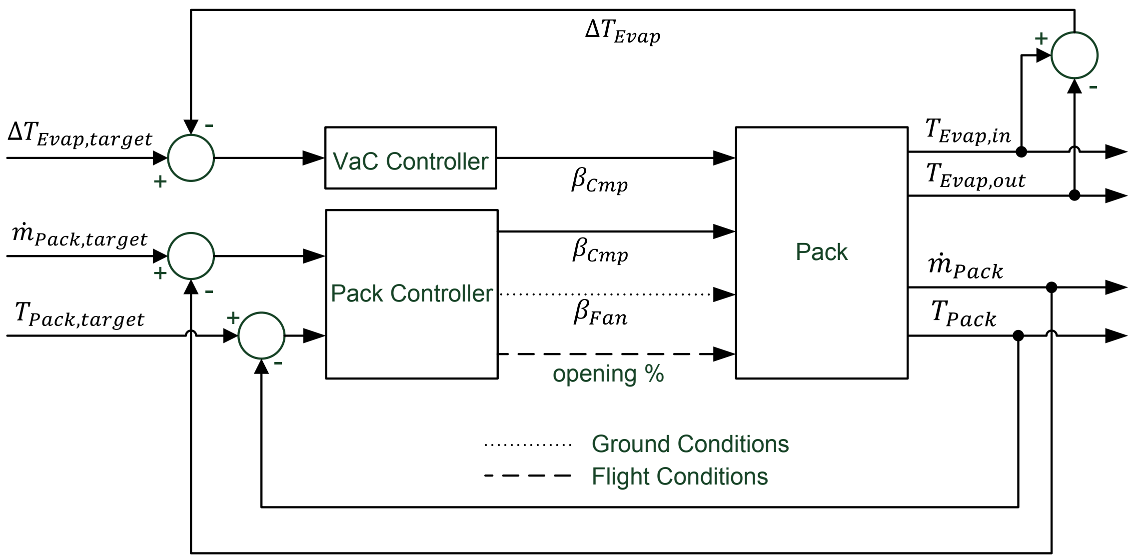

Figure 3.4: Control schematic of the electric driven vapor cycle pack.

The condensed water is discharged in the water separator. The dehumidified air is reheated in the reheater before it is expanded in the turbine and leaves the pack towards the mixing unit. The water separation branch including water extractor, reheater and turbine works only during ground and low altitude operations and is bypassed during high altitude operations and cruise. The ram air is fed by ambient air and works as a heat sink to discharge the surplus heat from the fresh air cycle. The condensate from the water extractor is injected into the ram air to use evaporative cooling to further decrease the ram air temperature. During ground operation the ram air inlet door is fully opened and the air flow is provided by the ram air fan located in the back of the ram air channel. The vapor cycle includes the evaporator, the vapor cycle compressor, condenser, reservoir and the expansion valve.

The electric driven vapor cycle pack has more degrees of freedom compared to the conventional bleed air driven pack. The base compressor and ram air fan are driven independently from the air cycle machine. In addition a vapor cycle is part of the eVCP architecture. The base compressor is bypassed during ground operations and is set to a fixed pressure ratio during flight conditions. The turbine is part of the ACM and mounted on one shaft with the ACM compressor. Further the water extraction branch is only used for ground and low altitude operations. During high altitude and cruise this branch is bypassed. The degrees of freedom decrease now to three control loops.

Figure 3.4 shows the control system for the eVCP model. The fresh air mass flow is set to a defined value. The mass flow is measured at the pack outlet (#9) and directed as process value to the pack controller. The controller output presets the pressure ratio for the ACM compressor until the target mass flow is reached. The second control loop of the pack controller affects the pack discharge temperature (Figure 3.3, #9). The desired temperature is set within the controller and compared to the actual value. The set point is achieved by controlling the ram air mass flow. This control loop knows two controller outputs.

During ground operations the controller presets the pressure ratio of the ram air fan in order to enforce the mass flow through the ram air channel. As soon as the ram air flow is provided by the aircraft speed, the ram air fan switches to flight mode, e.g. free rotation, to prevent damage and is partly bypassed. The second controller output is the opening of the ram air channel doors. During ground operations the doors are fully opened to allow maximum air flow. During flight conditions the opening is preset by the controller. The cooling power of the vapor cycle is ensured by the VaC controller. The temperature difference of the fresh air flow among the evaporator is measured and controlled at the desired target value by prescribing the pressure ratio of the VaC compressor. The mass flow of the refrigerant is used to control a desired subcooling temperature downstream the condenser which can be set within the subcooling control valve model.

Chapter 4
Methods

In this chapter, state of the art exergy-based methods are introduced and discussed in detail where necessary. Modifications for the adaptation to aircraft ECS applications are performed. Exergy balances for the components and on system level are developed with particular regards to the reference environment and requirements coming from the varying operating conditions of the ECS. A new approach for the combination of fuel weight penalties and the exergy of fuel consumption is presented including a detailed description how to calculate the fuel exergy of aviation fuel under consideration of the reference environment. Finally, the application of advanced exergy methods to aircraft ECS is discussed.

4.1 Conventional Exergy Analysis

4.1.1 General Assumptions

The environmental control system of an aircraft works similar to air conditioning systems installed in vehicles, buildings and other facilities. Heat exchangers, heat sinks and sources regulate the temperature and humidity. In order to provide a breathable environment inside the aircraft cabin, the air needs to be kept at a certain pressure level. This is achieved by turbomachines such as compressor and turbine. Within conventional aircraft ECSs the working fluid is moist air, including water extracted from condensation. The analysis shall provide an evaluation on system level. As usually done for the calculation of thermodynamic values of air conditioning applications, some simplifications are made for the exergy calculation of moist air:

- Moist air is regarded as an ideal mixture.
- The constituents of air are treated as ideal gases.
- The air is a mixture of two components: dry air with an averaged and fixed composition (Table 4.1) and pure water.
- Condensation and formation of ice are considered when condition of phase transformation is reached. Transformation enthalpies are assumed to be temperature-independent.
- Solubility of the components is neglected.

For most applications, the reference environment is set to the ambient environment. The working fluid under consideration operates either above or beneath the reference environment while the environment can be assumed to be constant. For the analysis of

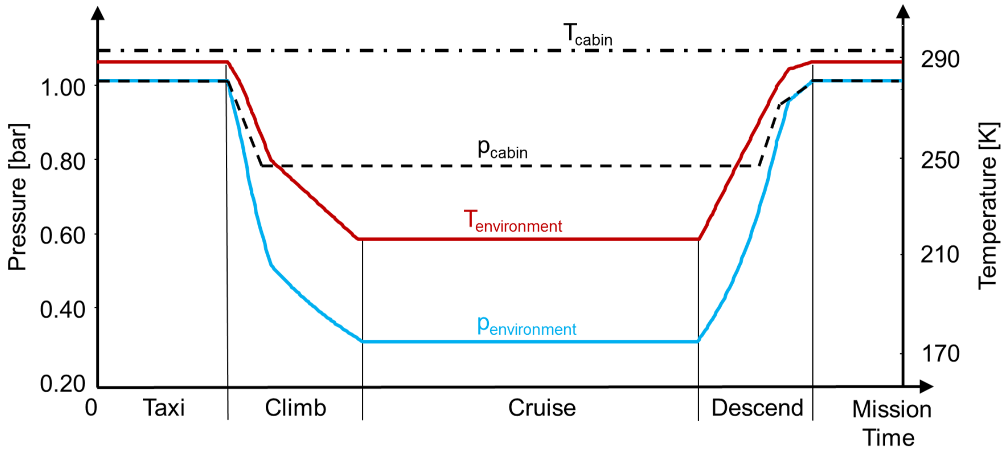

Figure 4.1: Temperature and pressure conditions of the cabin and the environment during a typical flight mission.

aircraft environmental control systems, this does not apply any more. Induced by the flight trajectory, the ambient conditions highly vary among the flight phases and the definition of the reference environment needs further discussion/considerations.

Table 4.1: Molar composition of dry air.

Constituent		Molar fraction x_i [kmol/kmol]
Nitrogen	N_2	0.7808
Oxygen	O_2	0.2095
Argon	Ar	0.0093
Carbon dioxide	CO_2	0.0004

Description of Environment Conditions

The environment conditions for an aircraft comprises a wide range. On the one hand, the operating conditions on ground cover all possible climate conditions. This ranges from high temperature (up to +55°C) with low humidity, such as desert environment, or high humidity, such as tropical climate, to cold conditions such as arctic weather (down to −54°C). For ground operation usually only the temperature and humidity changes. The pressure can be assumed to be relatively constant. During flight, the pressure decreases as well. For flight conditions, the international standard atmosphere (ISA) is used to describe the environment or ambient conditions. Figure 4.1 shows the trends of temperature and pressure of the ISA. The ground temperature is shown for a normal ISA day. Additional to the environment conditions, the pressure and temperature conditions of the cabin are plotted. The cabin temperature is controlled on a constant value at approximately 24°C. The pressure level decreases with raising altitude to a pressure level of approximately 0.79 bar at an altitude of 37000 ft.

In order to do an exergy analysis correctly, the whole thermodynamic state of the reference environment needs to be taken into account, i.e. not only temperature but also pressure and humidity (in case of moist air). Within this work, it is assumed that the components do not interact with the environment (such as surrounding structures and ambient air). This brings the advantage that the exergy balance over one component includes only the entering and leaving fluid and mechanical work flows.

4.1.2 Conventional Exergy Methods

The total flow exergy of a fluid stream i is expressed as:

$$\dot{E}_{\mathrm{t},i} = \dot{m} \cdot [h_i - h_0 - T_0 \cdot (s_i - s_0)] \tag{4.1}$$

where $\dot{m}_i$ is the mass flow, and h and s represent the specific enthalpy and specific entropy of the fluid stream i and reference environment 0. The flow exergy balance for the $k-$ th component is defined by:

$$\dot{E}_{\mathrm{F},k} = \dot{E}_{\mathrm{P},k} + \dot{E}_{\mathrm{D},k} \tag{4.2}$$

where subscripts F, P and D represent the fuel exergy, product exergy and destroyed exergy of the $k-$ th component [83]. The balance for the total system can be written as:

$$\dot{E}_{\mathrm{F,tot}} = \dot{E}_{\mathrm{P,tot}} + \sum_k \dot{E}_{\mathrm{D},k} + \dot{E}_{\mathrm{L,tot}} \tag{4.3}$$

with $_{\mathrm{tot}}$ representing the total amount of the overall system. The exergetic efficiency ϵ_k of the $k-$ th component is defined by the following expression:

$$\epsilon_k = \frac{\dot{E}_{\mathrm{P},k}}{\dot{E}_{\mathrm{F},k}} = 1 - \frac{\dot{E}_{\mathrm{D},k}}{\dot{E}_{\mathrm{F},k}} \tag{4.4}$$

And for the overall system:

$$\epsilon_{tot} = \frac{\dot{E}_{\mathrm{P,tot}}}{\dot{E}_{\mathrm{F,tot}}} = 1 - \frac{\dot{E}_{\mathrm{D,tot}} + \dot{E}_{\mathrm{L,tot}}}{\dot{E}_{\mathrm{F,tot}}} \tag{4.5}$$

The rate of exergy destroyed by the $k-$ th component related to the exergy of total fuel is expressed by the exergy destruction ratio:

$$y_{D,k} = \frac{\dot{E}_{\mathrm{D},k}}{\dot{E}_{\mathrm{F,tot}}} \tag{4.6}$$

The rate of exergy destroyed by the $k-$ th component related to the total exergy destruction of the system is expressed by the exergy destruction share:

$$y^*_{\mathrm{D},k} = \frac{\dot{E}_{\mathrm{D},k}}{\dot{E}_{\mathrm{D,tot}}} \tag{4.7}$$

4.1.3 Physical and Chemical Exergy

Following the proposed methodology of [83, 84], the exergy of a fluid stream is split into its physical and chemical parts. These parts are important for the definition of exergy of fuel and exergy of product under consideration of the reference environment. For the splitting of the flow exergy into its physical and chemical parts, this equation is written as:

$$e_{t,i} = e_i^{\mathrm{Ph}} + e_i^{\mathrm{Ch}} \tag{4.8}$$

The physical exergy e_i^{Ph} constitutes the exergetic potential of the working fluid when it is brought from its initial state (T, p, X) to the reference state (T_0, p_0, X) under the requirement that heat transfer happens only between the system and the environment.

For an open system, the physical specific exergy associated with the i-th material stream is:

$$e_i^{\mathrm{Ph}} = h_i - h_0 - T_0 \cdot (s_i - s_0) \tag{4.9}$$

In case of an ideal gas considering an ideal mixing of the constituents with constant specific heat, Equation (4.9) can be transformed into:

$$e_i^{\mathrm{Ph}} = c_{p,i} \left[(T - T_0) - T_0 ln \frac{T}{T_0} \right] + R_i T_0 ln \frac{p_i}{p_{0,i}} \tag{4.10}$$

The simplification of using a constant specific heat $c_{p,i}$ for the constituents is recommended to be applied for a temperature range from -50 °C to 70 °C [86]. However, the environmental conditions range from -74 °C to $+55$ °C and the working fluid, resp. bleed air, reaches temperatures up to 250 °C. Although the description of Equation (4.10) exceeds the range of application, it is used for the formulation of the physical exergy.

A more detailed view of the physical exergy is possible by further splitting it into a thermal and mechanical part. With this consideration, the impact of temperature and pressure deviation from the reference state is characterized separately:

$$e_i^{\mathrm{Ph}} = e_i^{\mathrm{T}} + e_i^{\mathrm{M}} \tag{4.11}$$

where e_i^{T} is the thermal part and e_i^{M} the mechanical part induced by pressure deviation. Equation (4.10) already contains both parts and can be regarded as:

$$e_i^{\mathrm{Ph}} = \underbrace{c_{p,i} \left[(T - T_0) - T_0 ln \frac{T}{T_0} \right]}_{e^T} + \underbrace{R_i T_0 ln \frac{p_i}{p_{0,i}}}_{e^{\mathrm{M}}} \tag{4.12}$$

The chemical exergy is defined in [87] with the following wording:

Table 4.2: Standard molar chemical exergy $\bar{e}_l^{\mathrm{Ch}}$ for constituents of moist air, $T_{\mathrm{ref}} = 298.15\,\mathrm{K}$ and $p_{\mathrm{ref}} = 1.01325\,\mathrm{bar}$ [92].

Substance		$\bar{e}_l^{\mathrm{Ch}}$ [kJ/mol] Model II[92]
Argon	Ar (g)	11.69
Carbon dioxide	CO_2 (g)	19.87
Nitrogen	N_2 (g)	0.72
Oxygen	O_2 (g)	3.97
Water	H_2O (g)	9.50
Water	H_2O (l)	0.90

Chemical exergy is the maximum theoretical useful work obtainable as the system having the temperature and pressure of the reference environment is brought into chemical equilibrium with this environment while interacting only with this environment.

In case of the considered working fluids for aircraft ECS and the reference environment, i.e. environment atmosphere, the chemical composition includes dry air constituents (see Table 4.1) and water content. The dry air composition is regarded as constant whereas the water content varies for the working fluids and reference environment. Due to the wide range of operation conditions, the moist air can take state as humid air, fog or ice fog. This applies to the working fluids (bleed and ram air) as well as to the reference environment. Our natural environment is usually not in equilibrium. Thus, an artificial exergy-reference environment needs to be modeled [16, 88, 89, 61, 90, 91, 92].

For engineering applications, two standard exergy reference environments have gained acceptance. The two models [91, 92] provide tabulated standard chemical exergy values for substances contained in the environment at standard conditions ($T_{\mathrm{ref}} = 298.15\,\mathrm{K}$ and $p_{\mathrm{ref}} = 1.01325\,\mathrm{bar}$). Table 4.2 lists the molar chemical exergy values taken from model II for the constituents of moist air.

For evaluations with small variations and deviations of the reference environment T_0 and p_0 to the standard conditions, the effect on the chemical exergy of reference substances might be neglected. This again does not apply on the evaluations of aircraft ECSs. However, introducing a small work-around, the tabulated standard chemical exergy values can be used to calculate the chemical part of the exergy of the working fluid with respect to the reference environment.

For reasons of simplification, the chemical composition of humid air ($\varphi \leq 1$) can be regarded as an ideal mixture of N ideal gases. The molar chemical exergy can be calculated in the following way:

$$\bar{e}^{\mathrm{Ch}}_{\substack{\mathrm{mixture}\\ \mathrm{ideal\ gases}}} = \sum_{l=0}^{N} x_l \bar{e}_l^{\mathrm{Ch}} + \bar{R} T_0 \sum_{l=0}^{N} x_l ln\left(x_l\right) \tag{4.13}$$

with x_l being the molar fraction of the l-th constituent and $\bar{R} = 8.3144598 \, \frac{\mathrm{J}}{\mathrm{mol \cdot K}}$ the molar gas constant.

Equation (4.13) describes the chemical exergy of a fluid stream at a certain state caused by its composition with respect to the standard reference conditions ($_{\mathrm{ref}}$) of the tabled data in Table 4.2. In other words, Equation (4.13) can be reformulated into:

$$\bar{e}_i^{\mathrm{Ch}} - \bar{e}_{\mathrm{ref}}^{\mathrm{Ch}} = \sum_{l=0}^{N} x_{l,i} \bar{e}_l^{\mathrm{Ch}} + \bar{R} T_0 \sum_{l=0}^{N} x_{l,i} ln \left(x_{l,i} \right) \tag{4.14}$$

For the reference state environment (T_0, p_0 and X_0) distinct from T_{ref} and p_{ref}, Equation (4.13) turns into:

$$\bar{e}_0^{\mathrm{Ch}} - \bar{e}_{\mathrm{ref}}^{\mathrm{Ch}} = \sum_{l=0}^{N} x_{l,0} \bar{e}_l^{\mathrm{Ch}} + \bar{R} T_0 \sum_{l=0}^{N} x_{l,0} ln \left(x_{l,0} \right) \tag{4.15}$$

Combining Equations (4.14) and (4.15), the chemical exergy of a fluid stream with respect to any arbitrary reference state environment can be calculated:

$$\bar{e}_i^{\mathrm{Ch}} - \bar{e}_{\mathrm{ref}}^{\mathrm{Ch}} - \left(\bar{e}_0^{\mathrm{Ch}} - \bar{e}_{\mathrm{ref}}^{\mathrm{Ch}} \right) = \bar{e}_i^{\mathrm{Ch}} - \bar{e}_0^{\mathrm{Ch}} \tag{4.16}$$

and

$$\bar{e}_i^{\mathrm{Ch}} - \bar{e}_0^{\mathrm{Ch}} = \sum_{l=0}^{N} x_{l,i} \bar{e}_l^{\mathrm{Ch}} + \bar{R} T_0 \sum_{l=0}^{N} x_{l,i} ln \left(x_{l,i} \right) - \left[\sum_{l=0}^{N} x_{l,0} \bar{e}_l^{\mathrm{Ch}} + \bar{R} T_0 \sum_{l=0}^{N} x_{l,0} ln \left(x_{l,0} \right) \right] \tag{4.17}$$

$x_{l,i}$ represents the molar fraction of the composition's substances l of the fluid stream i and $x_{l,0}$ the molar fractions of the composition's substances l of the reference state environment 0.

When the water content exceeds the saturation point ($\varphi > 1$), water begins to condensate and the fluid stream cannot be regarded as an ideal mixture anymore. It needs to be described as a two phase fluid consisting of saturated moist air and liquid water. The chemical exergy of the saturated moist air is furthermore calculated by Equation (4.17). The liquid part can easily be calculated with the help of Table 4.2:

$$\bar{e}_{\mathrm{L},0}^{\mathrm{Ch}} = \bar{e}_l^{\mathrm{Ch}} \tag{4.18}$$

for the reference state environment and

$$\bar{e}_{\mathrm{L},i}^{\mathrm{Ch}} = \bar{e}_l^{\mathrm{Ch}} + \bar{R} T_0 ln \left(\frac{1}{\varphi_0} \right) \tag{4.19}$$

for the working fluid with $\bar{e}_l^{\mathrm{Ch}}$ taken from Table 4.2 for H_2O (l) and φ_0 being the relative humidity of the reference environment.

The standard chemical exergy for a fluid stream in the fog region can then be formulated by combining Equations (4.14) and (4.19):

$$\left(e_i^{\text{Ch}} - e_{\text{ref}}^{\text{Ch}}\right)_{\varphi>1} = \left(\frac{1+\omega_{LV}}{1+\omega}\right)\left(\frac{1}{M_{\text{LV}}}\right)\left(\bar{e}_i^{\text{Ch}} - \bar{e}_{\text{ref}}^{\text{Ch}}\right) + \left(\frac{\omega_{\text{L}}}{1+\omega}\right)\left(\frac{1}{M_{\text{L}}}\right)\bar{e}_{\text{L},i}^{\text{Ch}} \quad (4.20)$$

here, the chemical exergy is already written with respect to the mass flow of the working fluid in [J/kg]. For the case that the reference environment is in the fog region, Equation (4.15) has to be adjusted in the same way. Concluding, three cases for the calculation of the specific chemical exergy of a fluid stream with respect to the reference environment can be developed:

- Working fluid & reference environment unsaturated (humid air):

$$\begin{aligned}\left(e_i^{\text{Ch}} - e_0^{\text{Ch}}\right)_{\varphi\le1} = \frac{1}{M_i}&\left(\sum_{l=0}^{N} x_{l,i}\bar{e}_l^{\text{Ch}} + \bar{R}T_0\sum_{l=0}^{N} x_{l,i}ln\left(x_{l,i}\right)\right)\\ -\frac{1}{M_i}&\left[\sum_{l=0}^{N} x_{l,0}\bar{e}_l^{\text{Ch}} + \bar{R}T_0\sum_{l=0}^{N} x_{l,0}ln\left(x_{l,0}\right)\right]\end{aligned} \quad (4.21)$$

- Working fluid in fog region, reference environment unsaturated:

$$\begin{aligned}\left(e_i^{\text{Ch}}\right)_{\varphi>1} - \left(e_0^{\text{Ch}}\right)_{\varphi\le1} = &\left(\frac{1+\omega_{\text{LV}}}{1+\omega}\right)\left(\frac{1}{M_{\text{LV}}}\right)\left(\bar{e}_i^{\text{Ch}} - \bar{e}_{\text{ref}}^{\text{Ch}}\right)_{\varphi\le1}\\ &+\left(\frac{\omega_{\text{L}}}{1+\omega}\right)\left(\frac{1}{M_{\text{L}}}\right)\bar{e}_{\text{L},i}^{\text{Ch}}\\ &-\frac{1}{M_i}\left(\sum_{l=0}^{N} x_{l,0}\bar{e}_l^{\text{Ch}} + \bar{R}T_0\sum_{l=0}^{N} x_{l,0}ln\left(x_{l,0}\right)\right)\end{aligned} \quad (4.22)$$

- Working fluid & reference environment in fog region:

$$\begin{aligned}\left(e_i^{\text{Ch}} - e_0^{\text{Ch}}\right)_{\varphi>1} = &\left(\frac{1+\omega_{\text{LV}}}{1+\omega}\right)\left(\frac{1}{M_{\text{LV}}}\right)\left(\bar{e}_i^{\text{Ch}} - \bar{e}_{\text{ref}}^{\text{Ch}}\right)_{\varphi\le1} + \left(\frac{\omega_{\text{L}}}{1+\omega}\right)\left(\frac{1}{M_{\text{L}}}\right)\bar{e}_{\text{L},i}^{\text{Ch}}\\ &-\left[\left(\frac{1+\omega_{0,\text{LV}}}{1+\omega_0}\right)\left(\frac{1}{M_{0,\text{LV}}}\right)\left(\bar{e}_0^{\text{Ch}} - \bar{e}_{\text{ref}}^{\text{Ch}}\right)_{\varphi\le1} + \left(\frac{\omega_{0,\text{L}}}{1+\omega_0}\right)\left(\frac{1}{M_{0,\text{L}}}\right)\bar{e}_{\text{L},0}^{\text{Ch}}\right]\end{aligned} \quad (4.23)$$

The specific exergy of a fluid stream can now be calculated with Equation (4.12) and the specific chemical exergy from Equations (4.21) - (4.23):

$$e_{\text{t},i} = c_{p,i}\left[\left(T - T_0\right) - T_0 ln\frac{T}{T_0}\right] + R_i T_0 ln\frac{p_i}{p_{0,i}} + \left(e_i^{\text{Ch}} - e_0^{\text{Ch}}\right)_{\varphi} \quad (4.24)$$

4.1.4 Exergy Balances

Having now the equations at hand for calculating the specific exergy of a moist air fluid stream, the next step is to set up the exergy balances. Different thermodynamic processes take place within an aircraft ECS. Starting with heat exchange with or without condensation, water extraction and injection, turbomachine induced processes such as compression and expansion, expansion due to valves, mixing of two streams, and fan ventilation (see Figure 3.1). There are two approaches for the definition of the exergy balance among a considered process, either on component or system level. The *exergy in-coming/exergy out-going* concept balances for the selected control volume the entering exergy flow with the exiting exergy flow summed up with the exergy destruction and exergy loss term. The concept of *exergy fuel/exergy product*, however, follows a different approach. The formulation of the exergy balances for the $k-$ th component and the overall system is presented later in this Chapter. In [83], the following guidelines for an objective and generally accepted definition of fuel and product have been proposed:

The *exergy of product* - $\dot{E}_{\mathrm{P}}$ is denoted as the desired result, expressed in exergy terms and achieved by the system (the $k-$ th component) being considered.
The *product* is defined to be equal to the sum of

- all the exergy values to be considered at the outlet (including the exergy of energy streams generated in the component) plus
- all the exergy increases between inlet and outlet (i.e., the exergy additions to the respective material streams) that are in accord with the purpose of the component.

The *exergy of fuel* - $\dot{E}_{\mathrm{F}}$ is denoted as the exergetic resources expended to generate the exergy of the product.
Similarly, the *fuel* is defined to be equal to

- all the exergy values to be considered at the inlet (including the exergy of energy streams supplied to the component) plus
- all the exergy decreases between inlet and outlet (i.e., the exergy removals from the respective material streams) minus
- all the exergy increases (between inlet and outlet) that are not in accord with the purpose of the component.

The term *fuel* is used here in a general sense and is not necessarily restricted to being an actual fuel such as coal, natural gas, or oil. Following observations emphasize the advantage of the fuel and product approach under the mandatory consideration of the reference environment for the state of the working fluids. The comprehensive development of Equation (4.24) to describe the specific exergy was necessary in order to cover all possible operating conditions of the working fluid: above, across or beneath the reference environment, applied to all three exergetic parts separately: thermal, mechanical, and chemical.

4.1.4.1 Component Level

The application of the introduced fuel and product methodology requires the knowledge of the specific trend of the thermal, mechanical and chemical specific exergy in Equation (4.24). Their behavior varies depending whether the component they operate above or beneath the reference environment. Particular care needs to be taken when the energy flows along a component cross the reference point. Figure 4.2 shows the trend-lines for the thermal, mechanical and chemical parts of the specific exergy with regards to the reference point 0. The thermal specific exergy has its minimum at the reference point and increases with growing distance to T_0, both for decreasing and increasing temperature. The thermal specific exergy therefore can have only positive values. The mechanical specific exergy changes proportional with the pressure itself. It becomes zero at p_0 and has negative values beneath and positive values above the reference pressure.

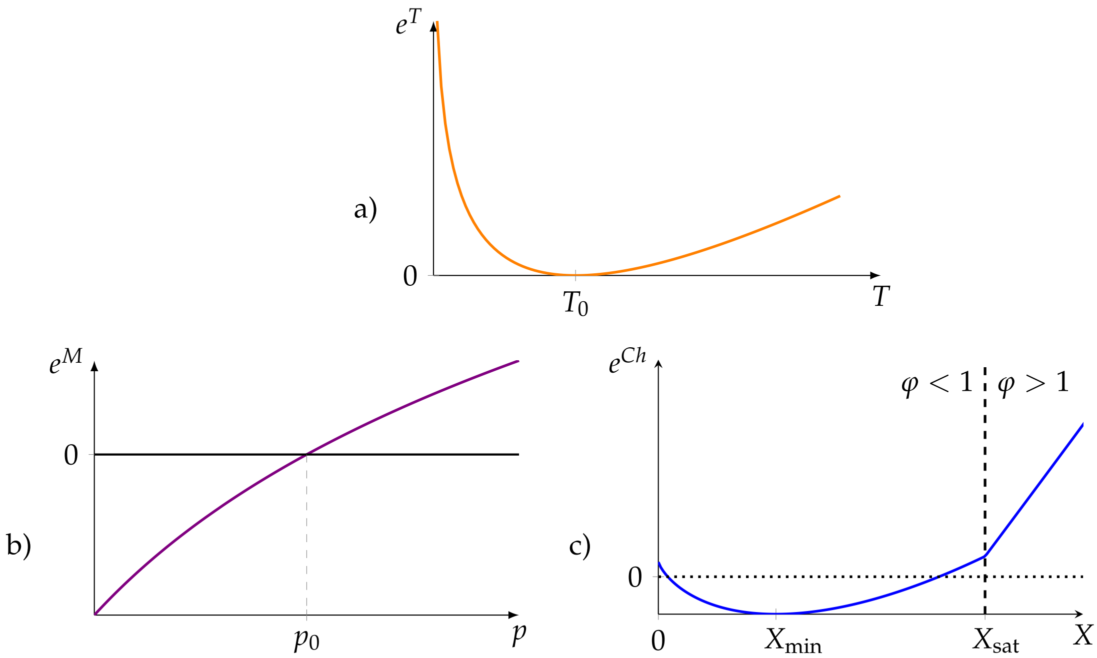

Figure 4.2: Impact on flow exergy through variation of: a) temperature, b) pressure, c) water content.

The chemical exergy e^{Ch} plays a more particular role. Equations (4.21) to (4.23) show that the calculation of the chemical exergy is more complex than the thermal or mechanical parts. Luckily, the chemical exergy does not change among many processes within an aircraft ECS and can be neglected for most of them. In general, only two cases need to be considered. The first one occurs when the amount of the water content changes, e.g. water extraction or injection. Here the chemical exergy changes among the trend-line of e^{Ch} shown in Figure 4.2 c). When the temperature of the working fluid changes within a process, the saturation point of the moist air changes as well. It could happen that the chemical exergy changes although the water content remains constant. This second case considers three scenarios (Figure 4.3):

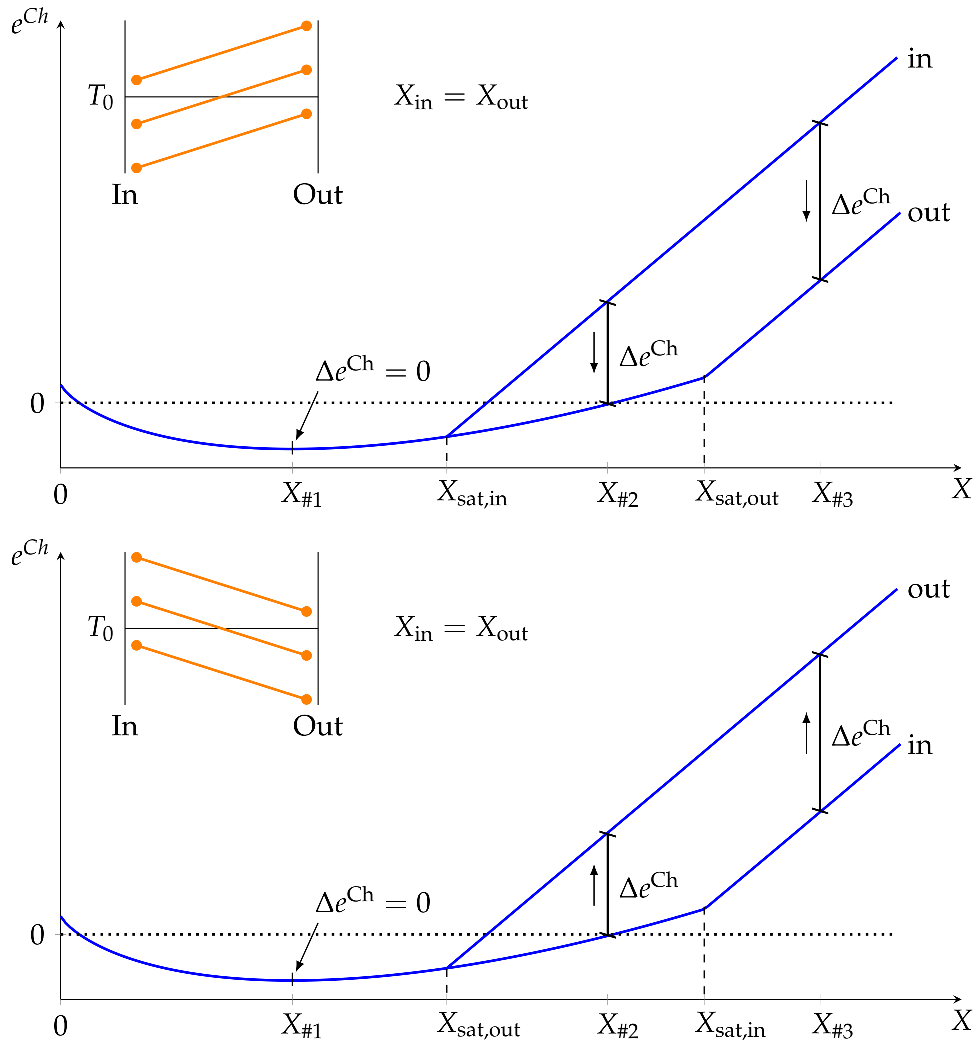

Figure 4.3: Behavior of chemical exergy for processes with temperature change.

Case #1: Both, entering and exiting flows are in unsaturated conditions

$$\Delta e^{Ch} = 0$$

Case #2: Either entering or exiting flow is unsaturated and the other one is in saturated condition

$$e^{Ch}_{out} > e^{Ch}_{in} \quad \text{if } T_{in} > T_{out}$$

$$e^{Ch}_{out} < e^{Ch}_{in} \quad \text{if } T_{in} < T_{out}$$

Case #3: Both, entering and exiting flows are in saturated condition

$$e^{Ch}_{out} > e^{Ch}_{in} \quad \text{if } T_{in} > T_{out}$$

$$e^{Ch}_{out} < e^{Ch}_{in} \quad \text{if } T_{in} < T_{out}$$

This missing brick now concludes the comprehensive view and allows the definition of the exergy rates of fuel and product for the different components. Table 4.3 lists the definitions of the exergy rates for the components of an aircraft ECS and all possible operation conditions. For reasons of clarity, the exergy rates are combined where appropriate. $\dot{E}_i$ includes all parts of the exergy stream, i.e. $\dot{E}_i = \dot{E}_i^{\mathrm{T}} + \dot{E}_i^{\mathrm{M}} + \dot{E}_i^{\mathrm{Ch}}$, and $\dot{E}_i^{\mathrm{Ph}}$ includes the physical parts, i.e. $\dot{E}_i^{\mathrm{Ph}} = \dot{E}_i^{\mathrm{T}} + \dot{E}_i^{\mathrm{M}}$. The exergy rates are organized according to the operation conditions depending on the temperature change and the relative position related to the reference environment. The fuel and product definition for the mechanical exergy can be defined independently from the relative position of the pressure to p_0. For processes with pressure loss, the mechanical exergy decreases and is assigned to exergy of fuel and for processes with increasing pressure, the mechanical exergy increases and affects the exergy of product. Some components are considered in general as dissipative components without any exergetic product, such as the water extractor, the mixer and flow resistances. In these cases, no fuel or product exergy can be identified and only the exergy destruction is calculated by balancing the entering and exiting energ flows. The exergy rates for the heat exchanger and the turbo components such as compressor and turbine are defined straight forward following the methodology of Chapter 4.1.4. The water injector is an exception among all components. In general this component can be seen as a dissipative component because there is no product identifiable from an exergetic view. The exception here is when it operates across or beneath the reference environment. Then thermal exergy is produced and this effect can be linked to the aim of the component, i.e. cooling the fluid stream through evaporation.

Table 4.3: Definition of exergy of fuel and exergy of product

<table>
<tr><th>Component schematic</th><th>Operation Conditions</th><th>Exergy Rates</th></tr>
<tr><td rowspan="5">
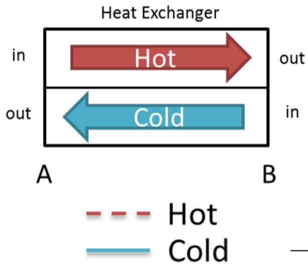

</td><td>
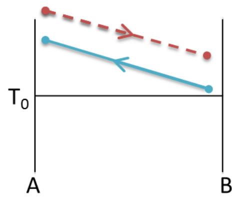

$T_{\text{hot, out}} \geq T_0$ and $T_{\text{cold, in}} \geq T_0$
</td><td>
$$\dot{E}_F = \dot{E}^{Ph}_{\text{hot, in}} - \dot{E}^{Ph}_{\text{hot, out}} + \dot{E}^{M}_{\text{cold, in}} - \dot{E}^{M}_{\text{cold, out}} + \dot{E}^{Ch}_{\text{cold, in}} - \dot{E}^{Ch}_{\text{cold, out}}$$

$$\dot{E}_P = \dot{E}^{T}_{\text{cold, out}} - \dot{E}^{T}_{\text{cold, in}} + \dot{E}^{Ch}_{\text{hot, out}} - \dot{E}^{Ch}_{\text{hot, in}}$$
</td></tr>
<tr><td>
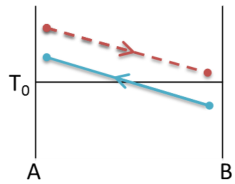

$T_{\text{hot, out}} \geq T_0$
and $T_{\text{cold, in}} \leq T_0 \leq T_{\text{cold, out}}$
</td><td>
$$\dot{E}_F = \dot{E}^{Ph}_{\text{hot, in}} - \dot{E}^{Ph}_{\text{hot, out}} + \dot{E}_{\text{cold, in}} - \dot{E}^{M}_{\text{cold, out}} - \dot{E}^{Ch}_{\text{cold, out}}$$

$$\dot{E}_P = \dot{E}^{T}_{\text{cold, out}} + \dot{E}^{Ch}_{\text{hot, out}} - \dot{E}^{Ch}_{\text{hot, in}}$$
</td></tr>
<tr><td>
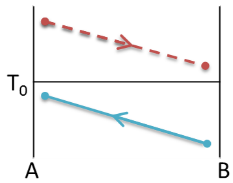

$T_{\text{hot, out}} \geq T_0$ and $T_{\text{cold, out}} \leq T_0$
</td><td>
Dissipative Component

$$\dot{E}_D = \dot{E}_{\text{hot, in}} - \dot{E}_{\text{hot, out}} + \dot{E}_{\text{cold, in}} - \dot{E}_{\text{cold, out}}$$
</td></tr>
<tr><td>
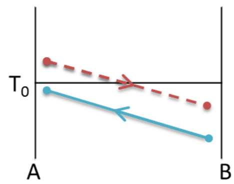

$T_{\text{hot, in}} \geq T_0 \geq T_{\text{hot, out}}$
and $T_{\text{cold, out}} \leq T_0$
</td><td>
$$\dot{E}_F = \dot{E}^{Ph}_{\text{hot, in}} - \dot{E}^{M}_{\text{hot, out}} + \dot{E}_{\text{cold, in}} - \dot{E}_{\text{cold, out}}$$

$$\dot{E}_P = \dot{E}^{T}_{\text{hot, out}} + \dot{E}^{Ch}_{\text{hot, out}} - \dot{E}^{Ch}_{\text{hot, in}}$$
</td></tr>
<tr><td>
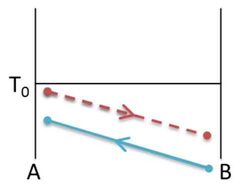

$T_{\text{hot, in}} \leq T_0$ and $T_{\text{cold, out}} \leq T_0$
</td><td>
$$\dot{E}_F = \dot{E}^{M}_{\text{hot, in}} - \dot{E}^{M}_{\text{hot, out}} + \dot{E}_{\text{cold, in}} - \dot{E}_{\text{cold, out}}$$

$$\dot{E}_P = \dot{E}^{T}_{\text{hot, out}} - \dot{E}^{T}_{\text{hot, in}} + \dot{E}^{Ch}_{\text{hot, out}} - \dot{E}^{Ch}_{\text{hot, in}}$$
</td></tr>
</table>

Component schematic	Operation Conditions	Exergy Rates
	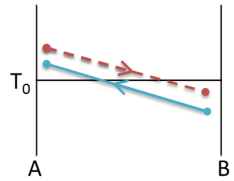 $T_{\text{hot, in}} \geq T_0 \geq T_{\text{hot, out}}$ and $T_{\text{cold, out}} \geq T_0 \geq T_{\text{cold, in}}$	$\dot{E}_{\text{F}} = \dot{E}^{\text{Ph}}_{\text{hot, in}} - \dot{E}^{M}_{\text{hot, out}} + \dot{E}_{\text{cold, in}} - \dot{E}^{\text{M}}_{\text{cold, out}} - \dot{E}^{\text{Ch}}_{\text{cold, out}}$ $\dot{E}_{\text{P}} = \dot{E}^{\text{T}}_{\text{hot, out}} + \dot{E}^{\text{T}}_{\text{cold, out}} + \dot{E}^{\text{Ch}}_{\text{hot, out}} - \dot{E}^{\text{Ch}}_{\text{hot, in}}$
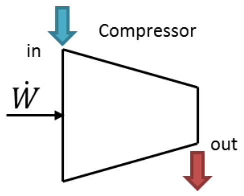	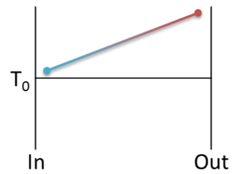 $T_{\text{in}} \geq T_0$	$\dot{E}_{\text{F}} = \dot{W} + \dot{E}^{\text{Ch}}_{\text{in}} - \dot{E}^{\text{Ch}}_{\text{out}}$ $\dot{E}_{\text{P}} = \dot{E}^{\text{Ph}}_{\text{out}} - \dot{E}^{\text{Ph}}_{\text{in}}$
	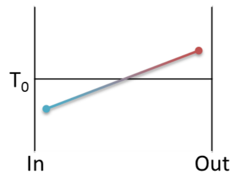 $T_{\text{in}} \leq T_0 \leq T_{\text{out}}$	$\dot{E}_{\text{F}} = \dot{W} + \dot{E}^{\text{T}}_{\text{in}} + \dot{E}^{\text{Ch}}_{\text{in}} - \dot{E}^{\text{Ch}}_{\text{out}}$ $\dot{E}_{\text{P}} = \dot{E}^{\text{Ph}}_{\text{out}} - \dot{E}^{\text{M}}_{\text{in}}$
	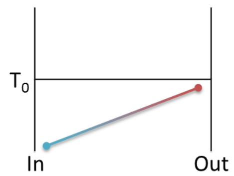 $T_{\text{out}} \leq T_0$	$\dot{E}_{\text{F}} = \dot{W} + \dot{E}^{\text{T}}_{\text{in}} - \dot{E}^{\text{T}}_{\text{out}} + \dot{E}^{\text{Ch}}_{\text{in}} - \dot{E}^{\text{Ch}}_{\text{out}}$ $\dot{E}_{\text{P}} = \dot{E}^{\text{M}}_{\text{out}} - \dot{E}^{\text{M}}_{\text{in}}$
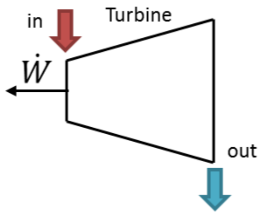	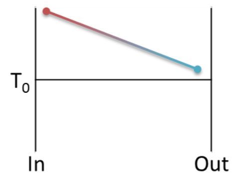 $T_{\text{out}} \geq T_0$	$\dot{E}_{\text{F}} = \dot{E}^{\text{Ph}}_{\text{in}} - \dot{E}^{\text{Ph}}_{\text{out}}$ $\dot{E}_{\text{P}} = \dot{W} + \dot{E}^{\text{Ch}}_{\text{out}} - \dot{E}^{\text{Ch}}_{\text{in}}$
	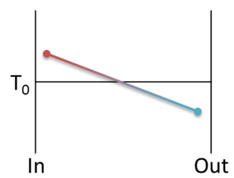 $T_{\text{in}} \geq T_0 \geq T_{\text{out}}$	$\dot{E}_{\text{F}} = \dot{E}^{\text{Ph}}_{\text{in}} - \dot{E}^{\text{M}}_{\text{out}}$ $\dot{E}_{\text{P}} = \dot{W} + \dot{E}^{\text{T}}_{\text{out}} + \dot{E}^{\text{Ch}}_{\text{out}} - \dot{E}^{\text{Ch}}_{\text{in}}$

<table>
<tr><th>Component schematic</th><th>Operation Conditions</th><th>Exergy Rates</th></tr>
<tr><td></td><td>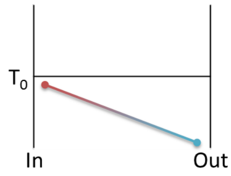

$T_{\text{in}} \leq T_0$</td><td>$\dot{E}_{\text{F}} = \dot{E}^{\text{M}}_{\text{in}} - \dot{E}^{\text{M}}_{\text{out}}$
$\dot{E}_{\text{P}} = \dot{W} + \dot{E}^{\text{T}}_{\text{out}} - \dot{E}^{\text{T}}_{\text{in}} + \dot{E}^{\text{Ch}}_{\text{out}} - \dot{E}^{\text{Ch}}_{\text{in}}$</td></tr>
<tr><td>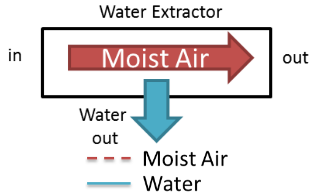
</td><td>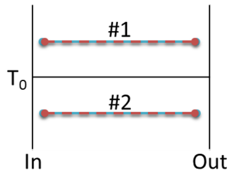

$T \geq T_0$ and $T \leq T_0$</td><td>Dissipative Component
$\dot{E}_{\text{D}} = \dot{E}_{\text{in}} - \dot{E}_{\text{out}} - \dot{E}_{\text{water, out}}$</td></tr>
<tr><td>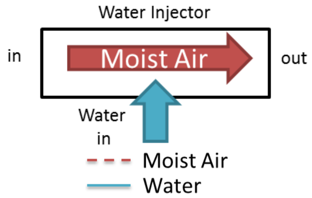
</td><td>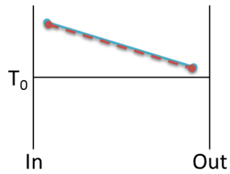

$T_{\text{out}} \geq T_0$</td><td>Dissipative Component
$\dot{E}_{\text{D}} = \dot{E}_{\text{in}} + \dot{E}_{\text{water, in}} - \dot{E}_{\text{out}}$</td></tr>
<tr><td rowspan="2">^{1} : $\dot{E}_{\text{water, in}^1}$ stands for actual part of entering water that is evaporated.
^{2} : $\dot{E}^{\text{T}}_{\text{out}^2}$ stands for thermal exergy of the entering flow that is cooled to T_{out}.</td><td>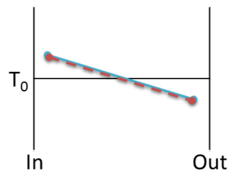

$T_{\text{in}} \geq T_0 \geq T_{\text{out}}$</td><td>$\dot{E}_{\text{F}} = \dot{E}_{\text{water, in}^1} - \dot{E}_{\text{water, evap}} + \dot{E}^{\text{T}}_{\text{in}}$
$\dot{E}_{\text{P}} = \dot{E}^{\text{T}}_{\text{out}^2}$</td></tr>
<tr><td>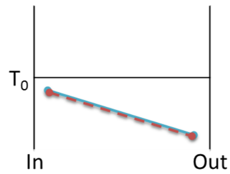

$T_{\text{in}} \leq T_0$</td><td>$\dot{E}_{\text{F}} = \dot{E}_{\text{water, in}^1} - \dot{E}_{\text{water, evap}}$
$\dot{E}_{\text{P}} = \dot{E}^{\text{T}}_{\text{out}^2} - \dot{E}^{\text{T}}_{\text{in}}$</td></tr>
<tr><td>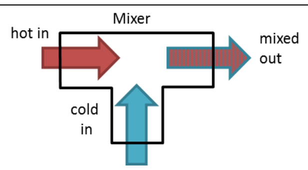
</td><td>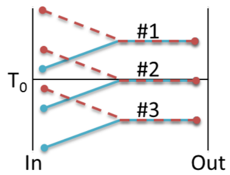

$T_{\text{out}} \geq T_0$</td><td>Dissipative Component
$\dot{E}_{\text{D}} = \dot{E}_{\text{hot, in}} + \dot{E}_{\text{cold, in}} - \dot{E}_{\text{out}}$</td></tr>
<tr><td>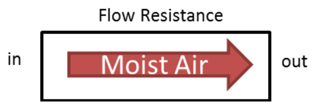
</td><td>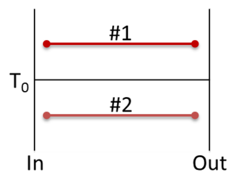

$T \geq T_{\text{out}}$ and $T \leq T_0$</td><td>Dissipative Component
$\dot{E}_{\text{D}} = \dot{E}_{\text{in}} - \dot{E}_{\text{out}}$</td></tr>
</table>

4.1.4.2 System Level

On component level, an explicit description of the exergy balances is in most cases obvious following the approach of fuel and product as presented in the beginning of Section 4.1.4. The difference of exergy of fuel and product denotes the exergy destruction of the component. On system level, the balance of the conventional exergy-based approach extends with the exergy of losses that describes the exergy flows leaving the system boundaries without being used (Equation 4.3).

The first step to define the exergy balance on system level is to identify the system boundaries. Figure 4.4 shows a simplified schematic of the bleed pack with the main components, air streams and system boundaries for the conventional exergy analysis. As shown in Figure 4.4, two fluid streams pass the conventional bleed air driven pack. The bleed air enters the pack at high temperature and pressure. The conditioned air is then discharged to the mixing unit where it meets the recirculated air from the cabin. The ram air enters the pack from outside the aircraft and is discharged to the environment downstream the pack. The only energy flows that cross the system boundaries are the two air flows. Within this thesis, it is assumed that there is no further interaction with the ambient environment, such as heat exchange. The bleed pack works autonomously and thus no additional work or electric power is supplied to the system. The exergy flows of fuel, product and loss need to be defined with the entering and exiting ram air flow and entering and exiting bleed air flow. The high energetic entering bleed air drives the air cycle machine and is the only source of energy for the pack. It is assigned as exergy of fuel. Referring to the pack's aim, the system shall condition the bleed air to satisfy the atmosphere requirements of the cabin. Therefore the discharge air could be regarded as

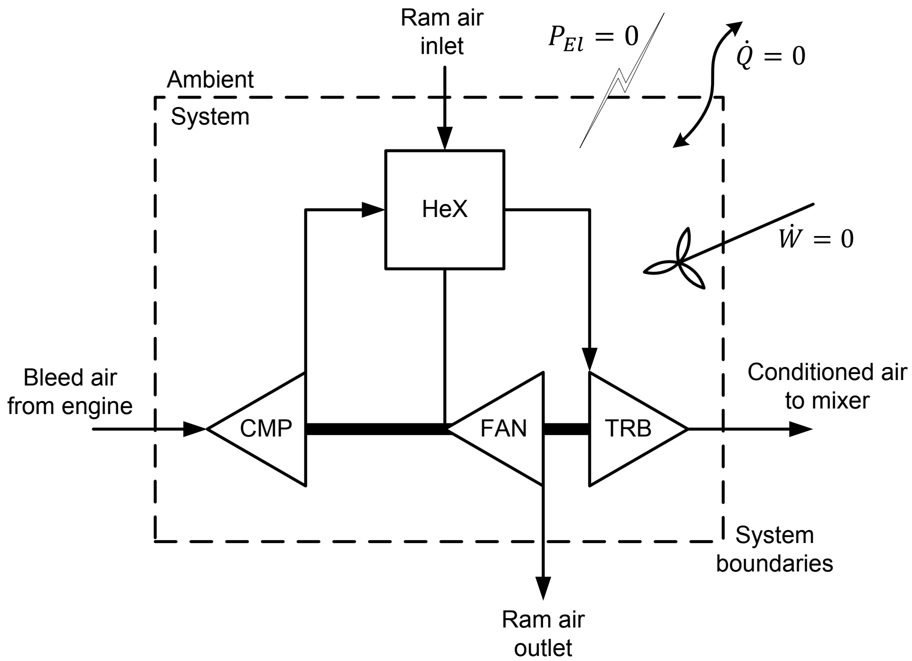

Figure 4.4: System boundaries for the conventional exergy analysis of the bleed air pack.

product of the process. However, from the exergetic perspective, the exergy of the bleed air stream decreases along the pack for any operating points. Setting the system boundaries as shown in Figure 4.4, there is no exergetic product. The exergy of the exiting bleed air flow needs to be considered as losses within the system balance. The same applies to the ram air flow. Along the ram air channel, the exergy of the ram air flow increases. The exergy stored to the ram air flow leaves the system boundaries to the ambient without any use and is thus assigned as losses.

Equation 4.3 can now be written for the conventional bleed air driven pack as:

$$\underbrace{\dot{E}_{\text{bleed,in}}}_{\dot{E}_{\text{F,tot}}} = \sum_k \dot{E}_{\text{D},k} + \underbrace{\dot{E}_{\text{bleed,out}} + \left(\dot{E}_{\text{ram,out}} - \dot{E}_{\text{ram,in}}\right)}_{\dot{E}_{\text{L,tot}}} \tag{4.25}$$

Components that have no exergetic product are regarded as dissipative components. The same applies to the bleed air pack on system level. No exergetic product can be extracted from the system. Hence, no exergetic efficiency can be defined for the overall system. The exergy destruction ratio $y_{\text{D},k}$ and exergy destruction share $y^*_{\text{D},k}$ give information about the magnitude of inefficiencies of the single components compared to the total system.

The second pack architecture regarded within this work is an electric driven vapor cycle pack (eVCP). Figure 4.5 shows the simplified schematic of the eVCP. Similar to the bleed air driven pack, two fluid streams cross the boundaries. The ram air enters the system from the ambient and exits to the same. Contrary to the conventional pack, the fresh air does not rise from the engine, but enters the pack from the outside at environment conditions. The requirements for the conditioned air leaving the eVCP equal the bleed air pack. An additional vapor cycle is integrated to the pack cycle and in contrast to the conventional pack, the eVCP does not run autonomously. The turbo components are driven by electrically powered motors. This includes the air flown compressors and fan, and the vapor cycle compressor. Thus, a third energy stream crosses the system boundaries in form of electric power. Heat transfer with the ambient is further neglected and there is no mechanical work supplied to the system.

The entering and exiting energy flows are now integrated to the exergy balance of the overall system. The electric power supplied to the eVCP is now the only source of fuel to the system from an exergetic perspective and thus assigned as fuel exergy rate. The ram air flow is considered the same way as for the bleed air pack. Heat is transfered to the ram air and discharged to the environment without any usage. The difference of the exergy rate among the ram air channel is regarded as losses. The process of the fresh air needs a more detailed discussion.

To develop a comprehensive formulation for the fresh air stream and place it into the system balance, the air flow is regarded with its thermal, mechanical and chemical parts. Beginning with the mechanical part, the pressure change throughout the pack is considered. During ground and low altitude operation, the cabin pressure level is slightly

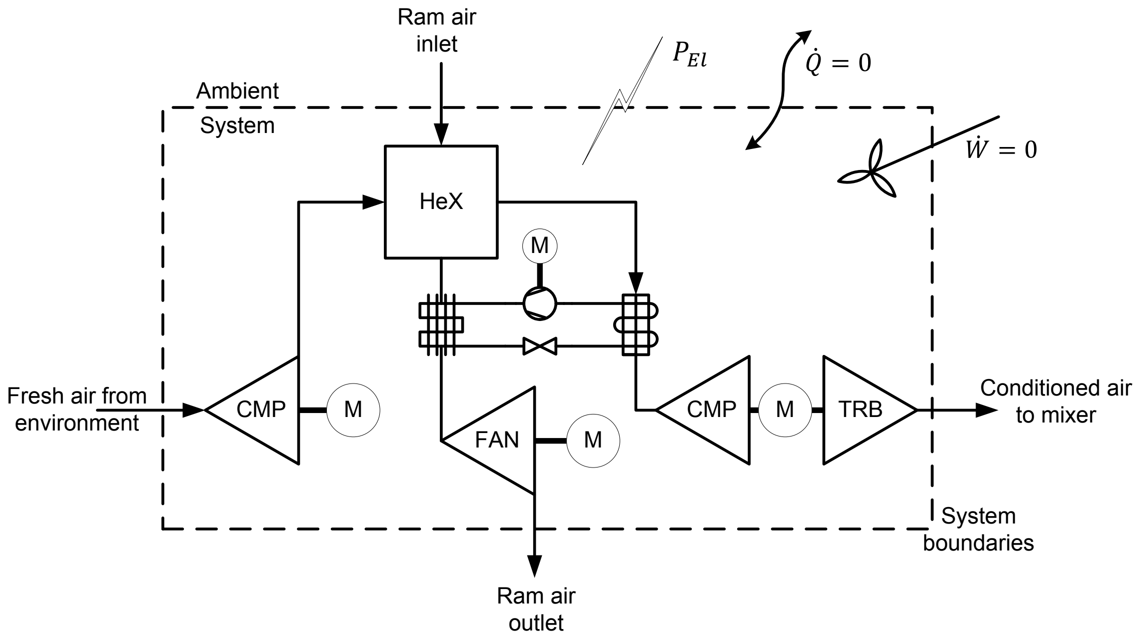

Figure 4.5: System boundaries for the conventional exergy analysis of the electric driven vapor cycle pack.

higher than the environment. As the mass flow from the mixer to the cabin is driven by pressure drop, the discharge pressure at the pack outlet is always above the ambient pressure. During flight conditions, the cabin needs to be pressurized and thus the pack provides an increase in pressure. Concluding, a pressure increase leads according to Figure 4.2 to an increase in mechanical exergy across the system boundaries and is regarded as fuel exergy.

For the discussion of the change in chemical exergy, the temperature change has to be taken into account. Replacing the eVCP by a surrogate process for the fresh air, it can be reduced to a heat exchanger with water extraction. With this simplified view, it can be handled as a component and the behavior can be explained with Figure 4.3. In general two cases can occur: heating and cooling. The water content remains constant or decreases, but never increases. Again, it is important if the appropriate stream is in saturated or unsaturated conditions.

The possible cases that can occur for the chemical exergy are listed in Table 4.5. It is devided into the general cases of cooling and heating. Further, the saturation state at the eVCP inlet and outlet is distinguished and if water separation takes place or not. The change of chemical exergy for the case of no water extraction is easy to identify. For the cooling case, the chemical part does not change or increase, so that the change can be assigned as product. For the heating case, the chemical exergy can remain constant or decreases, so that the change can be assigned as fuel. For the case of water separation, an explicit rule cannot be formulated due to the trends of the curves (Figure 4.3), there could be either an increase or decrease or no change in chemical exergy. Concluding the discussion for the chemical exergy change, it is recommended that the difference $e_{\text{in}}^{\text{Ch}} - e_{\text{out}}^{\text{Ch}}$

Table 4.5: Changes in chemical exergy for the fresh air stream among the eVCP.

	φ	$X_{\text{in}} = X_{\text{out}}$	$X_{\text{in}} > X_{\text{out}}$
cooling	$\varphi_{\text{in}} \leq 1$ $\varphi_{\text{out}} \leq 1$	$e^{\text{Ch}}_{\text{in}} - e^{\text{Ch}}_{\text{out}} = 0$	$e^{\text{Ch}}_{\text{in}} - e^{\text{Ch}}_{\text{out}} =$ #1 : < 0 $\rightarrow$ product #2 : > 0 $\rightarrow$ fuel
	$\varphi_{\text{in}} > 1$ $\varphi_{\text{out}} > 1$	$e^{\text{Ch}}_{\text{in}} - e^{\text{Ch}}_{\text{out}} < 0$ $\rightarrow$ product	$e^{\text{Ch}}_{\text{in}} - e^{\text{Ch}}_{\text{out}} =$ #1 : < 0 $\rightarrow$ product #2 : > 0 $\rightarrow$ fuel #3 : 0
heating	$\varphi_{\text{in}} \leq 1$ $\varphi_{\text{out}} \leq 1$	$e^{\text{Ch}}_{\text{in}} - e^{\text{Ch}}_{\text{out}} = 0$	$e^{\text{Ch}}_{\text{in}} - e^{\text{Ch}}_{\text{out}} =$ #1 : < 0 $\rightarrow$ product #2 : > 0 $\rightarrow$ fuel
	$\varphi_{\text{in}} > 1$ $\varphi_{\text{out}} > 1$	$e^{\text{Ch}}_{\text{in}} - e^{\text{Ch}}_{\text{out}} > 0$ $\rightarrow$ fuel	$e^{\text{Ch}}_{\text{in}} - e^{\text{Ch}}_{\text{out}} > 0$ $\rightarrow$ fuel
	$\varphi_{\text{in}} > 1$ $\varphi_{\text{out}} < 1$	$e^{\text{Ch}}_{\text{in}} - e^{\text{Ch}}_{\text{out}} > 0$ $\rightarrow$ fuel	$e^{\text{Ch}}_{\text{in}} - e^{\text{Ch}}_{\text{out}} =$ #1 : < 0 $\rightarrow$ product #2 : > 0 $\rightarrow$ fuel

is assigned to the appropriate part of the system balance depending on its sign. Positive means it is fuel, negative means it is product.

The discussion about the chemical exergy showed that the pack could either heat or cool the fresh air. The thermal part of the exergy rate hence has to be discussed the same way as the chemical part. Figure 4.2 is taken again to define the exergy rates for the thermal exergy change among the electric driven pack.

Table 4.6 lists the cases for the change of thermal exergy of the fresh air flow. Depending of the reference state environment, the process operates above, below or across the reference temperature T_0. This results in three cases each for cooling and heating and thus in total there are six cases for the change of thermal exergy. If the reference temperature is crossed, the assignment is the same for cooling and heating. Contrary to the chemical exergy, these two assignments are important as the thermal exergy is zero at T_0. From an exergetic point of view, there is no exergetic product for the first case of cooling and the last case of heating. There is no product and thus speaking for the thermal part, a dissipative process. These observations are directly linked to one of the main questions of this thesis: how to define the reference environment?

Table 4.6: Changes in thermal exergy for the fresh air stream among the eVCP.

	T	thermal exergy
cooling	$T_{\text{out}} \geq T_0$	$e^{\text{T}}_{\text{in}} - e^{\text{T}}_{\text{out}} > 0$ $\rightarrow$ fuel
	$T_{\text{in}} \geq T_0 \geq T_{\text{out}}$	e^{T}_{in} $\rightarrow$ fuel $e^{\text{T}}_{\text{out}}$ $\rightarrow$ product
	$T_{\text{in}} \leq T_0$	$e^{\text{T}}_{\text{in}} - e^{\text{T}}_{\text{out}} < 0$ $\rightarrow$ product
heating	$T_{\text{in}} \geq T_0$	$e^{\text{T}}_{\text{in}} - e^{\text{T}}_{\text{out}} < 0$ $\rightarrow$ product
	$T_{\text{in}} \leq T_0 \leq T_{\text{out}}$	e^{T}_{in} $\rightarrow$ fuel $e^{\text{T}}_{\text{out}}$ $\rightarrow$ product
	$T_{\text{out}} \leq T_0$	$e^{\text{T}}_{\text{in}} - e^{\text{T}}_{\text{out}} > 0$ $\rightarrow$ fuel

Following strictly the approach for fuel and product exergy, it could happen that both the thermal and chemical exergy decrease among the eVCP and only the mechanical exergy increases. The only product then would be the increase in pressure. The exergetic efficiency of Equation 4.5 would be very low. The results of the conventional exergy analysis for the overall system performance would be devastating, although the pack fulfills its task. The bleed air driven pack can be reduced to an expansion process with water extraction and explicitly identified as a dissipative component. The eVCP, however, performs a meaningful process by converting supplied electrical power to either cooling or heating power. The definition of the reference environment is the linchpin of the whole analysis. The fresh air enters the pack at environment conditions. Setting the reference point to ambient conditions, the exergy of the entering air flow would be zero. For both operations, cooling and heating, the thermal exergy increases among the eVCP and can be measured as product exergy and the energy conversion is described in a meaningful way. Nevertheless, the exergy-based methods are implemented into model-based design and need to meet all possible conditions. The definition of the fuel and product exergy rate for the exergy balances of the eVCP are listed in Table 4.7.

Table 4.7: Definition of fuel and product for the exergy balance of the overall eVCP system.

	$\dot{E}^{\mathrm{Ch}}_{\mathrm{in}} - \dot{E}^{\mathrm{Ch}}_{\mathrm{out}}$	T	Exergy balance
cooling	$\Delta\dot{E}^{\mathrm{Ch}} < 0$	$T_{\mathrm{out}} \geq T_0$	$\dot{E}_{\mathrm{F,tot}} = P_{\mathrm{el}} + \dot{E}^{\mathrm{T}}_{\mathrm{fA,in}} - \dot{E}^{\mathrm{T}}_{\mathrm{fA,out}}$ $\dot{E}_{\mathrm{P,tot}} = \dot{E}^{\mathrm{M}}_{\mathrm{fA,out}} - \dot{E}^{\mathrm{M}}_{\mathrm{fA,in}} + \dot{E}^{\mathrm{Ch}}_{\mathrm{fA,out}} - \dot{E}^{\mathrm{Ch}}_{\mathrm{fA,in}}$
		$T_{\mathrm{in}} \geq T_0 \geq T_{\mathrm{out}}$	$\dot{E}_{\mathrm{F,tot}} = P_{\mathrm{el}} + \dot{E}^{\mathrm{T}}_{\mathrm{fA,in}}$ $\dot{E}_{\mathrm{P,tot}} = \dot{E}^{\mathrm{M}}_{\mathrm{fA,out}} - \dot{E}^{\mathrm{M}}_{\mathrm{fA,in}} + \dot{E}^{\mathrm{Ch}}_{\mathrm{fA,out}} - \dot{E}^{\mathrm{Ch}}_{\mathrm{fA,in}} + \dot{E}^{\mathrm{T}}_{\mathrm{fA,out}}$
		$T_{\mathrm{in}} \leq T_0$	$\dot{E}_{\mathrm{F,tot}} = P_{\mathrm{el}}$ $\dot{E}_{\mathrm{P,tot}} = \dot{E}^{\mathrm{M}}_{\mathrm{fA,out}} - \dot{E}^{\mathrm{M}}_{\mathrm{fA,in}} + \dot{E}^{\mathrm{Ch}}_{\mathrm{fA,out}} - \dot{E}^{\mathrm{Ch}}_{\mathrm{fA,in}} + \dot{E}^{\mathrm{T}}_{\mathrm{fA,out}}$ $- \dot{E}^{\mathrm{T}}_{\mathrm{fA,in}}$
	$\Delta\dot{E}^{\mathrm{Ch}} > 0$	$T_{\mathrm{out}} \geq T_0$	$\dot{E}_{\mathrm{F,tot}} = P_{\mathrm{el}} + \dot{E}^{\mathrm{T}}_{\mathrm{fA,in}} - \dot{E}^{\mathrm{T}}_{\mathrm{fA,out}} + \dot{E}^{\mathrm{Ch}}_{\mathrm{fA,in}} - \dot{E}^{\mathrm{Ch}}_{\mathrm{fA,out}}$ $\dot{E}_{\mathrm{P,tot}} = \dot{E}^{\mathrm{M}}_{\mathrm{fA,out}} - \dot{E}^{\mathrm{M}}_{\mathrm{fA,in}}$
		$T_{\mathrm{in}} \geq T_0 \geq T_{\mathrm{out}}$	$\dot{E}_{\mathrm{F,tot}} = P_{\mathrm{el}} + \dot{E}^{\mathrm{T}}_{\mathrm{fA,in}} + \dot{E}^{\mathrm{Ch}}_{\mathrm{fA,in}} - \dot{E}^{\mathrm{Ch}}_{\mathrm{fA,out}}$ $\dot{E}_{\mathrm{P,tot}} = \dot{E}^{\mathrm{M}}_{\mathrm{fA,out}} - \dot{E}^{\mathrm{M}}_{\mathrm{fA,in}} + \dot{E}^{\mathrm{T}}_{\mathrm{fA,out}}$
		$T_{\mathrm{in}} \leq T_0$	$\dot{E}_{\mathrm{F,tot}} = P_{\mathrm{el}} + \dot{E}^{\mathrm{Ch}}_{\mathrm{fA,in}} - \dot{E}^{\mathrm{Ch}}_{\mathrm{fA,out}}$ $\dot{E}_{\mathrm{P,tot}} = \dot{E}^{\mathrm{M}}_{\mathrm{fA,out}} - \dot{E}^{\mathrm{M}}_{\mathrm{fA,in}} + \dot{E}^{\mathrm{T}}_{\mathrm{fA,out}} - \dot{E}^{\mathrm{T}}_{\mathrm{fA,in}}$
heating	$\Delta\dot{E}^{\mathrm{Ch}} < 0$	$T_{\mathrm{in}} \geq T_0$	$\dot{E}_{\mathrm{F,tot}} = P_{\mathrm{el}}$ $\dot{E}_{\mathrm{P,tot}} = \dot{E}^{\mathrm{M}}_{\mathrm{fA,out}} - \dot{E}^{\mathrm{M}}_{\mathrm{fA,in}} + \dot{E}^{\mathrm{Ch}}_{\mathrm{fA,out}} - \dot{E}^{\mathrm{Ch}}_{\mathrm{fA,in}} + \dot{E}^{\mathrm{T}}_{fA,ont}$ $- \dot{E}^{\mathrm{T}}_{\mathrm{fA,in}}$
		$T_{\mathrm{in}} \leq T_0 \leq T_{\mathrm{out}}$	$\dot{E}_{\mathrm{F,tot}} = P_{\mathrm{el}} + \dot{E}^{\mathrm{T}}_{\mathrm{fA,in}}$ $\dot{E}_{\mathrm{P,tot}} = \dot{E}^{\mathrm{M}}_{\mathrm{fA,out}} - \dot{E}^{\mathrm{M}}_{\mathrm{fA,in}} + \dot{E}^{\mathrm{Ch}}_{\mathrm{fA,out}} - \dot{E}^{\mathrm{Ch}}_{\mathrm{fA,in}} + \dot{E}^{\mathrm{T}}_{\mathrm{fA,out}}$
		$T_{\mathrm{out}} \leq T_0$	$\dot{E}_{\mathrm{F,tot}} = P_{\mathrm{el}} + \dot{E}^{\mathrm{T}}_{\mathrm{fA,in}} - \dot{E}^{\mathrm{T}}_{\mathrm{fA,out}}$ $\dot{E}_{\mathrm{P,tot}} = \dot{E}^{\mathrm{M}}_{\mathrm{fA,out}} - \dot{E}^{\mathrm{M}}_{\mathrm{fA,in}} + \dot{E}^{\mathrm{Ch}}_{\mathrm{fA,out}} - \dot{E}^{\mathrm{Ch}}_{\mathrm{fA,in}}$
	$\Delta\dot{E}^{\mathrm{Ch}} > 0$	$T_{\mathrm{in}} \geq T_0$	$\dot{E}_{\mathrm{F,tot}} = P_{\mathrm{el}} + \dot{E}^{\mathrm{Ch}}_{\mathrm{fA,in}} - \dot{E}^{\mathrm{Ch}}_{\mathrm{fA,out}}$ $\dot{E}_{\mathrm{P,tot}} = \dot{E}^{\mathrm{M}}_{\mathrm{fA,out}} - \dot{E}^{\mathrm{M}}_{\mathrm{fA,in}} + \dot{E}^{\mathrm{T}}_{\mathrm{fA,out}} - \dot{E}^{\mathrm{T}}_{\mathrm{fA,in}}$
		$T_{\mathrm{in}} \leq T_0 \leq T_{\mathrm{out}}$	$\dot{E}_{\mathrm{F,tot}} = P_{\mathrm{el}} + \dot{E}^{\mathrm{T}}_{\mathrm{fA,in}} + \dot{E}^{\mathrm{Ch}}_{\mathrm{fA,in}} - \dot{E}^{\mathrm{Ch}}_{\mathrm{fA,out}}$ $\dot{E}_{\mathrm{P,tot}} = \dot{E}^{\mathrm{M}}_{\mathrm{fA,out}} - \dot{E}^{\mathrm{M}}_{\mathrm{fA,in}} + \dot{E}^{\mathrm{T}}_{\mathrm{fA,out}}$
		$T_{\mathrm{out}} \leq T_0$	$\dot{E}_{\mathrm{F,tot}} = P_{\mathrm{el}} + \dot{E}^{\mathrm{Ch}}_{\mathrm{fA,in}} - \dot{E}^{\mathrm{Ch}}_{\mathrm{fA,out}} + \dot{E}^{\mathrm{T}}_{\mathrm{fA,in}} - \dot{E}^{\mathrm{T}}_{\mathrm{fA,out}}$ $\dot{E}_{\mathrm{P,tot}} = \dot{E}^{\mathrm{M}}_{\mathrm{fA,out}} - \dot{E}^{\mathrm{M}}_{\mathrm{fA,in}}$

The overall exergy balance of the eVCP can then be written in the following way:

$$\dot{E}_{\text{F,tot}} = \dot{E}_{\text{P,tot}} + \sum_k \dot{E}_{\text{D},k} + \underbrace{\left(\dot{E}_{\text{ram,out}} - \dot{E}_{\text{ram,in}}\right)}_{\dot{E}_{\text{L,tot}}} \tag{4.26}$$

with $\dot{E}_{\text{F,tot}}$ and $\dot{E}_{\text{P,tot}}$ taken from Table 4.7. Based on these equations, the dimensionless factors ϵ_k, ϵ_{tot}, $y_{\text{D},k}$ and $y^*_{\text{D},k}$ according to Equations 4.5-4.7 can be calculated.

The developed equations of this section now provide a comprehensive tool set to perform a conventional exergy-based analysis of a conventional bleed air driven pack and an electric driven vapor cycle pack.

4.2 Exergoaeronautic Analysis

With the conventional exergy-based methods presented in the previous section, it is possible to identify the thermodynamic inefficiencies within an aircraft air conditioning pack. On system level, the exergy balance contains the fuel exergy rate supplied to the system, exergy that is destroyed within the system due to thermodynamic inefficiencies of the components, exergy losses that leave the system without being used and the exergetic product that represents the system's aim. With the help of the dimensionless factors of Equations 4.5-4.7, the results of the system balance can further be split up and discover the components' share of the thermodynamic inefficiencies on system level. However, the conventional exergy-based method gives only information about the thermodynamic behavior and is limited to the system boundaries, as defined in Figures 4.4 and 4.5.

In modern aircraft design, the main design drivers are the minimization of fuel consumption and inefficiencies. The so-called "traditional" design parameters include weight, fuel consumption and drag. Basic calculations such as trade-off analyses rule most optimization studies. They rely on rules-of-thumb, individual experience and non-integrated, non-interdisciplinary approaches [14, 15]. Cost-benefit studies among various options are performed on different basis and thus may lead to sub-optimal solutions [14].

Many authors demand a common basis for the comparison of different architectures in aircraft design [53, 36, 93, 94, 95, 96]. Moorhouse [36] explains the possibility of defining aircraft design parameters as energy functions. These traditional fuel penalty factors [38] link the energy demanding disciplines of an aircraft ECS, i.e. bleed air mass flow, weight, drag and power consumption, with additional fuel consumption on system level. The optimization problem can now be characterized by minimizing additional weight and losses constrained by energy requirements of the customer, such as weight to be transported [14]. In 1997, Tipton et al. [17] already compared first and second law analysis methods for the analysis and evaluation of aircraft ECS. They concluded that there is a strong need to define direct correlations between fuel penalties due to the ECS and second law methods (in this case entropy generation). Some years later, Figliola et al. [53] came to similar conclusions after they applied first law methods and exergy-based appraoch to an advanced ECS in order to minimize gross take-off weight (GTW). Endeavors on the formulation of coupling functions for ECS with gross take-off weight or specific fuel consumption, were made around 2000 by Muñoz et al. [54, 55, 56]. The equations used in this thesis for describing the aircraft fuel weight penalties due to air conditioning, follow the manual of the SAE AIR1168/8 [38].

Gandolfi et al. [57] introduced an index that relates the exergy of aircraft fuel that is consumed by the ECS and the total exergy of fuel burnt in the engine. The specific exergy consumption gives information about the impact in overall aircraft performance. The same authors applied this approach to a complete flight mission analysis [58] and more-electric-aircraft analysis [59]. The consideration of the exergetic performance of the air conditioning unit confines to the entering and exiting streams, such as ram air flow, bleed air flow and supplied power. A more detailed analysis on component level using the latter approach is to the author's knowledge not reported in literature.

This section provides a methodology to close the gap between the isolated analysis of the ECS and its evaluation on the aircraft level. A formulation is presented that expresses the fuel weight penalty parameters in terms of exergy rates of fuel consumption. An integration of these exergy rates into the previously defined system balances of fuel and product exergy is further suggested. All presented developments are performed with regard to the integration into the model-based design process of aircraft ECS.

4.2.1 Aircraft Fuel Weight Penalties

Modern aircraft design parameters always rely on fuel consumption and gross take-off weight. The impact on aircraft performance caused by the installation of an air conditioning unit can be split into four categories:

- weight,
- bleed air off-take from the engine,
- aerodynamic drag induced by the ram air,
- shaft power off-take from the engine.

All four categories impact the aircraft performance in different ways different magnitudes. Nevertheless, all of them result in fuel consumption. The increase in fuel consumption consists of two parts. The additional fuel actually consumed and the fuel that has to be carried until the point it is expended. The SAE aerospace information report AIR1168/8 [38] provides a manual with coupling functions to calculate the penalty on aircraft level induced by the listed points. The following sections introduce the fuel weight penalties and present a way to transform them into exergy rates of fuel consumption.

4.2.1.1 Exergy of Fuel Consumption Related to Weight

Due to the laws of physics, energy must be spent to lift weight. The additional weight of the ECS results in a higher fuel consumption to carry this weight. Two types of weight are distinguished. The fixed weight of a system or material that is carried during the whole flight and does not change. The weight of the fuel that is needed to carry the fixed weight until it is expended is called dead weight. Expendable materials that are used during flight are considered as variable weight penalty. This penalty is neglected within this work as the considered systems do not contain expendable materials.

According to [38], the fixed weight penalty is calculated with:

$$\frac{W_{\mathrm{f}_0} + W_{\mathrm{F}}}{W_{\mathrm{F}}} = exp\left(\frac{(SFC)_{\mathrm{th}} \cdot \tau}{L/D}\right) \tag{4.27}$$

It consists of the system fixed weight W_{F} and the additional fuel weight W_{f_0} required to carry the system. $(SFC)_{\mathrm{th}}$ denotes the thrust specific fuel consumption, τ the mission time and L/D the lift-to-drag ratio. The thrust specific fuel consumption and lift-to-drag ratio are engine as well as aircraft specific data and vary for each flight phase. The appropriate equations and data can be found in the appendix.

The general idea of coupling the exergy of fuel consumption with the system weight is to introduce a specific exergy parameter per weight of the system. The exergy of fuel consumption related to system weight can then be calculated in the following way:

$$E_{\mathrm{FC}}^{\mathrm{W}} = e_{\mathrm{FC}}^{\mathrm{W}} \cdot W \tag{4.28}$$

with W being the weight of the system and $e_{\mathrm{FC}}^{\mathrm{W}}$ constitutes the specific exergy per kg of weight. The specific exergy factor $e_{\mathrm{FC}}^{\mathrm{W}}$ is described by the relation:

$$e_{\mathrm{FC}}^{\mathrm{W}} = \frac{\text{exergy of fuel required}}{\text{system weight}} = \frac{e_{\mathrm{f}} \cdot W_{\mathrm{f}_0}}{W_{\mathrm{F}}} = e_{\mathrm{f}} \cdot \frac{W_{\mathrm{f}_0}}{W_{\mathrm{F}}} \tag{4.29}$$

with e_f being the specific exergy of fuel (i.e. jet fuel), W_{f_0} weight of the additional fuel needed for the system weight and W_{F} the fixed weight of the system. Here, the link to the penalty factor is made. The fixed fuel weight penalty of Equation 4.27 can be transformed into

$$\frac{W_{\mathrm{f}_0}}{W_{\mathrm{F}}} = exp\left(\frac{(SFC)_{\mathrm{th}} \cdot \tau}{L/D}\right) - 1 \tag{4.30}$$

and thus integrated into Equation 4.29. $E_{\mathrm{FC}}^{\mathrm{W}}$ constitutes the total exergy of fuel consumption required to carry the system weight. The time dependent exergy flow rate of fuel consumption due to fixed weight can then be determined by:

$$\dot{E}_{\mathrm{FC}}^{W} = \frac{E_{\mathrm{FC}}^{\mathrm{W}}}{\tau} \tag{4.31}$$

with τ being the mission time within which $E_{\mathrm{FC}}^{\mathrm{W}}$ is consumed.

4.2.1.2 Exergy of Fuel Consumption Related to Shaft Power Off-Take

The engine is the only significant power source aboard the aircraft. Here the chemical energy stored in the fuel is transformed into different kinds of power. Besides thrust, bleed air and hydraulic power, generators are mounted on the shaft to produce electricity. Power that is extracted from the engine shaft results in a power loss for the net thrust. This loss is compensated by an increased fuel flow rate to the engine. The increased fuel consumption leads to a take-off fuel weight penalty. Assuming a constant power consumption during a mission phase, the fuel weight penalty according to [38] is expressed as:

$$\frac{W_{f_0}}{P \cdot (SFC)_{P}} = \frac{L/D}{(SFC)_{th}} \cdot \left[exp\left(\frac{(SFC)_{th} \cdot \tau}{L/D} \right) - 1 \right] \tag{4.32}$$

with W_{f_0} being the weight of additional fuel needed for the shaft power off-take P. $(SFC)_{th}$ is the thrust specific fuel consumption, SCF_{P} the power specific fuel consumption, and τ the mission time. Both, the thrust and power specific fuel consumption are engine specific data and can be obtained from aircraft specific datasets available in the appendix.

The general idea of coupling the exergy of fuel consumption with the shaft power off-take is to introduce a specific exergy parameter per power off-take of the system. The exergy of fuel consumption related to power off-take can then be calculated in the following way:

$$E_{FC}^{P} = e_{FC}^{P} \cdot P \tag{4.33}$$

with P being the shaft power off-take extracted from the engine. e_{FC}^{P} constitutes the specific exergy per power off-take:

$$e_{FC}^{P} = \frac{\text{exergy of fuel required}}{\text{shaft power off-take}} = \frac{e_{f} \cdot W_{f_0}}{P} = e_{f} \cdot \frac{W_{f_0}}{P} \tag{4.34}$$

with e_{f} being the specific exergy of fuel (i.e. jet fuel). Here, the link to the penalty factor is made. The fuel weight penalty of Equation 4.32 can be transformed into:

$$\frac{W_{f_0}}{P} = \frac{L/D \cdot (SFC)_{P}}{(SFC)_{th}} \cdot \left[exp\left(\frac{(SFC)_{th} \cdot \tau}{L/D} \right) - 1 \right] \tag{4.35}$$

and thus integrated into Equation 4.34. E_{FC}^{P} constitutes the total exergy of fuel consumption required to compensate the consumed power P. The time-dependent exergy flow rate of fuel consumption due to shaft power off-take can then be determined by:

$$\dot{E}_{FC}^{P} = \frac{E_{FC}^{P}}{\tau} \tag{4.36}$$

with τ being the mission time within which E_{FC}^{P} is consumed.

4.2.1.3 Exergy of Fuel Consumption Related to Ram Air

The waste and cooling heat of the air conditioning unit needs to be discharged. Outside air enters the ram air channel through inlet located at the fuselage and passes the heat exchanger(s) of the ECS pack. The ram air works as the heat sink of the ECS.

The exergy of fuel consumption related to ram air use can be calculated the following way. During ground operations, the ram air mass flow is enforced by a powered fan. In flight the airspeed provides the mass flow. The kinetic energy of the air speed is used to overcome the momentum losses caused by the flow resistances within the ram air channel. The momentum loss causes an additional aerodynamic drag that has to be compensated by an additional fuel consumption. According to [38], the ram air penalty in terms of take-off fuel weight is expressed by:

$$\frac{W_{\mathrm{f_0}}}{\dot{m}_{\mathrm{R}} \cdot v} = \frac{L/D}{g} \cdot \left[exp \left(\frac{(SFC)_{\mathrm{th}} \cdot \tau}{L/D} \right) - 1 \right] \tag{4.37}$$

with $W_{\mathrm{f_0}}$ being the weight of additional fuel caused by the ram air mass flow $\dot{m}_{\mathrm{R}}$ as well as the airspeed v. $(SFC)_{\mathrm{th}}$ is the thrust specific fuel consumption, L/D the lift-to-drag ratio, τ the mission time, and g the gravitational acceleration. The thrust specific fuel consumption and lift-to-drag ratio are engine as well as aircraft specific data and vary for each flight phase. The appropriate equations and data can be found in the appendix. The approach of coupling the exergy of fuel consumption with the ram air is to introduce a specific exergy parameter per drag caused by the ram air mass flow. The exergy of fuel consumption related to ram air mass flow can then be calculated in the following way:

$$E_{\mathrm{FC}}^{D} = e_{\mathrm{FC}}^{\mathrm{D}} \cdot D \tag{4.38}$$

with D being the additional drag caused by ram air. $e_{\mathrm{FC}}^{\mathrm{D}}$ constitutes the specific exergy per drag:

$$e_{\mathrm{FC}}^{\mathrm{D}} = \frac{\text{exergy of fuel required}}{\text{drag caused by ram air}} = \frac{e_{\mathrm{f}} \cdot W_{\mathrm{f_0}}}{D} = e_{\mathrm{f}} \cdot \frac{W_{\mathrm{f_0}}}{\dot{m}_{\mathrm{R}} \cdot v} \tag{4.39}$$

where e_{f} constitutes the exergy of jet fuel and $\frac{W_{\mathrm{f_0}}}{\dot{m}_{\mathrm{R}} \cdot v}$ the ram air penalty given in Equation 4.37. E_{FC}^{D} is the total exergy of fuel consumption required to overcome the aerodynamic drag caused by the ram air mass flow. The time-dependent exergy flow rate of fuel consumption due to ram air mass flow can then be determined by:

$$\dot{E}_{\mathrm{FC}}^{D} = \frac{E_{\mathrm{FC}}^{\mathrm{D}}}{\tau} \tag{4.40}$$

with τ being the mission time within which $E_{\mathrm{FC}}^{\mathrm{D}}$ is consumed.

4.2.1.4 Exergy of Fuel Consumption Related to Bleed Air

Bleed air is extracted at the compressor stage of the turbojet engine. Power has already been spent to compress the air. Thus, the bleed air off-take results in a power extraction from the engine. Similar to the shaft power off-take, this loss has to be compensated to avoid power loss in net thrust. Additional fuel flow rate is needed to fill this gap. The increased fuel consumption leads to a take-off weight penalty. According to [38], the bleed air penalty in terms of take-off fuel weight can be calculated in the following way:

$$\frac{W_{f_0}}{\dot{m}_B} = 0.0335 \cdot \frac{L/D}{g \cdot (SFC)_{th}} \cdot \frac{T_{tb}}{2000} \cdot \left[exp \left(\frac{(SFC)_{th} \cdot \tau}{L/D} \right) - 1 \right] \tag{4.41}$$

with W_{f_0} being the weight of the additional fuel needed for the extraction of bleed air mass flow $\dot{m}_B$ from the engine. $(SFC)_{th}$ is the thrust specific fuel consumption and L/D the lift-to-drag ratio. The gravitational acceleration g is not present in the original equation of [38], but was subsequently added to comply with the correct units. T_{tb} is the turbine inlet temperature of the engine. The thrust specific fuel consumption, lift-to-drag ratio and turbine inlet temperature are engine and aircraft specific data and can be obtained from aircraft specific datasets and depend on the flight phase. The appropriate equations and data are listed in the Appendix B.

Following the approach of the previous described fuel weight penalties, a specific exergy parameter per bleed air mass flow is introduced. The exergy of fuel consumption related to ram air mass flow can then be described as:

$$E^B_{FC} = e^B_{FC} \cdot \dot{m}_B \tag{4.42}$$

with $\dot{m}_B$ being the bleed air mass flow extracted from the engine. e^B_{FC} constitutes the specific exergy per mass flow of bleed air:

$$e^B_{FC} = \frac{\text{exergy of fuel required}}{\text{bleed air mass flow}} = \frac{e_f \cdot W_{f_0}}{\dot{m}_B} = e_f \cdot \frac{W_{f_0}}{\dot{m}_B} \tag{4.43}$$

where e_f represents the specific exergy of jet fuel and $\frac{W_{f_0}}{\dot{m}_B}$ the bleed air penalty given in Equation 4.41. E^B_{FC} is the total exergy of fuel consumption required to compensate the extracted bleed air mass flow from the compressor stage of the turbojet engine. It is transformed into an exergy rate of fuel consumption due to bleed air mass flow by:

$$\dot{E}^B_{FC} = \frac{E^B_{FC}}{\tau} \tag{4.44}$$

with τ being the mission time within which E^B_{FC} is consumed.

4.2.2 Exergy of (Jet) Fuel

The only significant energy source aboard modern civil aircraft is fuel. The turbojet engine converts the chemical energy stored in the fuel into thrust, pneumatic power (bleed air for ECS, anti-ice, etc.), hydraulic power (e.g. hydraulic pumps) and electric power (e.g. avionics, in-flight entertainment, etc.). The previous sections introduced a method to combine aircraft fuel weight penalty induced by the environmental control system with exergy of the fuel consumed to compensate the different penalties. The exergetic value considered by this approach is the chemical exergy stored in the jet fuel.

In aviation, fuels can be classified in three main categories. Aviation gasoline (AvGas), turbine fuels and air-breathing missile fuels. AvGas is used for reciprocating or piston engines. Most piston engine aircraft can be found in the general aviation sector. Missile fuels are further distinguished into ramjet and turbine missile fuels. Turbine fuels are categorized in commercial and military fuels. The U.S. military holds several types of turbine fuels for different operational needs of service or specific applications. Some examples are: JP-4, JP-5, JP-7 and JP-8. Both, the military fuels and aviation gasoline are mentioned for the sake of completeness, but are not of further interest as this thesis focuses on civil aircraft. [97]

All aviation fuels are characterized and controlled by specifications. They are based less upon the detailed chemistry of the fuels, but more upon usage requirements.There is only one composition requirement for all aircraft fuels. They shall consist completely of hydrocarbon compounds except for specific additives. Limits on particular hydrocarbons are primarily driven by performance factors. Requirements for the fuels include items such as fluidity, combustion properties, corrosion protection, fuel stability, and some more. The specifications are listed in detail in [97]. Turbine fuels consist of many hydrocarbons, although there are only four types of main compounds. They can be grouped into paraffins, cycloparaffins or naphthenes, aromatics and olefins. For the definition of the chemical exergy of the fuel, their physical properties are important.

According to the specifications, jet fuel is a mixture of pure hydrocarbons. These hydrocarbons are not present in the environment with their composition. Following Bejan et al. [16], the standard chemical exergy of a substance not present in the environment can be calculated by using an idealized reaction of the substance with its reaction compounds for which the chemical exergy is known. Hydrocarbons react in an idealized reaction with oxygen to form carbon dioxide and liquid water. The stoichiometric equation for the combustion process of a hydrocarbon C_aH_b with air is [87]:

$$C_aH_b + \left(a + \frac{b}{4}\right)(O_2 + 3.76N_2) \rightarrow aCO_2 + \frac{b}{2}H_2O + \left(a + \frac{b}{4}\right)3.76N_2 \tag{4.45}$$

Assuming that all substances enter and exit unmixed the combustion at T_0 and p_0, the chemical exergy can be calculated as:

$$\bar{e}_{\mathrm{F}}^{\mathrm{Ch}} = \left(\frac{\dot{W}_{\mathrm{cv}}}{\dot{n}_{\mathrm{F}}}\right)_{\mathrm{int\ rev}} + a\bar{e}_{\mathrm{CO_2}}^{\mathrm{Ch}} + \frac{b}{2}\bar{e}_{\mathrm{H_2O}}^{\mathrm{Ch}} - \left(a + \frac{b}{4}\right)\bar{e}_{\mathrm{O_2}}^{\mathrm{Ch}} \tag{4.46}$$

The nitrogen parts does not have any impact on the chemical exergy as it exists on both sides of the reaction equation at the same concentration. $\left(\frac{\dot{W}_{\mathrm{cv}}}{\dot{n}_{\mathrm{F}}}\right)_{int\ rev}$ is the maximum value of work developed per mole of fuel assuming an ideal process:

$$\begin{aligned}\left(\frac{\dot{W}_{\mathrm{cv}}}{\dot{n}_{\mathrm{F}}}\right)_{\mathrm{int\ rev}} &= \left\{\left[\bar{h}_{\mathrm{F}} + \left(a + \frac{b}{4}\right)\bar{h}_{\mathrm{O_2}} - a\bar{h}_{\mathrm{CO_2}} - \frac{b}{2}\bar{h}_{\mathrm{H_2O}}\right]_{(T,p)}\right\} \\ &\quad -T\left[\bar{s}_{\mathrm{F}} + \left(a + \frac{b}{4}\right)\bar{s}_{\mathrm{O_2}} - a\bar{s}_{\mathrm{CO_2}} - \frac{b}{2}\bar{s}_{\mathrm{H_2O}}\right]_{(T,p)}\end{aligned} \tag{4.47}$$

According to [16], the first part of Equation 4.47 in curly brackets is recognized as $-h_{RP}$ and represents the specific enthalpy per unit of mole of the reaction product [87]. On condition that $T = 298.15K$ and $p = 1.013bar$, $-h_{RP}$ corresponds to the standard heating value. Within this work it is assumed that the water exits the combustion process as vapor. Hence, the standard heating value complies with the lower heating value ($\overline{LHV}$). The higher heating value ($\overline{HHV}$) assumes liquid water exiting the combustion. Equation 4.47 integrated into Equation 4.46 leads to:

$$\begin{aligned}\bar{e}_{\mathrm{F}}^{\mathrm{Ch}} &= \overline{LHV}_{(T_0,p_0)} - T_0\left[\bar{s}_{\mathrm{F}} + \left(a + \frac{b}{4}\right)\bar{s}_{\mathrm{O_2}} - a\bar{s}_{\mathrm{CO_2}} - \frac{b}{2}\bar{s}_{\mathrm{H_2O(g)}}\right]_{(T_0,p_0)} \\ &\quad + \left\{a\bar{e}_{\mathrm{CO_2}}^{\mathrm{Ch}} + \frac{b}{2}\bar{e}_{\mathrm{H_20}O(\mathrm{g})}^{\mathrm{Ch}} - \left(a + \frac{b}{4}\right)\bar{e}_{\mathrm{O_2}}^{\mathrm{Ch}}\right\}_{(T_0,p_0)}\end{aligned} \tag{4.48}$$

The standard molar chemical exergies $\bar{e}^{\mathrm{Ch}}$ for various substances can be found in [91, 98] at $T_0 = 298\,K$ and $p_0 = 1.019\,bar$, and in [92] at $T_0 = 298\,K$ and $p_0 = 1.0\,bar$.
A simple correlation between the higher heating value and chemical exergy is suggested by [87] as the HHV is the main contributor to the chemical exergy in case of fossil fuel. Applied to the jet fuel, the molar chemical exergy of jet fuel can be estimated with:

$$\frac{\bar{e}_{\mathrm{F}}^{\mathrm{Ch}}}{\overline{LHV}} \approx 0.98 - 1.00 \quad \text{for liquid fuels} \tag{4.49}$$

The Handbook of Aviation Fuel Properties [97] provides an overview of typical net heat combustion ranges for various aviation fuels. The range for Jet-A and Jet-A1 can be gathered from Figure 4.6. The lower heating values cover the range of $42.8 - 43.4\,\mathrm{MJ/kg}$.

Similar values for Jet-A are presented by other authors:

- $18.580\,\mathrm{BTU/lb} = 43.2171\,\mathrm{MJ/kg}$ [99],
- $6.55\,\mathrm{MJ/mol} = 43.323\mathrm{MJ/kg} \quad \left(\overline{M} = 151.19\,\mathrm{kg/kmol}\right)$ [100],

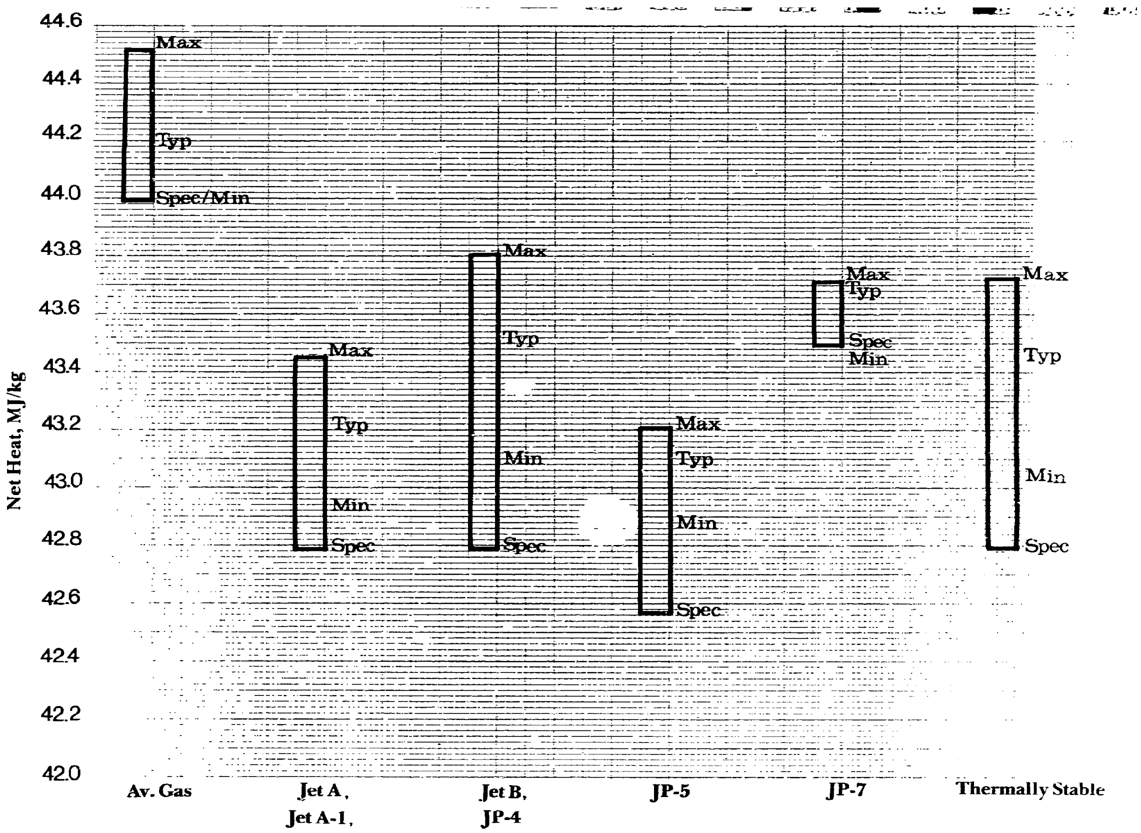

Figure 4.6: Net heat of combustion for typical aircraft fuels. [97]

- 6.76 MJ/mol = 43.0958 MJ/kg $\left(\overline{M} = 156.86\,\mathrm{kg/kmol}\right)$ [100].

Using Equation 4.49, the chemical exergy for fuel equals the lower heating or net heat of combustion.

Equations 4.48 and thus 4.49 rely on the assumption that all substances enter and exit the system unmixed at T_0 and p_0 and heat transfer occurs only at temperature T_0 [16]. One major contribution of this work is the detailed discussion of the reference environment within the application of aircraft ECSs. In Section 4.1.3 much effort has been put into the formulation of the chemical exergy of the moist air mixture considering the reference environment. The coupling of the conventional exergy analysis with the fuel weight penalties would not follow the proposed comprehensive approach if the chemical exergy of the jet fuel neglects the impact of the reference environment. The following paragraphs will now present a methodology how the reference environment is integrated to the calculation of the fuel chemical exergy.

Etele and Rosen [68] studied the effects of using different reference environmental models for the exergy analysis of a turbojet engine. They considered varying flight altitudes from sea level to 15000 m. For their study they used the approach of Clarke and Horlock [101] to determine the specific fuel exergy of methane (CH_4) which they assumed as aviation fuel. Clarke and Horlock presented a way to evaluate the steady-flow essergy ('exergy of extraction and delivery' [102]), i.e. in today's nomenclature [61] flow exergy, in an arbitrary state. With the knowledge of the hydrocarbon composition, the atmospheric composition, relative* enthalpies and entropies of each constituent of the fuel and atmosphere, and the standard† enthalpies and entropies, the specific flow exergy can be calculated with the following equation:

$$
\begin{aligned}
e_{\mathrm{F}}^{\mathrm{Ch}} = & \left[\sum_i \left(\beta_i h_{is} - \gamma_i h_{is}\right) + \sum_i \left(\beta_i \Delta h_{i1} - \gamma_i \Delta h_{i\infty}\right)\right] \\
& - T_\infty \left[\sum_i \left(\beta_i s_{is} - \gamma_i s_{is}\right) + \sum_i \left(\beta_i \Delta s_{i1} - \gamma_i \Delta s_{i\infty}\right)\right] \\
& + \left[\sum_i \beta_i \frac{C_{i1}^2}{2}\right]
\end{aligned}
\tag{4.50}
$$

with subscript is standing for the data of constituent i at standard state s, $i1$ the data at state 1 which is assumed to be inflow state of the fuel, and $i\infty$ constituent i at atmospheric conditions ∞. Standard state is at $T_{\mathrm{s}} = 298\,K$ and $p_{\mathrm{s}} = 1.013\,bar$. The data for standard enthalpies h_{is} and standard entropies s_{is} is taken from thermodynamic data tables. Clarke and Horlock suggest [103, 104] for standard enthalpies and [105] for standard entropies. A huge dataset for the calculation of standard specific heat, standard enthalpy and standard entropy based on empirical equations is provided in [106].

For the calculation of the relative enthalpies and entropies it is assumed that all constituents are perfect gases [101]:

$$\Delta h_{i1} = c_{pi}\left(T_{i1} - T_{\mathrm{s}}\right) \tag{4.51}$$

$$\Delta s_{i1} = c_{pi}\, ln \left\{\frac{T_{i1}}{T_{\mathrm{s}}}\right\} - R_i \left\{\frac{p_{i1}}{p_{\mathrm{s}}}\right\} \tag{4.52}$$

$$\Delta h_{i\infty} = c_{pi}\ \left(T_{i\infty} - T_{\mathrm{s}}\right) \tag{4.53}$$

and

$$\Delta s_{i\infty} = c_{pi}\, ln \left\{\frac{T_{i\infty}}{T_{\mathrm{s}}}\right\} - R_i \left\{\frac{p_{i\infty}}{p_{\mathrm{s}}}\right\} \tag{4.54}$$

c_{pi} is the specific heat of constituent i and $R_i = 8314.34\,\mathrm{J}/\,(\mathrm{kmol\,K})$ [107] the universal gas constant. The equation of reaction of the combustion is considered in Equation 4.50 by β_i and γ_i. β_i is the proportion by mass of constituent i in fuel and γ_i is the sum of $\beta_i + \delta_i$

*The difference Δh, between the enthalpy at the specific state and that at a standard state for the same constituent is defined as the relative enthalpy. The relative entropy Δs, is defined similarly. [101]

†The proper value of the different enthalpy levels of the different constituents at the same temperature and pressure constitutes the standard enthalpy h_{s}. The standard entropy s_{s} is similarly defined and its existence stems from the interpretation of entropy as a quantity having an absolute value. [101]

Table 4.9: Reaction coefficients of the hydrocarbon combustion reaction equation.

	β_i	δ_i	γ_i
N_2	0.0	0.0	0.0
O_2	0.0	$-\left(a+\frac{b}{4}\right)\frac{M_{O_2}}{M_{C_aH_b}}$	$-\left(a+\frac{b}{4}\right)\frac{M_{O_2}}{M_{C_aH_b}}$
CO_2	0.0	$a\,\frac{M_{CO_2}}{M_{C_aH_b}}$	$a\,\frac{M_{CO_2}}{M_{C_aH_b}}$
H_2O	0.0	$\frac{b}{2}\,\frac{M_{H_2O}}{M_{C_aH_b}}$	$\frac{b}{2}\,\frac{M_{H_2O}}{M_{C_aH_b}}$
C_aH_b	1.0	-1.0	0.0

where δ_i constitutes the change in mass of constituent per unit fuel burned, i.e.:

$$\delta_i = \frac{\Delta M_i}{M_{C_aH_b}} \tag{4.55}$$

with M_i and $M_{C_aH_b}$ being the molar mass of constituent i and the hydrocarbon of fuel. With Equation 4.45 the coefficients β, δ and γ can be determined. The constituents of moist air are listed in Table 4.2.

Aviation fuel for turbines, in particular Jet-A, are mixtures of many hydrocarbons [97]. In order to determine the specific exergy of the fuel with Equation 4.50 without putting huge effort in calculating the specific exergy for each constituent of the mixture, a surrogate composition is needed. In [108], a version of ASTM D2425 is used to characterize a number of jet fuels from a world fuel survey. The provided data can be taken for combustion and physical property modelling as well as for the development of surrogates for kerosene fuel. In [100], two formulae for Jet-A fuel from surrogate models are presented: $C_{10.8}H_{20.9}$ and $C_{11.3}H_{21.1}$. These are very similar to [99] who suggests using $C_{11}H_{21}$. A little divergent formula is used by [109] who assumed $C_{12}H_{23}$ to represent Jet-A. The latter one used the thermodynamic data of [110] to derive the necessary coefficients to include Jet-A in the thermodynamic data library of the NASA Lewis Chemical Equilibrium Program [111, 106]. Having these coefficients and equations available, the standard enthalpies, standard entropies and standard specific heats can be calculated and Equation 4.50 finally applied for Jet-A fuel $C_{12}H_{23}$.

Figure 4.7 shows the sensitivity of the specific fuel exergy for Jet-A for varying environments. It was calculated for altitudes up to 15000 m. The change with increasing altitude is small. At 15000 m there is a deviation of 1.83% compared to sea level. The trend line calculated with Equation 4.50 fits the data from literature of Figure 4.6. The surrogate model of $C_{12}H_{23}$ can be seen as validated for the application within this thesis and will be used for all further calculations of the fuel exergy of Jet-A.

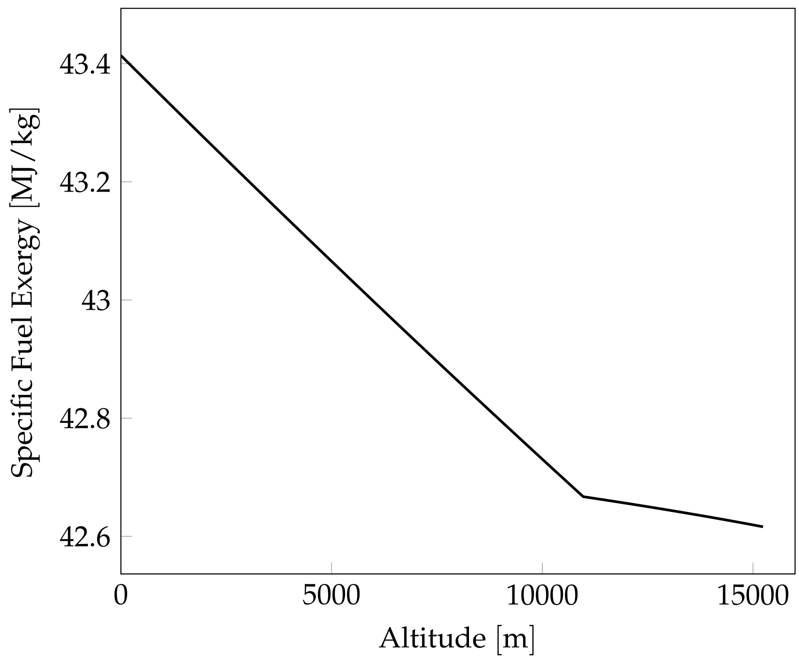

Figure 4.7: Sensitivity of the specific fuel exergy for Jet-A ($C_{12}H_{23}$) for varying altitudes.

4.2.3 System Balances

The previous two sections presented the necessary equations for the description of exergy of fuel consumption due to fuel weight penalties. The total exergy of fuel consumption can be expressed with the following term:

$$\dot{E}_{\mathrm{FC}} = \dot{E}^{\mathrm{W}}_{\mathrm{FC}} + \dot{E}^{\mathrm{P}}_{\mathrm{FC}} + \dot{E}^{\mathrm{D}}_{\mathrm{FC}} + \dot{E}^{\mathrm{B}}_{\mathrm{FC}} \tag{4.56}$$

All terms represent the appropriate exergy rate of jet fuel consumed. Depending on the type of environmental control system, some terms on the right side disappear. In the case of the conventional bleed air pack (Section 3.2), neither electrical nor mechanical power is supplied to the system. Therefore, the fuel penalty due to shaft power off-take $\dot{E}^{\mathrm{P}}_{\mathrm{FC}}$ ceases and Equation 4.56 reduces to:

$$\dot{E}_{\mathrm{FC}} = \dot{E}^{\mathrm{W}}_{\mathrm{FC}} + \dot{E}^{\mathrm{D}}_{\mathrm{FC}} + \dot{E}^{\mathrm{B}}_{\mathrm{FC}} \tag{4.57}$$

Instead of using bleed air, the electric driven vapor cycle pack (Section 3.3) obtains the fresh air directly from the environment through air inlets. The conditioning of the fresh air is performed with the help of externally supplied electrical power. The total exergy of fuel consumption is described without the bleed air penalty part $\dot{E}^{\mathrm{B}}_{\mathrm{FC}}$ and Equation 4.56 reduces to:

$$\dot{E}_{\mathrm{FC}} = \dot{E}^{\mathrm{W}}_{\mathrm{FC}} + \dot{E}^{\mathrm{P}}_{\mathrm{FC}} + \dot{E}^{\mathrm{D}}_{\mathrm{FC}} \tag{4.58}$$

The fuel weight penalty for drag $\dot{E}_{\mathrm{FC}}^{\mathrm{D}}$ increases for the eVCP architecture as the fresh air enters the pack through an air inlet similar to the ram air channel.

4.3 Advanced Exergy Analysis

The advanced exergy analysis proposes a further splitting of the exergy destruction for the *k*-th component [74]. The exergy destruction can be split into four parts. Avoidable and unavoidable exergy destruction provide a measurement instrument for the optimization potential of the thermodynamic efficiency of the component. Endogenous and exogenous exergy destruction give information on how the components impact each other within the system.

4.3.1 Methodology

Avoidable and Unavoidable Exergy Destruction

The thermodynamic performance of a component is limited due to technological limitations such as availability and cost of materials, and manufacturing methods. In case of the application for the aircraft industry additional limitations such as weight, volume, noise and reliability must be considered. The exergetic destruction due to these limitations is defined as the unavoidable $\dot{E}_{\mathrm{D}}^{\mathrm{UN}}$ part and cannot be reduced by optimization. The remaining part is called the avoidable exergy destruction $\dot{E}_{\mathrm{D}}^{\mathrm{AV}}$. The splitting in the k-th component $\dot{E}_{\mathrm{D},k} = \dot{E}_{\mathrm{D},k}^{\mathrm{UN}} + \dot{E}_{\mathrm{D},k}^{\mathrm{AV}}$ gives a realistic assessment of the potential for optimization of the thermodynamic efficiency of a component. [74]

Endogenous and Exogenous Exergy Destruction

The endogenous part $\dot{E}_{\mathrm{D},k}^{\mathrm{EN}}$ of the total destroyed exergy in the *k*-th component results from the irreversibilities happening within the component under the assumption that all other components of the system operate in the ideal way and the *k*-th component operates with its current efficiency. The remaining exogenous part $\dot{E}_{\mathrm{D},k}^{\mathrm{EX}}$ can be reduced to the exergy destruction within the component that are caused by irreversibilities of other components of the system. Together they yield the total exergy destruction $\dot{E}_{\mathrm{D},k} = \dot{E}_{\mathrm{D},k}^{\mathrm{EN}} + \dot{E}_{\mathrm{D},k}^{\mathrm{EX}}$ of the *k*-th component. [74]

Combination of the Splitting

The combination of the four parts allows a detailed analysis of the total destroyed exergy within a component. The unavoidable endogenous exergy destruction $\dot{E}_{\mathrm{D},k}^{\mathrm{UN,\,EN}}$ cannot be reduced due to technical limitations of the k-th component. The unavoidable exogenous part $\dot{E}_{\mathrm{D},k}^{\mathrm{UN,\,EX}}$ will remain because of technical limitations related to all the other components of the system structure. The other two parts can be reduced through optimization. The avoidable endogenous ($\dot{E}_{\mathrm{D},k}^{\mathrm{AV,\,EN}}$) part can be reduced by optimizing the thermodynamic efficiency of the *k*-th component. The remaining part, the avoidable exogenous exergy destruction $\dot{E}_{\mathrm{D},k}^{\mathrm{AV,\,EX}}$ can be reduced by improving the efficiency of the other components of the overall system. [74]

4.3.2 Adaption to Aircraft ECS

The analysis using advanced exergy methods needs to cover the varying operation conditions. The evaluation of single operation points would result in insufficient or misleading statements. Within this thesis, the focus for the application of advanced exergy methods is the integration into model-based design and system simulation. Further, the splitting of the exergy destruction into avoidable and unavoidable parts is considered. For the calculation of the unavoidable exergy destruction $\dot{E}_{\mathrm{D},k}^{\mathrm{UN}}$, [71] suggests two approaches.

The first approach introduces unavoidable efficiencies for all components simultaneously [72]. In the frame of system simulations, this is only possible for simple systems. Aircraft ECS are balanced systems designed to operate within a broad range of ambient conditions and deliver fresh air at a defined state. The control laws for the two example packs have been introduced in Figures 3.2 and 3.4. The multitude of operating points can only be achieved to the detriment of the individual component performance. Setting the components efficiencies to unavoidable conditions simultaneously either results in a non-working simulation or the system is not capable of delivering the demanded conditioning. For environmental control systems this procedure is not applicable.

The second approach [112] suggests the separate (in isolation) simulation of each component with unavoidable conditions. The number of simulations increases to the number of regarded components, but the risk for a crash of the simulation and insufficient working system can be reduced significantly. Although the splitting into avoidable and unavoidable parts is a theoretically method, setting only one component to unavoidable conditions gives a more realistic result as the impact of the real-working system is not neglected. On this basis the adaption to aircraft ECS is made.

The unavoidable exergy destruction shall be valid for all operation conditions. The objective is to identify the least possible exergy destruction, assuming that the component operates at conditions that cannot be achieved in the foreseeable future [71]. From this particular operation point, the value $\left(\frac{\dot{E}_{\mathrm{D},k}}{\dot{E}_{\mathrm{P},k}}\right)^{\mathrm{UN}}$ can be obtained. The unavoidable exergy destruction within the $k-$th component can then be calculated by [74]:

$$\dot{E}_{\mathrm{D},k}^{\mathrm{UN}} = \dot{E}_{\mathrm{P},k}^{\mathrm{real}} \left(\frac{\dot{E}_{\mathrm{D},k}}{\dot{E}_{\mathrm{P},k}}\right)^{\mathrm{UN}} \tag{4.59}$$

$\dot{E}_{\mathrm{P},k}^{\mathrm{real}}$ is the product exergy of the $k-$th component at real conditions. The factor $\left(\frac{\dot{E}_{\mathrm{D},k}}{\dot{E}_{\mathrm{P},k}}\right)^{\mathrm{UN}}$ constitutes the ratio of the exergy destruction and product exergy of the $k-$th component at unavoidable conditions. This factor is determined by simulating the air conditioning model for a whole flight mission and setting the efficiency of the $k-$th component to the hypothetical value that is assumed for the unavoidable operation condition. The ratio is evaluated for each time step and the minimum value is then assigned as the

Table 4.10: Thermodynamic effectivenesses and isentropic efficiencies for unavoidable operation conditions.

Component	Eff.	%	Reference
Turbine	η_{is}	98.89	[81]
Compressor	η_{is}	96.0	[81]
PHX	η_{th}	92.0	[113]
MHX	η_{th}	92.0	[113]
Reheater	η_{th}	92.0	[113]
Condenser	η_{th}	83.0	control limitations

unavoidable factor $\left(\frac{\dot{E}_{\mathrm{D},k}}{\dot{E}_{\mathrm{P},k}}\right)^{\mathrm{UN}}$. This factor is regarded as valid for each flight phase at any operation condition. The unavoidable exergy destruction of the $k-$th component can then be calculated for any operation condition of the considered flight phase by applying Equation 4.59.

The splitting of the exergy destruction into avoidable and unavoidable parts is done within this work for the conventional bleed air driven pack (Figure 3.1). The components that are regarded with the splitting are listed in Table 4.10. From an exergetic point of view, the ram air fan operates only during ground conditions as a productive component and turns into a dissipative component during flight condition. Thus, it is not taken into account as well as all other dissipative components.

The regarded components are either heat exchangers or turbo components. Table 4.10 shows the efficiencies assigned with the components and the references the numbers are based on. The one exception for the condenser relates to the behavior of the pack model. A higher efficiency than the one listed results in working conditions that exceed the controllable limits of the system. For the turbine and compressor, the efficiency constitutes the isentropic efficiency, and for the heat exchangers, the thermodynamic efficiency is the ratio of the actual transfered heat and the maximum possible heat.

Figure 4.8 illustrates the procedure of how the unavoidable factor is determined. $\left(\frac{\dot{E}_{\mathrm{D},k}}{\dot{E}_{\mathrm{P},k}}\right)^{\mathrm{UN}}$ is plotted for the turbine among a full flight mission and the minimum is determined. For the case of the turbine, a value of 0.2538 can be calculated. This value can now be used in Equation 4.59 to calculate the splitting of the exergy destruction into avoidable and unavoidable parts.

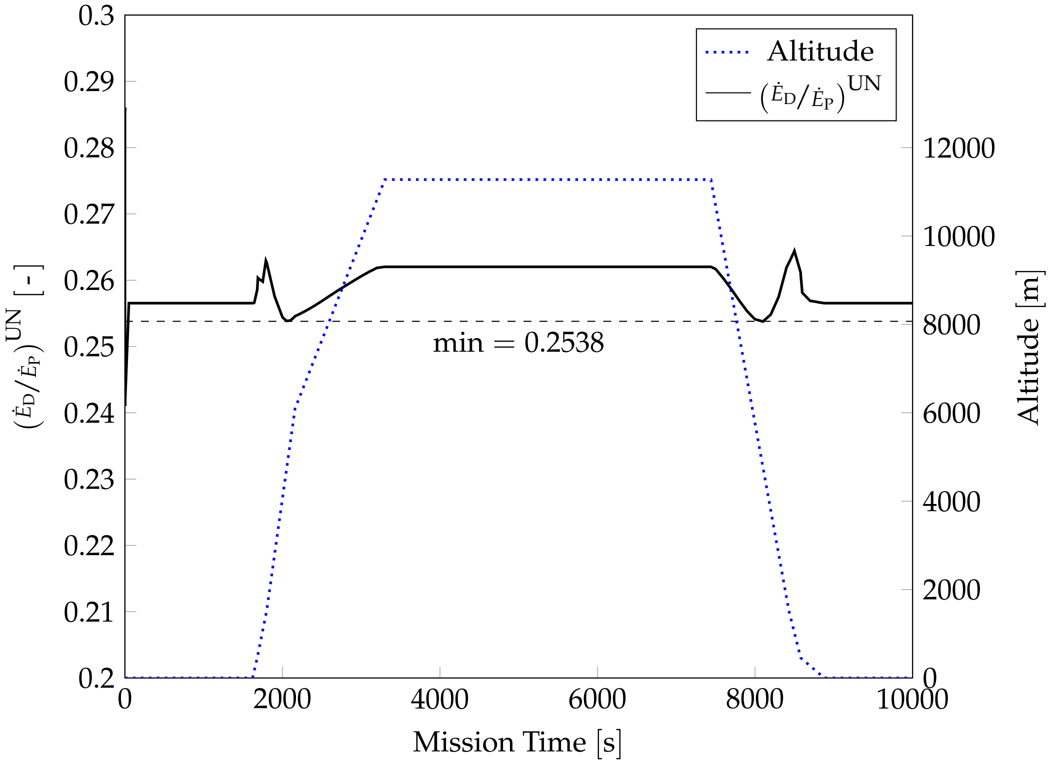

Figure 4.8: Ratio of exergy destruction to product exergy for a full flight simulation with the turbine operating in unavoidable condition.

Chapter 5
Modeling & Simulation

5.1 Modeling Language and Environment

Model-based design methods have become a crucial tool in the development of environmental control systems for aircraft - whether to support trade-off studies during the pre-design phase or for detailed performance simulation of system models. Thanks to sufficient computing power, such simulations can be performed on single workstations. Equation-based object-oriented modeling languages allow the modeling of multi-physics systems without the need to be a computer scientist. Modelica [25] is a free language that has been developed by the Modelica Association since 1996 and is used in industry since 2000. Its goal is to provide the modeling of technical systems and their dynamic behavior in a convenient way. The models are described by differential-algebraic and discrete equations. Models of similar technical fields tend to be organized in libraries. For example equipment such as heat exchangers, compressors, turbines, ducts, etc. can be modeled as single components and stored in a library. Using these component models, a system model can be assembled to simulate its behavior. In this way, different architectures do not have to be modeled from scratch as the single component models can be reused and slight modifications can easily be made with little effort. Many free and commercial libraries based on the Modelica language have been developed for different physical fields and applications [114].

For this thesis, all modeling and simulation work was performed with Modelica and the modeling and simulation environment Dymola [49]. Dymola is a commercial software distributed by Dassault Systèmes®.

Two different pack architectures have been selected to apply the exergy-based methods and evaluate them. Both systems were introduced in Chapter 3. Now, the Modelica libraries that have been used to model the architectures are described. Both libraries are purpose-built model libraries and constitute a toolkit for the design of ECSs. They contain physical models in an acausal formulation. The two libraries aim for the same applications of early design assessment and off-design simulations. Different levels of detail are available for the components, such as fixed efficiencies, performance maps or geometry based performance. The distinction between the two libraries is the concept of how the equations of the fluid network are set up.

The older library, DENECS [2], was developed over a decade ago at the DLR Institute of System Dynamics and Control in cooperation with Airbus Deutschland GmbH. The infrastructure, e.g. connector definitions and boundary conditions, is based on the definition of the Modelica Fluid library [115] which is part of the Modelica Standard Library (MSL) [25] since version 3.1. The fluid connector provides the interface for quasi one-dimensional fluid flows of incompressible or compressible fluids including one or more phases and one or more substances. The following quantities are given at the connector: absolute pressure, mass flow, specific enthalpy, mass fractions of the mixture and potential properties of the substances of the fluid. Listing 5.1 shows the Modelica code of such a fluid port.

Listing 5.1: Modelica code of FluidPort connector from MSL. [25]

```
connector FluidPort
replaceable package Medium = Modelica.Media.Interfaces.PartialMedium
    "Medium model";

flow Medium.MassFlowRate m_flow "Mass flow rate";
Medium.AbsolutePressure p "Thermodynamic pressure";
stream Medium.SpecificEnthalpy h_outflow "Specific thermodynamic
    enthalpy";
stream Medium.MassFraction Xi_outflow[Medium.nXi] "Independent
    mixture mass fractions m_i/m";
stream Medium.ExtraProperty C_outflow[Medium.nC] "Properties c_i/m";
end FluidPort;
```

It is apparent that the quantities have different types of connector variables. The mass flow rate is assigned as a `flow` variable, which means that the sum of all flow variables in a connection set is zero. The thermodynamic pressure is a potential variable and the port pressures of connected ports have the same value. The `stream` variable was introduced with the Modelica Fluid Library 1.0 [116]. It assigns a specific quantity carried by the `flow` variable. It was introduced with the purpose of providing reliable handling of convective mass and energy transport in thermo-fluid systems with bi-directional flow of matter. Relevant boundary conditions and mass and energy balance equations are fulfilled in an idealized connection point between two or more connected ports. A detailed description can be found in [116]. The connector ports of a component (two or more) are then connected with physical equations enforcing mass, energy and momentum balances and representing the component's physical behavior. The governing equations within the components used for the modeling of the pack architectures are introduced later in this chapter.

The second library, HEXHEX [29], follows a very new concept that has been recently developed at the DLR Institute of System Dynamics and Control. The motivation of the new approach roots from reoccurring problems with the current way of modeling mostly addressing the resolvability of (larger) non-linear equation systems [29]. Finding working initialization settings took huge effort in some cases and thus, is perceived from an end-user perspective a lack of robustness and slowed down development time significantly. The new approach now aims to avoid the creation of large non-linear equation systems, which provides a very robust fluid library. [29]

In the scope of the new approach, the inertial pressure r is introduced with the following equation:

$$\frac{d\dot{m}}{dt}\frac{\Delta s}{A} = \Delta r \tag{5.1}$$

with Δs being the length of a fluid element and A its cross area. This formulation is implemented in every component and causes the mass flow to be a state variable. The inertial pressure is defined in every connector and builds together with the mass flow a pair of potential and flow variable. Δr constitutes the difference between the r at the connector port. Contrary to the approach of the Modelica Fluid library, the connectors work unidirectional. The following listings show the Modelica code of the inlet and outlet connectors [29]:

```
connector Inlet
replaceable package Medium = Modelica.Media.Interfaces.PartialMedium;
Modelica.SIunits.Pressure r;
flow Medium.MassFlowRate m_flow;
input Medium.AbsolutePressure p;
input Medium.SpecificEnthalpy h;
input Medium.MassFraction Xi[Medium.nXi];
end Inlet;

connector Outlet
replaceable package Medium = Modelica.Media.Interfaces.PartialMedium;
Modelica.SIunits.Pressure r;
flow Medium.MassFlowRate m_flow;
output Medium.AbsolutePressure p;
output Medium.SpecificEnthalpy h;
output Medium.MassFraction Xi[Medium.nXi];
end Outlet;
```

The remaining quantities, such as static pressure, specific enthalpy and mass fraction are defined as specific quantities and transmitted signal based in an unidirectional way. Unlike the latter connectors of the MSL, no `stream` variable has to be used anymore. The detailed methodology of this approach can be found in [29].

Both libraries cover all domains of an aircraft ECS. These are the fuselage, covering the cabin, flight deck and compartment, air mixing and distribution, the ram air channel, air generation and the vapor cycle and electric heating. Within this work, only the ECS packs are considered what excludes the air mixing and distribution, fuselage domain and electric heating. They are regarded indirectly as they affect the boundary conditions at the system boundaries. In the following, a brief overview of the physical components and the modeling approach is given. Figure 5.1 shows the Modelica diagram of the conventional bleed air pack architecture of Figure 3.1. The Modelica diagram of the electric driven vapor cycle pack architecture of Figure 3.3 is shown in the appendix (see Figure 5.5). The

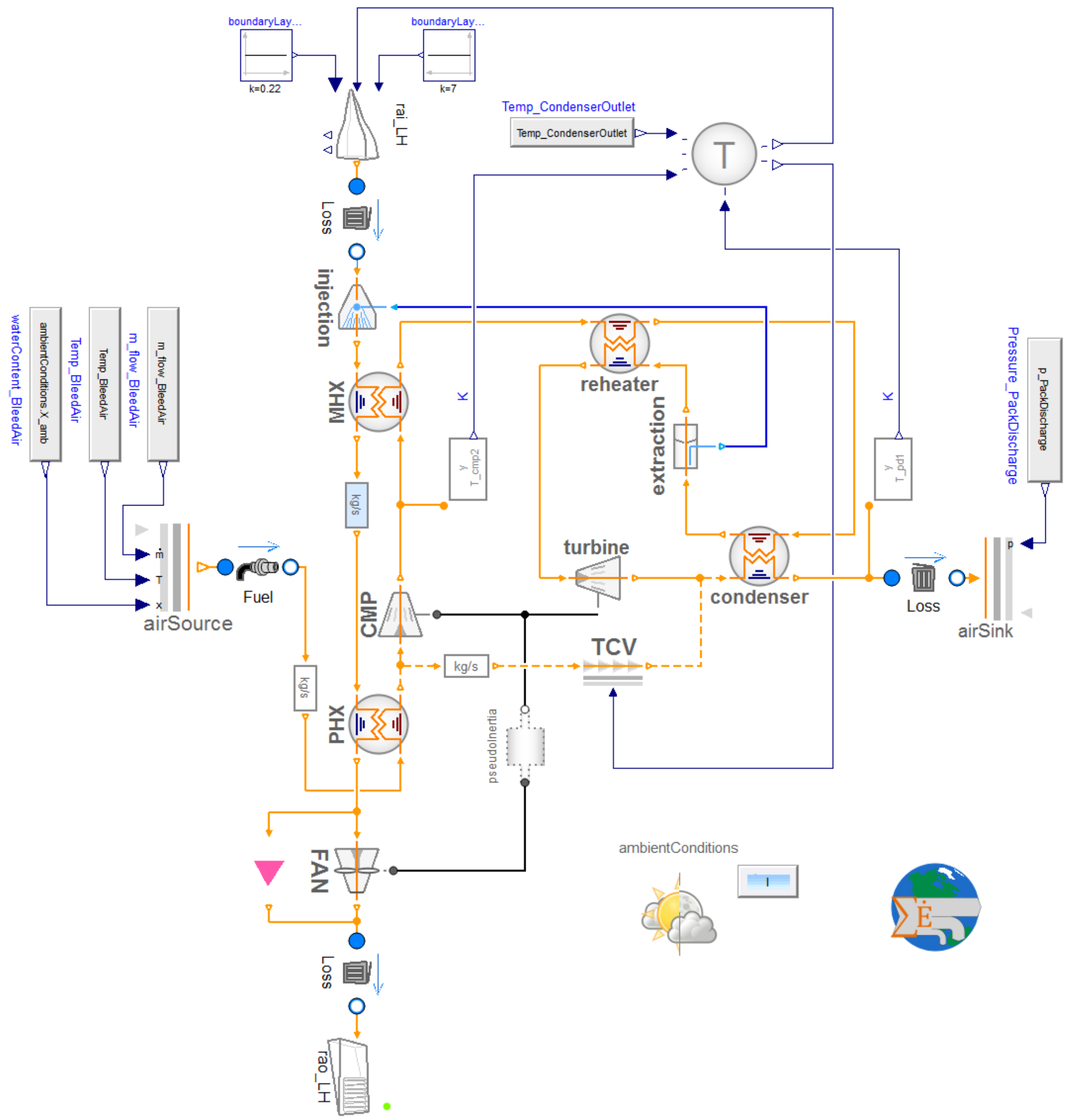

Figure 5.1: Modelica diagram of the conventional bleed air pack model.

ambient conditions and WorldEx model in the lower right are explained in the subsequent section.

The components of both packs can be grouped in ten categories (see Table 5.1). All components are regarded as 0-dimensional models. That means no discretization is implemented. The physical properties at the fluid connectors consist of specific enthalpy, pressure, mass fraction of water content and mass flow. The physical modeling of the component categories is presented in the following.

Table 5.1: Component categories for the conventional and electric pack.

Component Category	Working Fluid
Heat Exchanger	Moist Air
Compressor/Fan	Moist Air
Turbine	Moist Air
Water Exctraction	Moist Air & Water
Water Injection	Moist Air & Water
Mixer	Moist Air
Flow Resistance	Moist Air
Condenser/Evaporator	Moist Air & Refrigerant
Expansion Valve	Refrigerant
VaC Compressor	Refrigerant

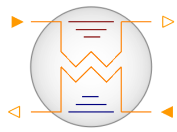

Heat Exchanger

The air-to-air heat exchanger model uses the simple approach of efficiency-based heat transfer. The enthalpy change of the hot side is accomplished by applying the efficiency to the maximum temperature difference between the hot inlet and cold inlet. It is described with the following equation:

$$\eta = \frac{\dot{m}_{\text{hot}} \cdot \Delta h_{\text{hot}}}{C_{\text{min}} \left(T_{\text{hot, in}} - T_{\text{cold, in}} \right)} \tag{5.2}$$

with $C_{\text{min}} = min \left(\dot{m}_{\text{hot}} \cdot c_{\text{p, hot}}, \dot{m}_{\text{cold}} \cdot c_{\text{p, cold}} \right)$. c_{p} constitutes the specific heat capacity. The efficiency is read from characteristic maps based on the mass flows of the hot and cold side. The pressure loss is modeled using a power law equation for pressure drop:

$$\Delta p = k \cdot \dot{m}^{m} \tag{5.3}$$

The parameters k and m are specific data for each type of heat exchanger. The heat transfer to the cold side is determined by the energy conservation:

$$\dot{m}_{\text{cold}} \cdot \Delta h_{\text{cold}} = \dot{m}_{\text{hot}} \cdot \Delta h_{\text{hot}} \tag{5.4}$$

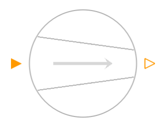

Compressor & Fan

Both the compressor and fan represent an energy flow into the working fluid to provide a pressure increase among the component. Performance maps describe the physical behavior. In case of the conventional bleed pack, all turbo components are mounted on the same shaft. A 1-dimensional flange connector represents the power link to the shaft.

The power P is expressed in the model as:

$$P = \omega \cdot \tau \tag{5.5}$$

with τ being the torque transmitted by the shaft and ω the time derivative of the rotational angle of the shaft $\dot{\varphi}$.

The power is then transmitted to the fluid by:

$$\eta_{\text{mech}} \cdot P = \dot{m} \cdot \Delta h \tag{5.6}$$

with η_{mech} being the mechanical efficiency of the compressor. The efficiency of the compressor and fan are described by the isentropic efficiency:

$$\eta_{\text{is}} = \frac{\frac{k}{k-1} \, R \, T_{\text{in}}}{\Delta h} \left(\beta^{\frac{k-1}{k}} - 1 \right) \tag{5.7}$$

β represents the pressure ratio among the component and k the isentropic coefficient for ideal gas for which the value of 1.4 is set. R denotes the ideal gas constant.

In case of the compressor, the performance maps provide the pressure ratio β and isentropic efficiency η_{is} based on the rotational speed of the flange and entering mass flow. The fan performance maps provide the pressure ratio β and relative temperature increase $\Delta T / T_{\text{in}}$ among the component based on the same input variables.

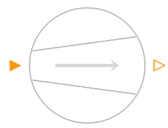

Turbine

The turbine is linked to the shaft in the same way as the compressor and fan (see Equation 5.5). The process is described with an isentropic expansion:

$$\Delta h_{\text{is}} = \frac{k}{k-1} \, R \, T_{\text{in}} \left(1 - \beta^{\frac{k-1}{k}} \right) \tag{5.8}$$

The power extracted from the fluid and transmitted to the shaft is expressed as:

$$P = \dot{m} \cdot \Delta h_{\text{is}} \cdot \eta_{\text{is}} \cdot \eta_{\text{mech}} \tag{5.9}$$

Similar to the compressor and fan, the turbine is based on performance maps. The pressure ratio is provided based on the rotational speed of the flange and a speed factor. The isentropic efficiency is than determined from tables based on the pressure ratio and a velocity factor.

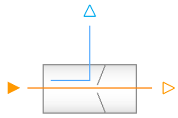

Water Extraction

In the case of saturated moist air, water is extracted from the working fluid. The amount of water that can be separated is defined by an efficiency and set by the user. Following the mass conservation, the mass flow of liquid water and moist air at the air outlet are calculated. There is no pressure drop considered within the water extractor.

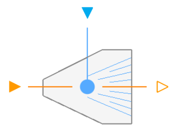

Water Injection

The water separated in the water extractor is injected to the working fluid. The rate of evaporation is set with a user defined efficiency η. The energy conservation is formulated in the following way:

$$\dot{m}_{\text{out}} \cdot h_{\text{out}} = \dot{m}_{\text{in}} \cdot h_{\text{in}} + \left(\eta \cdot \dot{m}_{\text{water}} \cdot h_{\text{water, liquid}} + (1-\eta)\dot{m}_{\text{water}} \cdot h_{\text{water, vapor}}\right) \tag{5.10}$$

$h_{\text{water, liquid}}$ denotes the enthalpy of the injected water in liquid phase and $h_{\text{water, vapor}}$ in vapor phase. There no pressure drop considered within the water extractor.

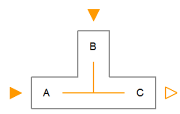

Mixer

The energy conservation for two working fluids meeting in a junction is described with the following equation:

$$h_{\text{out}} = \frac{\dot{m}_{\text{in, 1}} h_{\text{in, 1}} + \dot{m}_{\text{in, 2}} h_{\text{in, 2}}}{\dot{m}_{\text{in, 1}} + \dot{m}_{\text{in, 2}}} \tag{5.11}$$

The pressure at the outlet is assumed to be equal to both entering working fluids.

Flow Resistance

There are several components installed in both pack architectures that represent different kinds of flow resistances. The pressure drop inside the diffuser and divergent plenum of the ram air channel is calculated based on geometry following correlations of [117]. The remaining flow resistance component provides different options for calculating the pressure drop:

- linear with respect to a reference design 0: $\Delta p = \Delta p_0 \frac{\dot{m}}{\dot{m}_0}$,
- quadratic with respect to a reference design 0: $\Delta p = \Delta p_0 \left(\frac{\dot{m}}{\dot{m}_0}\right)^2$,
- resistance coefficient ζ: $\Delta p = \frac{\dot{m}^2 \zeta \rho}{2 A^2}$,
- constant: $\Delta p = \Delta p_{\text{fixed}}$,

- detailed base on flow and geometry characteristics:
  $\Delta p = f\,(\dot{m}, \rho, \mu, l, d, roughness, Re)$.

The resistance models do not interact thermally with the environment.

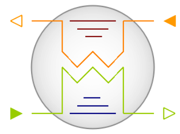

Condenser & Evaporator

The condenser and evaporator are part of the vapor cycle and interact with the fresh air through the evaporator and with the ram air through the condenser. The heat transfer is described with an efficiency based approach. Ideal conditions assuming a $\Delta T = 0$ for both sides are calculated. Based on the ideal temperatures, ideal enthalpy differences Δh are determined and thus ideal heat transfers are calculated. The minimum of the ideal heat flows, which depends on if the heat exchanger works as a condenser or evaporator, is then applied with the user defined efficiency. This model is very basic and pressure drop is neglected for both the air and refrigerant side.

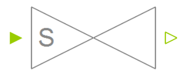

Expansion Valve

The pressure drop within the expansion valve of the vapor cycle is prescribed by a quadratic correlation with respect to a reference mass flow $\dot{m}_0$ and reference pressure p_0. It is controlled by an external signal u ranging from $0 \ldots 1$:

$$\Delta p = \frac{1}{u}\,\Delta p_0\,\frac{\dot{m}}{\dot{m}_0} \tag{5.12}$$

An enthalpy change is neglected ($\Delta h = 0$).

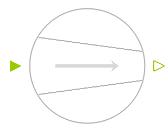

VaC Compressor

The vapor cycle compressor is modeled similar to the air compressor. The process is described as isentropic compression:

$$\eta_{\text{is}} = \frac{\frac{k}{k-1}\,R\,T_{\text{in}}}{\Delta h}\,\left(\beta^{\frac{k-1}{k}} - 1\right) \tag{5.13}$$

The power transmitted to the refrigerant is expressed as:

$$\eta_{\text{mech}} \cdot P = \dot{m} \cdot \Delta h \tag{5.14}$$

Contrary to the moist air compressor, the efficiencies are not based on performance maps, but user defined fixed values. The flange of this model complies with an external power signal.

5.2 Ambient Conditions

The ambient and flight conditions during the flight phases are provided by an additional model. The ambientConditions model is displayed in the lower right of Figure 5.1. This model is part of the Aircraft System Interface Library [118]. Its aim is to provide data about ambient conditions at fixed flight phases or predefined flight missions. The following data are globally provided at each time step by the ambientConditions model and can be accessed by all other components:

- Aircraft altitude,
- Static temperature,
- Aircraft speed,
- Static pressure,
- Humidity.

Aircraft altitude and speed are always prescribed by the user. The static temperature can be either prescribed or calculated by the standard atmospheric temperature profile [119]. The same applies for the pressure. The humidity can either be set to an absolute value of water content or prescribed by relative humidity. Based on the relative humidity, the water content is calculated depending on the actual atmospheric conditions.

5.3 Exergy Library

The analysis of thermo-fluid energy conversion systems using exergy-based methods is usually performed in two steps. The system is simulated in a first step using a simulation environment, such as Ansys, Aspen or Modelica. The produced thermodynamic data is then used to do the exergy analysis in a subsequent step. This requires a data transfer to another calculation software (e.g. EES or MS Excel). If the analysis is limited to one or a few operation points, the amount of data remains manageable. But if the exergy analysis shall be performed for several operation points or include dynamic behavior of a system, the data points exceed soon a practicable amount for subsequent exergy analyses.

Modelica is already used for the application of large thermo-fluid systems. Evaluation criteria based on the first law of thermodynamics such as energetic efficiencies are provided in most components that describe energy conversion processes. The advantage of the model-based approach that system models can be built from scratch or modified using available libraries within a short time shall now be extended with the capability of exergy-based methods. The exergy analysis is a subsequent calculation step and does not impact the system behavior.

5.3.1 Requirements

In order to achieve a solution as generic as possible some requirements need to be formulated derived from both, the exergy-based methods and the model-based environment:

Exergy-based Methods

- Retrieve thermodynamic state of all energy streams entering and exiting a component.
- Identify the aim of the component energy conversion process.
- Select the appropriate exergy balance of fuel and product exergy rates depending on the operation condition and reference environment.
- Allow a user defined exergy analysis on system level using the component's based analysis.
- Global propagation of the reference environment on system level.
- Media models must provide appropriate functions to calculate further thermodynamic data.

Model-based environment

- Generic approach for easy integration into any thermo-fluid library.
- Compliant with Modelica Standard Library (usage of MSL Media models and connectors).
- Minor impact on numerical computation.

The best way to put these requirements into action would require the screening of the modeled system architecture. The structure could be gathered to identify the components' aims and link them with their appropriate fuel and product definition. This procedure can be seen as a preceding step before the simulation starts. Unfortunately, Modelica at its recent stage of development used for this work [25] does not provide sufficient practical sequential capabilities. Therefore the integration needs to be realized in a different way.

5.3.2 Library Structure

The top level and partly unfolded structure of the library is shown in Figure 5.2. The `WorldEx` model is available on the top level. Besides the User's Guide and Examples package there are three packages on the top layer. The Functions package includes all functions that are necessary to calculate the exergy flows and are called from the exergy sensor models. The Sensors package contains all sensor models. It is organized according to the fluid medium. Currently there are sensors available for air, liquid, refrigerant, and mixed media. Typical applications for mixed media sensors are for example heat exchangers with two media. The Examples package aims at the understanding of how the sensor models are applied. Finally, there is an additional package for advanced analysis applications such as advanced exergy analysis and exergy analysis of fuel consumption.

The Sensors package is further organized in component and system level. The Component package contains the sensors for the different component types. Currently eight processes are covered: flow resistances and valves, heat exchangers, power demanding and producing turbo components, junctions such as splitter and mixer, and water extraction and injection. The System package provides sensor models to perform exergy analysis on system level according to Equation 4.3. The sensor models equal mass flow sensors and need to be integrated into a flow stream. These sensors must be compatible with the infrastructure, i.e. have the same connectors, of the used library. For the moment there are sensors provided that are compatible with the Modelica Standard Library and the new approach of HEXHEX that has been introduced in the first section of this Chapter.

5.3.3 Component Level

The exergetic analysis on component level includes the exergy balance of Equation (4.2) and the calculation of the exergetic efficiency with Equation (4.5). Table 4.3 lists the fuel and product exergy rates on component level. To calculate the appropriate exergy flows, the thermodynamic data at the component connectors must be provided. As mentioned before, it is hardly manageable to catch the data from outside the component without huge effort for the user. Therefore, the approach of a sensor model was chosen to integrate the exergy equations to the component. To keep the usability as simple as possible, the sensor model must be dropped to the component model and linked to the component connectors and some other variables. Figure 5.3 shows the Modelica diagram layer of

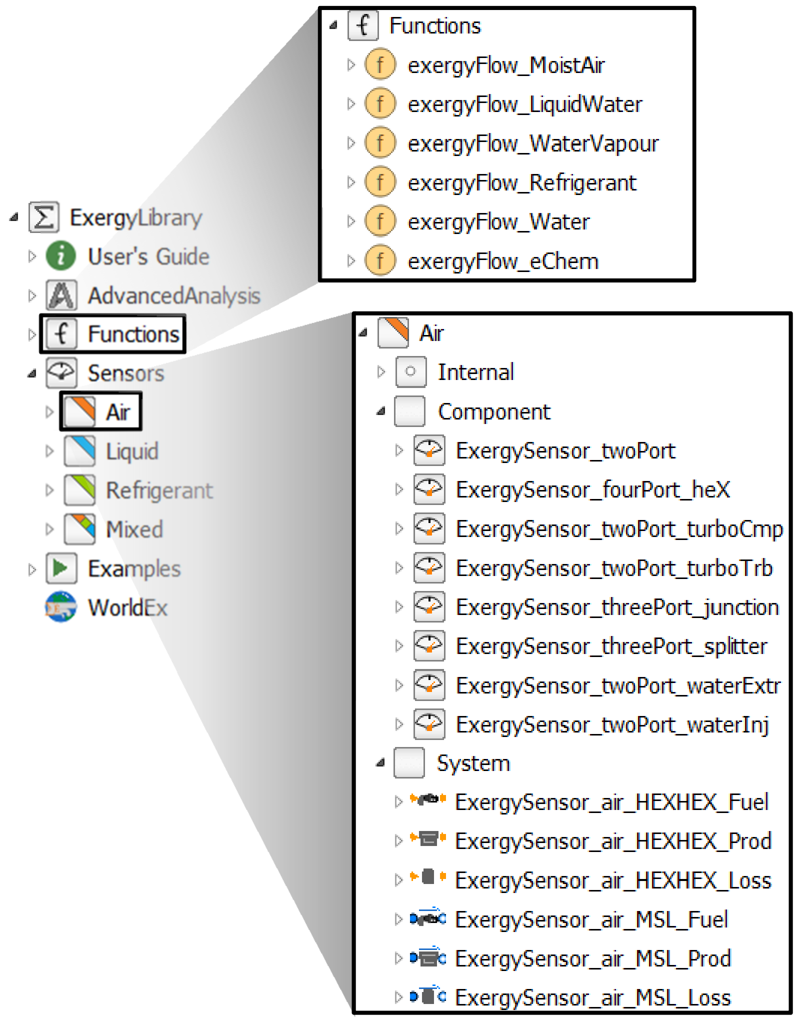

Figure 5.2: Library structure of the exergy library.

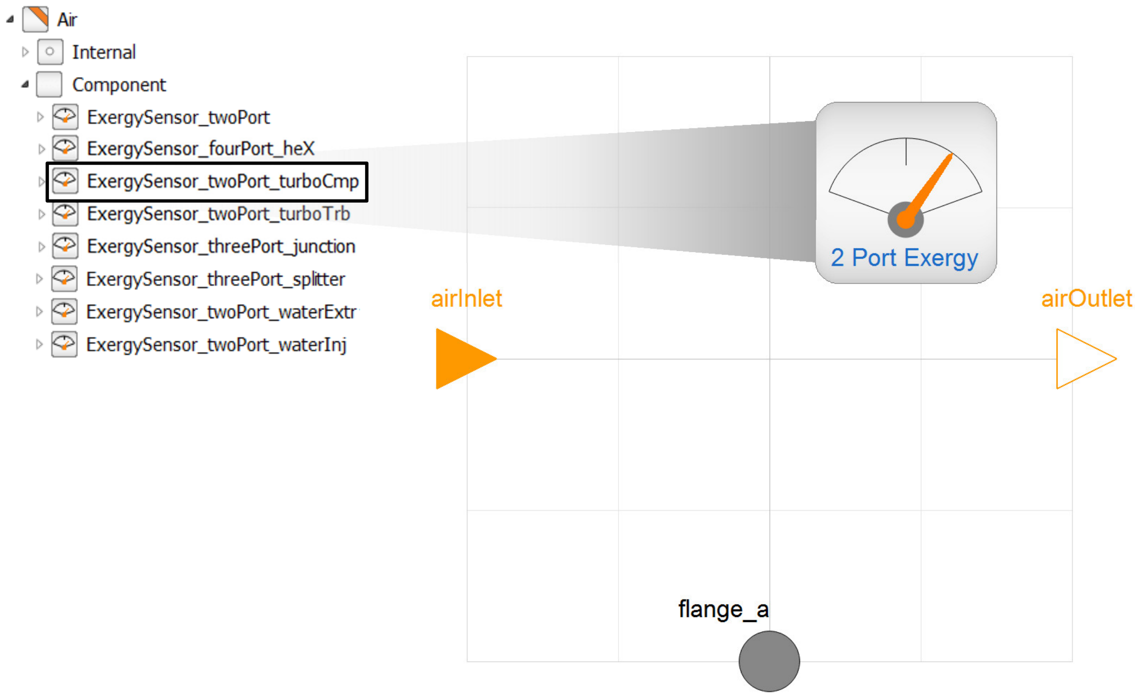

Figure 5.3: Modelica diagram of the StaticPipe model with an exergy sensor integrated.

the compressor model after the exergy sensor has been integrated on component level. The sensor model is then linked with the component by adding standardized code to the component model to supply the reference environment and the `WorldEx` model. Listing 5.2 shows an example of an exergy sensor integrated to a compressor model.

Besides the thermodynamic state at the connectors, the flow medium, mass flow, reference environment and in this particular case of the compressor, the power is transferred. The propagation of the thermodynamic state enables to be independent from the type of connectors used for the system modeling. The same applies for the flow medium. Here, the same medium model that is used for the component is propagated to the exergy sensor. As long as the medium model provides basic equations similar to the MSL, any medium model can be used. All calculations for the exergy flows and the definitions of the exergy rates depending on the operation condition (Table 4.3) happen within the sensor model. First the specific exergy at the inlet and outlet of the component are calculated. Function models provide the algorithms to determine the specific exergy split into its thermal, mechanical and chemical parts. Listing 5.3 shows how the function call works. The thermodynamic states at the connector and of the reference environment are committed to the function and the specific exergy values are returned. Then the exergy flows are calculated depending on the dry air and mass flow. The exergy flows of thermal ($\dot{E}^T$), mechanical ($\dot{E}^M$), and chemical ($\dot{E}^{Ch}$) parts, and the exergy of work ($\dot{W}$) are then used to formulate the fuel and product balances. The Modelica code of the compressor exergy sensor for the exergy rates of Table 4.3 is presented in Listing 5.3.

This approach allows the calculation of the exergy destruction within each component. The user integrates the sensor to the component level and does not have to care about the formulation of the exergy equations. The recent exergy library contains a sensor model for each category listed in Table 5.1.

5.3.4 System Level

A `WorldEx` model controls the exergy analysis on system level. It is responsible for the definition of the reference environment and collects the exergetic information for the exergy balance on system level. The reference environment can be either defined with fixed values or it can be linked to an environment model with variable conditions.

The exergy balance for the total system is formulated by Equation (4.3). The exergy flows for the total fuel, product and losses must be defined by the user as they depend on the system architecture. For each of the exergy flows, sensor models are available to integrate them to fluid flows. Similar to mass flow sensors, they must be implemented within the appropriate fluid stream. The exergy of the stream is calculated without any impact on the flow. In some cases, it is not possible to use fluid sensors to catch fuel, product, or loss exergy of the system, e.g. pure power that is supplied to or extracted from the system. For such cases the `WorldEx` model provides input boxes for each part of the exergy balance where the variable names can be entered. A mixed usage of sensors and entered variable names is possible as all parts are captured and summed up automatically.

The capability of automatically collecting the exergy data for the system balance requires the identification of all implemented exergy objects. Unfortunately, during runtime,

Listing 5.2: Modelica code of the implementation of the exergy sensor model into a compressor component model.

```
// Reference environment
SIunits.Temperature T_ref = worldEx.T_ref;
SIunits.Pressure p_ref = worldEx.p_ref;
SIunits.MassFraction X_ref[:] =  worldEx.X_ref;

outer ExergyLibrary.World worldEx;

//*************Sensors*************
Sensors.Air.ExergySensor_twoPort_turboCmp exergySensor_twoPort(
        airMediumA(state=AirMedium.setState_phX(
                portA.p,
                portA.h,
                portA.Xi), redeclare package AirMedium = AirMedium),
        airMediumB(state=AirMedium.setState_phX(
                portB.p,
                portB.h,
                portB.Xi), redeclare package AirMedium = AirMedium),
        m_flow=m_flow,
        power=power,
        T_ref = T_ref,
        p_ref = p_ref,
        X_ref = X_ref);
```

Listing 5.3: Modelica code of the exergy calculation within a sensor model.

```
// Exergy implementation
(e_t_in,e_therm_in,e_mech_in,e_chem_in) =
   Functions.exergyFlow_MoistAir(airMediumA.state, state_ref);
(e_t_out,e_therm_out,e_mech_out,e_chem_out) =
   Functions.exergyFlow_MoistAir(airMediumB.state, state_ref);

E_t_in = e_t_in * airMediumA.X[2] * m_flow;
E_t_out = e_t_out * airMediumB.X[2] * m_flow;
E_therm_in = e_therm_in * airMediumA.X[2] * m_flow;
E_therm_out = e_therm_out * airMediumB.X[2] * m_flow;
E_mech_in = e_mech_in * airMediumA.X[2] * m_flow;
E_mech_out = e_mech_out * airMediumB.X[2] * m_flow;
E_chem_in = e_chem_in * airMediumA.X[2] * m_flow;
E_chem_out = e_chem_out * airMediumB.X[2] * m_flow;

// Calculation of fuel and product Exergy
if m_flow <= 0 then
E_fuel = 0;
E_prod = 0;
case_T = 0;
else
if airMediumA.T > state_ref.T then
case_T = 1;
E_fuel = abs(power) + E_chem_in - E_chem_out;
E_prod = E_therm_out - E_therm_in + E_mech_out - E_mech_in;
elseif airMediumB.T >= state_ref.T and airMediumA.T <= state_ref.T
   then
case_T = 2;
E_fuel = abs(power) + E_therm_in + E_chem_in - E_chem_out;
E_prod = E_therm_out + (E_mech_out - E_mech_in);
elseif airMediumB.T < state_ref.T then
case_T = 3;
E_fuel = abs(power) + (E_therm_in - E_therm_out) + E_chem_in -
   E_chem_out;
E_prod = E_mech_out - E_mech_in;
else
case_T = 100;
E_fuel = 0;
E_prod = 0;
end if;
end if;
E_D = E_fuel - E_prod;
exergy_eff = E_prod / max(0.001,E_fuel);
```

Modelica does not provide such capabilities to screen a system model for its data structure. With the help of the `UID Library` [120], all exergy sensors are equipped with a unique identifier which can be identified on system level and used for the system balance. Listing 5.4 shows the implementation of the unique identifier to the exergy sensor for the implementation to the components.

Listing 5.4: Modelica code of the implementation of the unique identifier into an exergy sensor model.

```
UID.UniqueID uniqueID(group="exergy");
parameter String instanceName = getInstanceName();
equation
worldEx.E_D[uniqueID.uid+1] = E_D;
worldEx.instanceName[uniqueID.uid+1] = instanceName;
```

The `UniqueID` model is added to the sensor model and assigned with a group. A unique integer value uid is then provided within the group. In this way, it is possible to propagate the exergy destruction calculated within each sensor and the instance name of the component to the `WorldEx` model. The uid value starts at 0 and is in the range $[0 \ldots total]$. The `WorldEx` model contains a `GroupTotal` object that provides the total number of values assigned within a certain group and is illustrated in Listing 5.5. This

Listing 5.5: Modelica code of the implementation of the unique identifier variables into the `WorldEx` model.

```
UID.GroupTotal groupTotal(group="exergy");
Modelica.SIunits.Power E_D[groupTotal.total];
Modelica.SIunits.Power E_D_total = sum(E_D) + E_D_user;
String instanceName[groupTotal.total];
```

allows to summarize single values of the exergy destruction to the total destroyed exergy within the considered system. The collection of the fuel, product and loss exergy flows works in a similar way using additional `GroupTotal` objects having different group names assigned.

The `WorldEx` model displays in the *Dymola Message* Window the list of the collected instance names of the components having an exergy sensor integrated and writes them into an extra text file.

5.4 Implementation to ECS Models

Within this chapter, the implementation of the exergy library into the two ECS architectures is presented. Both systems are modeled with different libraries (see Section 5.1) and demonstrate the generic applicability of the exergy library.

Conventional Bleed Air Driven Pack

The Modelica diagram of the conventional pack is displayed in the beginning of this chapter in Figure 5.1. The `WorldEx` model and the exergy sensors for the system balance are dropped to the top layer. According to the system balance of Equation 4.25, a fuel exergy sensor is installed to the entering bleed air flow. The loss exergy sensors are added to the entering and exiting ram air and to the exiting bleed air. Figure 4.4 illustrates that there are no further energy streams crossing the system boundaries. Additional variables do not need to be taken into account for the exergy analysis. All components are equipped with appropriate exergy sensors from the exergy library. An example illustrates the integration of the compressor model in Figure 5.3.

In the beginning of the simulation a text file "ExComponentNames_*modelName*.txt", where *modelName* is replaced with the name of the simulated model, is created. It lists all components of the simulated model with exergy sensors inside (Listing 5.6) and a list of used exergy sensors for the system balance, i.e. fuel, product and loss. The bleed pack contains 12 components listed with their names and paths to the exergy sensor, and one fuel and three loss exergy sensors.

The path to the exergy sensors show that the naming of the sensors is the same independent of the exergy sensor model. A default name is set for all exergy sensor models. For example, in Figure 5.2 when the "ExergySensor_twoPort_turboCmp" model is dropped into a compressor model, the name of the sensor model is automatically set to "exergySensor_twoPort_turboCmp". To simplify an optional post processing of the results by using the generated *.mat file, the exergy sensor name is now set to "exergySensor" per default for all models. For the exergy analysis the type of exergy sensor is no longer important as the appropriate balances are included already.

Electric Driven Vapor Cycle Pack

The eVCP model is modeled using the approach for robust modeling of directed thermo-fluid flows [29]. A brief introduction was given in Section 5.1. Figure 5.5 shows the diagram layer of the electric driven vapor cycle pack architecture. Unlike the conventional bleed air driven air cycle pack, unconditioned outside air instead of bleed air from the engine enters the eVCP and all turbo-machines within the eVCP are electrically powered (see Section 3.3 for detailed description). Similar to the conventional pack model, the `WorldEx` model and the exergy sensors for the system balances are dropped to the top layer. Unfortunately, the exergy balance on system level cannot be described by fuel, product and loss sensors only. The exergy balances for fuel and product are listed in Table 4.7. The definition of the losses does not depend on the operation condition or the reference environment and the loss exergy sensors can be added to the entering and exiting ram air flow. The equations for fuel and product exergy are written to the Modelica code on system level. Using conditional clauses for the cases of Table 4.7, variables for fuel and product exergy for the fresh air stream are defined. These variables are written to the `WorldEx` GUI to the appropriate boxes. Last, the variables assigned with the power of the turbo components are added to the fuel and product boxes. Figure 5.4 shows the `WorldEx` GUI with the user defined fuel and product entries.

Listing 5.6: Generated text file with a list of components with exergy sensors.

```
Total Number of components containing exergy sensors = 12
Structure of vectors based on E_D:
[1]turbine
[2]compressor
[3]PHX
[4]MHX
[5]reheater
[6]condenser
[7]fan
[8]injection
[9]extraction
[10]temperatureControlValve
[11]dp
[12]junction
Full paths to exergy sensors:
CruiseFL370.turbine.exergySensor
CruiseFL370.compressor.exergySensor
CruiseFL370.PHX.exergySensor
CruiseFL370.MHX.exergySensor
CruiseFL370.reheater.exergySensor
CruiseFL370.condenser.exergySensor
CruiseFL370.fan.exergySensor
CruiseFL370.injection.exergySensor
CruiseFL370.extraction.exergySensor
CruiseFL370.temperatureControlValve.exergySensor
CruiseFL370.dp.exergySensor
CruiseFL370.junction.exergySensor
Total Number of fuel exergy sensors = 1
Structure of E_fuel vector:
[1]CruiseFL370.exergySensor_air_MSL_Fuel
Total Number of prod exergy sensors = 0
Structure of E_prod vector:
Total Number of loss exergy sensors = 3
Structure of E_loss vector:
[1]CruiseFL370.exergySensor_air_MSL_Loss
[2]CruiseFL370.exergySensor_air_MSL_Loss1
[3]CruiseFL370.exergySensor_air_MSL_Loss2
```

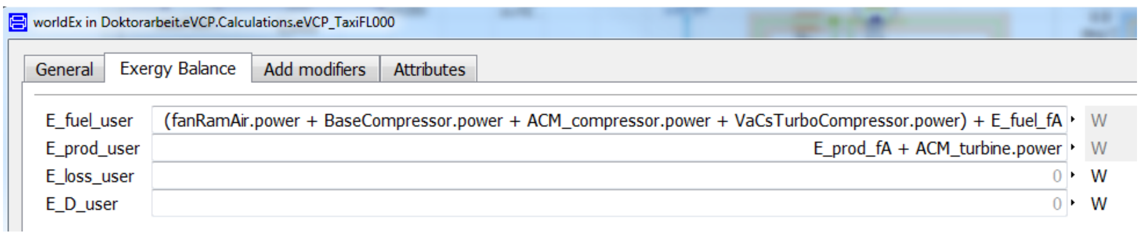

Figure 5.4: Extract of the `WorldEx` GUI showing the assignment of the fuel and product exergy to the system balance.

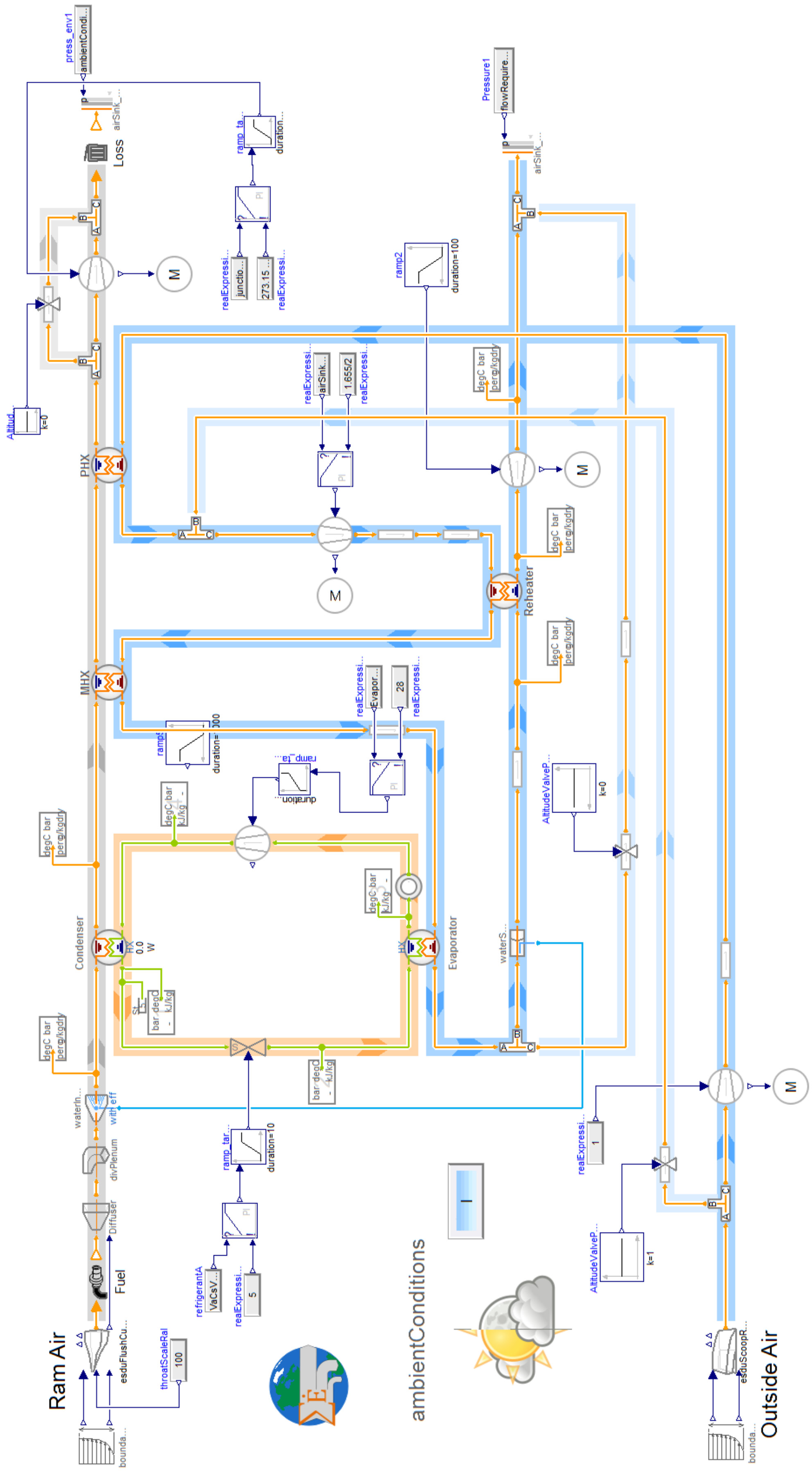

Figure 5.5: Modelica diagram of the electric driven vapor cycle pack.

Within the electric driven vapor cycle pack model, a total number of 30 components with exergy sensors was identified by the exergy library. The generated text file can be found in the appendix (Listing C.1) Although there are 30 components listed, the exergy sensor was not integrated 30 times manually to the component models. The work has to be done once for each different component class and can then be reused without limitations.

5.5 Conclusion

The motivation for the presented exergy library resulted from the idea of doing exergy analyses for aircraft environmental control systems within a model-based design. A solution had then to be found how to integrate exergy-based methods into the model-based design environment of Modelica.

The exergy analysis treats every component different, depending on its aim and particular energy conversion process. The derived requirements for such a library coming from both, the exergetic and model-based design, parties resulted in the presented work. An exergy sensor model is implemented into the component model and linked to the entering and exiting energy flows. The sensor then does all calculations for the component level exergy analysis and propagates its instance name and exergy destruction to a `WorldEx` model. Concurrently, the `WorldEx` model provides the reference environment for all exergy sensors. The exergy sensor model can be applied independently from the thermofluid modelling approach. This was achieved by linking the sensor model not by connecting any fluid connectors but by propagating the thermodynamic states of the entering and exiting fluid flows. The exergy balance on system level can be performed by using additional exergy sensors that work similar to mass flow sensors and need to be connected within the appropriate fluid stream. Unfortunately, these models have to be compatible with the fluid library, i.e. have the same or compatible connectors. The current version of the exergy library provides sensors that can be used with the Modelica Standard Library and the approach of HEXHEX [29]. Non-accessible energy streams that should be included to the system balance can be added by writing their variable names into the GUI of the `WorldEx` model. Here a box is provided for exergy desctruction, fuel, product and loss exergy. Additional evaluation numbers such as exergy destruction rate (component and system level) or the ratio of $E_{D,k}/E_{D,tot}$ are provided by the `WorldEx` model.

With the experience gained during the development of this exergy library, one can say that there is no universal solution as exergy-based methods by their nature, have the individual aspect on the component's aim. But there usually is a limited number of energy conversion processes and component classes. The work for integrating the exergy sensors to the components, needs to be done only once, and one can benefit from it any time after. The structure of the library allows an easy extension for new energy conversion processes. The advantage of this concept is that the exergy analysis is totally detached from the component development and behavior and allows an individual use for the modeler.

Remarks

The current version of the exergy library uses mainly the media models of the Modelica Standard Library. For moist air, water and single gases that can be treated as ideal gases, the provided models of the MSL might be sufficient. The second example architecture presented here, has a vapor cycle included that runs with refrigerant. For this purpose, an additional media library was used. The linchpin of the exergy analysis is the correct calculation of the thermodynamic properties. The current thermodynamic state record of the MSL or most other medium models does supply only basic properties which are not sufficient for an exergy analysis. Therefore, an extended thermodynamic state record was created in the exergy library by using the appropriate equations from the medium models. To further ensure a generic applicability of the exergy library for different kinds of fluids, it is recommended to provide a standardized formulation and naming of equations for the thermodynamic properties.

Chapter 6
Results

This chapter presents the results of the analysis of the conventional bleed and electric driven packs. In the first part, the mission based analysis of an example full flight mission was performed for the conventional bleed pack. The impact on the exergy analysis of the reference environment selection is illustrated comparing simulation results for three different reference environments. Using the mission based analysis, the unavoidable factor for the advanced exergy analysis is determined. The results are presented for the components of the conventional bleed pack.

The second part presents the results of the fixed operation point analysis. Both pack system have been simulated and analyzed for taxi and cruise flight phase. Different analysis methods have been applied. The traditional design parameters such as fuel weight penalties are presented. Conventional exergy analysis is applied on component and system level. Further, the exergy destruction is split into avoidable and unavoidable parts and finally the results of the exergoaeronautic analysis are presented.

Before the results are presented, the mission cases are introduced with the environment, operation, and boundary conditions for the two ECS packs.

6.1 Mission Cases

The boundary and environment conditions for the taxi and cruise flight phases are listed in Table 6.1. For the cruise phase, a duration of 1.5 h is chosen. The ambient air is assumed to be saturated during taxiing. The actual water content is calculated by the ambientConditions model (see Section 5.2). The environment conditions apply for both pack simulations.

The performance and aircraft data for the conventional bleed and electric driven packs are listed in Table 6.2. The bleed air and fresh air intake for the eVCP were set to the same

Table 6.1: Flight conditions for taxi and cruise phases.

Mission Phase	Taxi	Cruise
Cruise Time	-	1.5 h
Altitude	0 ft	37000 ft
Flight Speed	0.0 Ma	0.77 Ma
Env. Pressure	1.01325 bar	0.22 bar
Env. Temperature	30.0 °C	−56.3 °C
Humidity	100.0 %	60.0 %

Table 6.2: ECS performance and aircraft data for taxi and cruise phases.

Pack Architecture	Bleed		eVCP	
Mission Phase	Taxi	Cruise	Taxi	Cruise
$\dot{m}_{\text{bleed/fresh}}$	0.5 kg/s	0.5 kg/s	0.5 kg/s	0.5 kg/s
W_{system}	118 kg	118 kg	141.6 kg	141.6 kg
T_{tb}	932 °C	932 °C	–	–

value. The mass of the bleed pack is the same as introduced in Section 2.3.3. To the best knowledge of the author, there is no public data available for the electric driven ECS. The eVCP contains a vapor cycle and an additional compressor. The turbo components are driven by individual motors. Considering the technological advances for the eVCP in terms of lightweight materials and efficiency improvements, a 20 % higher system weight is assumed for the eVCP. The turbine inlet temperature T_{tb} is taken from [48] for both architectures. All other aircraft performance data such as thrust and power specific fuel consumption, and lift-to-drag ratio are calculated during simulation by the exergy library.

The environment conditions for the mission-based analysis are displayed in Figure 6.1. Besides the curves of ambient temperature, ambient pressure, and ambient water content, the conditions at sea level and cruise level are plotted. Each plot contains the altitude of the flight trajectory. The three different conditions are used to study the sensitivity of the reference environment definition on the exergy analysis. The water content changes according to a relative humidity of 60 % for all flight phases. The total mission time is 10000 s.

6.2 Full Flight Mission Analysis

The ambient conditions at the different flight levels are taken for a standard ISA day [119]. For the exergy analysis, three approaches for the reference environment were chosen. Figure 6.1 shows the charts for temperature, pressure and water content of the reference environments. The first case defines the reference environment at sea level (dotted blue line). The second approach assumes ambient condition as reference environment (red line). The third reference environment is set to the peak altitude of the flight trajectory at 37000ft (dash-dotted green line).

Three simulations of the conventional pack (Figure 3.1) were carried out, each with another reference environment. In the following paragraphs, selected results of the exergy analysis are presented comparing the different reference environments in order to show the sensitivity of the approaches.

Figure 6.2 shows the destroyed exergy and exergy efficiency for the main heat exchanger. The operation condition cases in terms of fuel and product definition are plotted in the upper chart. The case definitions are plotted in Table 4.3 and are used within this section to explain certain trends of the curves. For a direct comparison, the results for the three reference environment approaches are plotted all together in one chart. The destroyed

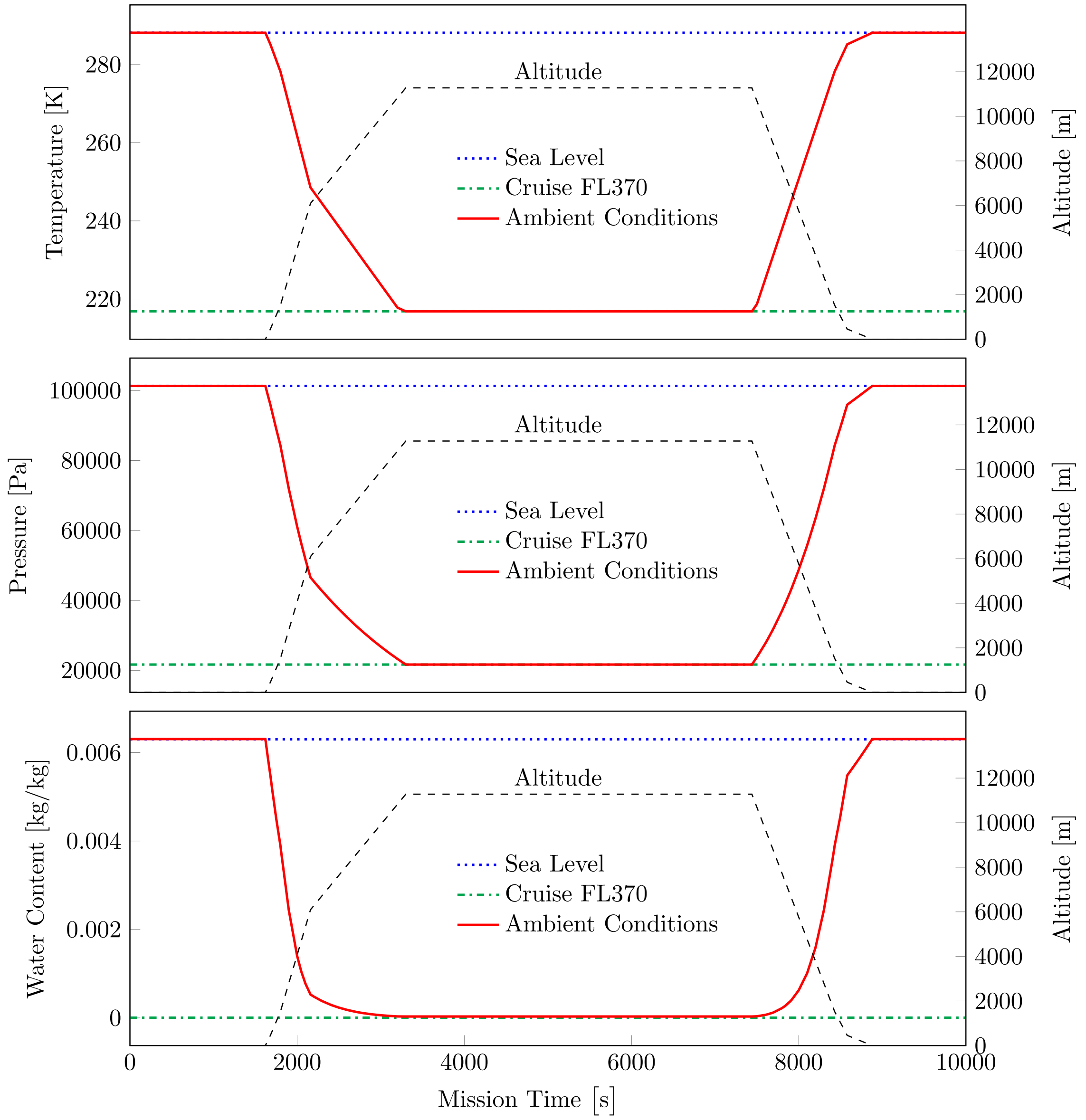

Figure 6.1: Ambient and reference environment conditions for a full flight mission.

exergy shows a similar course for all simulations. The exergy destruction is approximately 3 times higher during cruise operations for the sea and cruise level reference environments. The curve with the reference environment being at ambient conditions first complies with the sea level values and then changes to the cruise level curve.

The exergy efficiency graphs in the lower plot show a different behavior. The efficiency for the cruise level reference environment decreases by 11 % during flight to about 67 %. The operation condition plot shows that the MHX works among the whole mission at case #1, i.e. all streams work above the reference environment. The exergy efficiency with respect to sea level behaves totally different. During ground conditions, the MHX operates with almost zero efficiency. In the first part of the climb phase, there is a step up to approximately 50 % followed by a sudden drop back to 0 % before it steps again up to 50 % and decreases to about 31 % during cruise. The low performance levels can

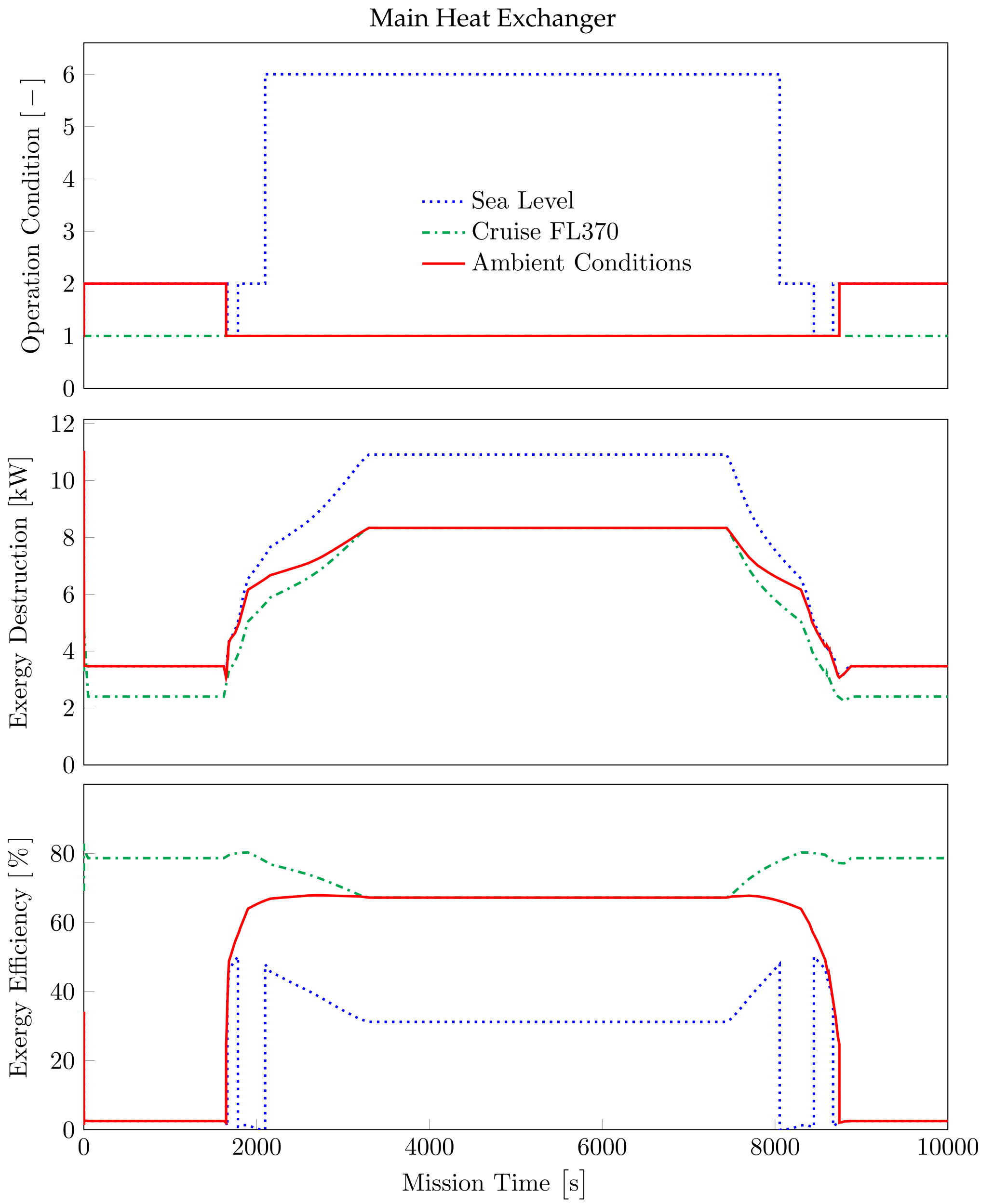

Figure 6.2: Results of exergy analysis of the MHX for a full flight mission.

be explained with the operation condition at case #2. This is one of the worst productive operation condition from an exergetic point of view. The temperature decrease of the hot side is assigned completely as fuel exergy. Additionally, the temperature increase of the cold side crosses the reference temperature and thus is only partly assigned as product exergy. During cruise, the MHX operates at case #6 and both sides cross the reference temperature. The variable reference environment curve switches from the sea level curve to the cruise level curve.

The analysis of the turbine shows interesting results that vary significantly from the previous ones. Figure 6.3 presents the destroyed exergy, exergy efficiency and the fuel and product definition cases (Table 4.3) of the turbine. The exergy destruction for the reference

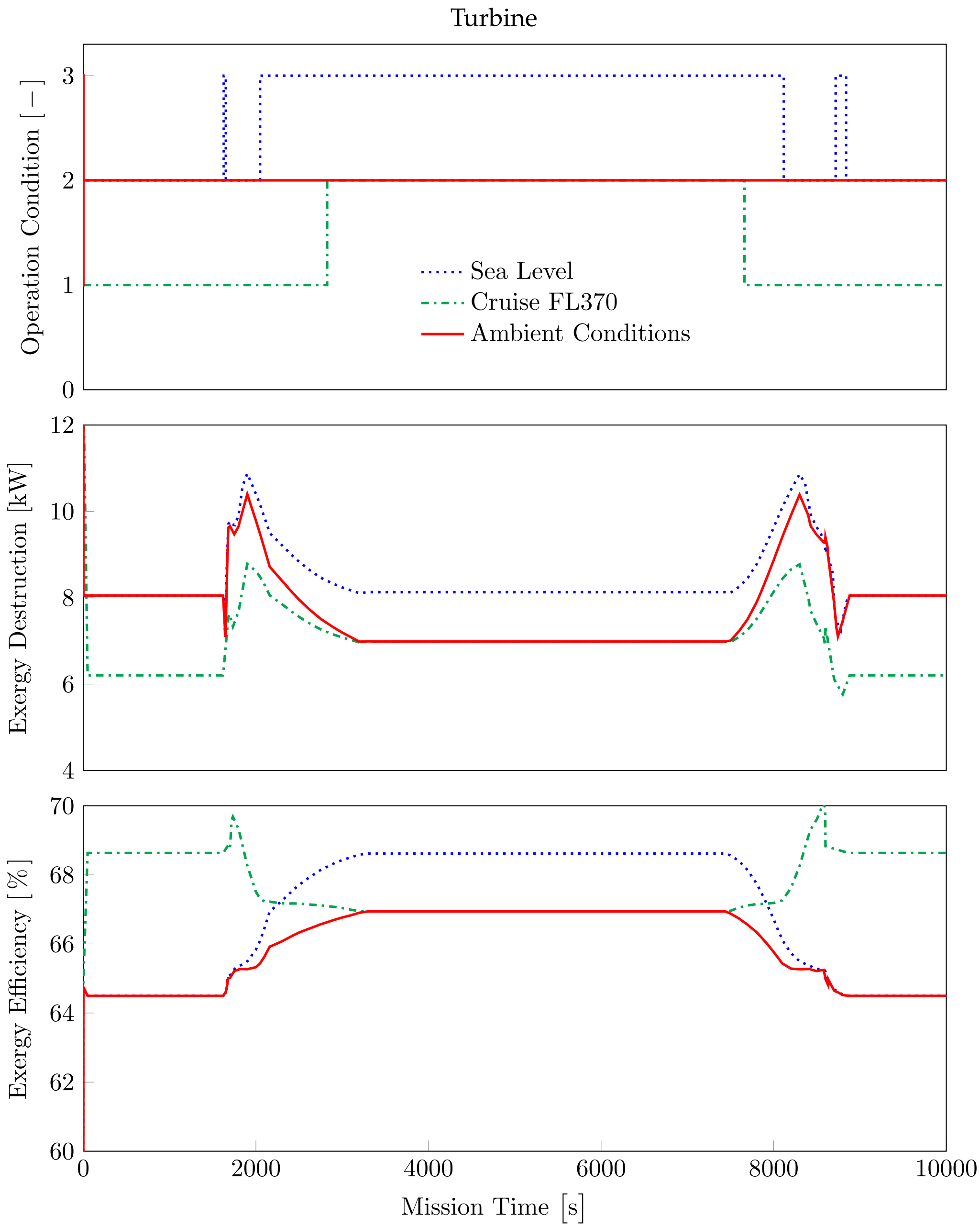

Figure 6.3: Results of exergy analysis of the Turbine for a full flight mission.

environment at sea level during cruise is similar to taxi operations. It increases during the transitions of climb and descend. The cruise FL370 approach, however, results in exergy destructions similar to the sea level approach, although higher values are reached during cruise. Looking at the reference environment set to ambient conditions, the exergy destruction decreases by approximately 1 kW. The courses of the exergetic efficiency conclude in two different statements. Following the cruise FL370 definition, the turbine operates at lower efficiency (about −1.5 %) during cruise, while the sea level approach predict a higher efficiency of approximately +4 % during cruise. The varying reference environment results in an efficiency increase of about +2 % during cruise.

The selected results show the sensitivity of the exergy analysis regarding the reference environment selection. For the main heat exchanger and the turbine, the sea level and cruise FL370 approach show each similar trends for the exergy destruction. The sea level approach results in higher exergy destructions than the cruise approach. For the MHX, the difference between the the two fixed reference environments remains almost constant for all flight phases. In case of the turbine, this difference is smaller during cruise. Although the results of the exergy destruction show similar trends, they must be interpreted carefully because according to the definition of exergy [61], there is an interaction between the system and the reference environment. This is valid only for parts of the flight mission. The different trends of the exergy efficiencies support this assessment. Looking at the MHX, one would draw contradictory conclusions. Setting the reference environment at cruise conditions, the results show that the heat exchanger should be improved for cruise. However, the sea level approach states the opposite. The varying reference environment supports for the MHX the trend of the sea level approach.

The exergy efficiency trends for the turbine do not show such large discrepancies. Nevertheless, the two fixed reference environment approaches again would end in contrary conclusions. Using the cruise FL370 approach leads to optimization during cruise and the sea level approach suggests improvements for ground operations.

Two important conclusions can be drawn from this study. No matter which approach for setting the reference environment is followed, it is mandatory to consider the operation condition regarding the reference environment for the formulation of the fuel and product exergy rates. Both components change the operation conditions during the flight. Without such definitions, an exergy analysis is not applicable for the particular operation conditions of an aircraft ECS.

The second conclusion regards the question where the reference environment should be defined. This issue has already been addressed in the beginning of this thesis and is one of the main objectives. The exergy destruction is less affected by the case of operation condition, but the exergy efficiency changes significantly as it measures the exergetic productivity of the component. The plots of the MHX results illustrate this effect. The varying reference environment predicts low performance during ground conditions and a significant increase during cruise. However, these results show the significance of this discussion, but an explicit conclusion cannot be drawn.

The methodology for the definition of fuel and product exergy itself can help at this point. Table 4.7 lists the exergy balances on system level for the electric driven vapor cycle pack. The pack can operated in cooling or heating mode. That means that the fresh air from the environment entering the system is either heated or cooled within the eVCP. The eVCP is supplied with electric power. Broudly speaking, this power is converted into compression and heating or cooling power. But, the conditioning of the fresh air always starts at ambient conditions and can be measured in a meaningful way with respect to the environment. Coming back to the definition of the exergy balances of Table 4.7. Beginning with the cooling mode. Assuming that the ambient air enters the system at 20 °C and is cooled by 15 °C. If one would set the reference environment to cruise FL370 conditions and the chemical exergy would decrease, case # 4 would apply. The exergetic product in this case restricts to the pressure increase within the system. During ground conditions, only small pressure increase is needed to overcome the flow resistances. From an exergetic point of view, there is hardly any product and the exergy efficiency is vanishing small, although the eVCP produces something meaningful: cooling power. The same effect occurs for case # 6 of the heating mode when the reference temperature is greater than the pack discharge temperature. This could happen for a cold day on ground when the reference temperature is set to standard ISA day conditions.

The discussion of the formulation of the exergy balances for the eVCP system allows to conclude with a recommendation for the definition of the reference environment. Components such as the MHX or the turbine do not interact directly with the environment at ambient conditions. The same applies for the conventional bleed air driven pack. The entering conditions of the bleed air are almost the same for all flight conditions and it is regarded as a dissipative component. The system boundaries for the bleed pack include just the pack system on purpose. The analysis methods presented in this thesis focus on the detailed analysis of the packs. Otherwise, the engine and the bleed air system would have to be taken into account additionally. However, the eVCP interacts directly with the environment and the formulation of the exergy of fuel and product can be compared with the physical energy conversion process. The final conclusion from this study is that for systems that operate in varying environment conditions and interact with this environment, is that the reference environment shall be set to the ambient conditions that the system is interacting with.

6.3 Conventional Exergy Analysis

The conventional exergy analysis was performed for both pack architectures. This section is divided into two parts: results of the bleed air driven pack, and results of the electric driven vapor cycle pack. For each system, the thermodynamic cycle is presented for taxi and cruise phase. The results of the exergy analysis are then shown and discussed.

The environment conditions for both flight phases have been shown in the beginning of this chapter in Table 6.1. The reference environment for the exergy analysis is set to the ambient conditions for all following analyses.

6.3.1 Conventional Bleed Air Driven Pack

Figure 6.4 and 6.5 show the thermodynamic cycles of the bleed pack for taxi and cruise phase. Both T-s diagrams are scaled to the same range. The temperature values on the ordinate are normalized. The flow schematic of the bleed air driven pack was introduced in Figure 3.1. All numbers of the state points in the T-s diagrams refer to this figure.

The bleed air enters the pack at the same conditions for both phases (1). The temperature decrease within the PHX ($1 - 2$) is higher during taxi and the temperature level downstream the compressor (3) is lower for taxi. Ram air enters the main heat exchanger at ambient temperature or slightly below in case of water injection. The temperature difference of the ram and bleed air within the MHX is greater during cruise than during taxi. The result is a larger temperature decrease $(3-4)$ and lower temperature level for the exiting bleed air in the cruise phase. The reheater $(4-5/7-8)$ and condenser $(4-5/9b-10)$ work at different conditions for taxi and cruise conditions. The reheater $(4-5)$ and condenser $(5-6)$ cool the bleed air during taxi before water is extracted $(6-7)$ and the temperature is increased again in the reheater $(7-8)$. During cruise, both heat exchangers cause a temperature raise and due to the insignificant water content of the ambient air, no condensation and water extraction 6/7 take place. The expansion within the turbine $(8-9a)$ causes a significant higher entropy increase during taxi compared to the cruise phase. The bypass flow passing the TCV is almost zero during taxi and causes only a small increase in temperature $(9a-9b)$. During cruise, the ACM is bypassed by a larger mass flow of hot air what results in a considerable temperature raise of the main bleed air stream. Finally, the air is heated in the condenser $(9b-10)$ during taxi and slightly cooled during cruise.

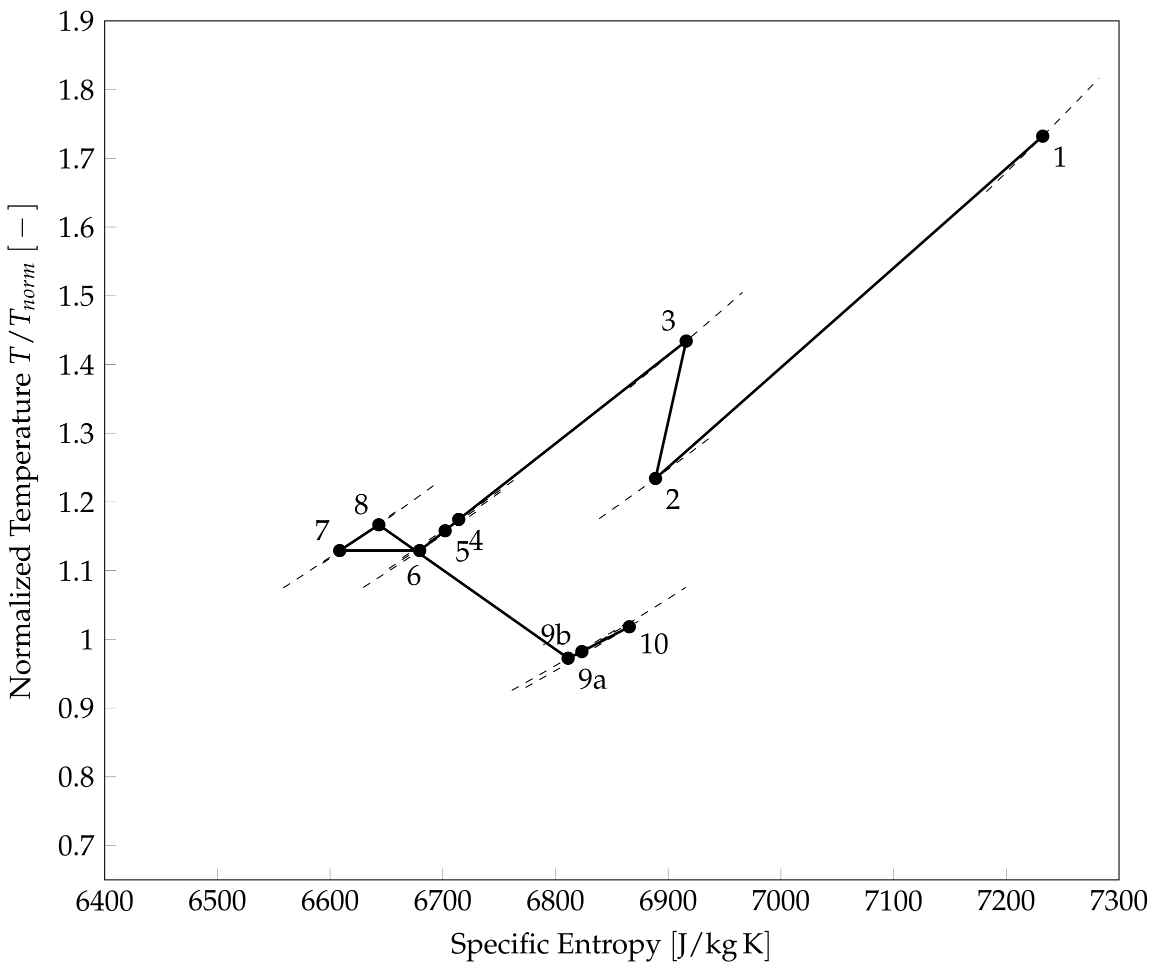

Figure 6.4: T-s diagram at taxi phase for the conventional bleed pack.

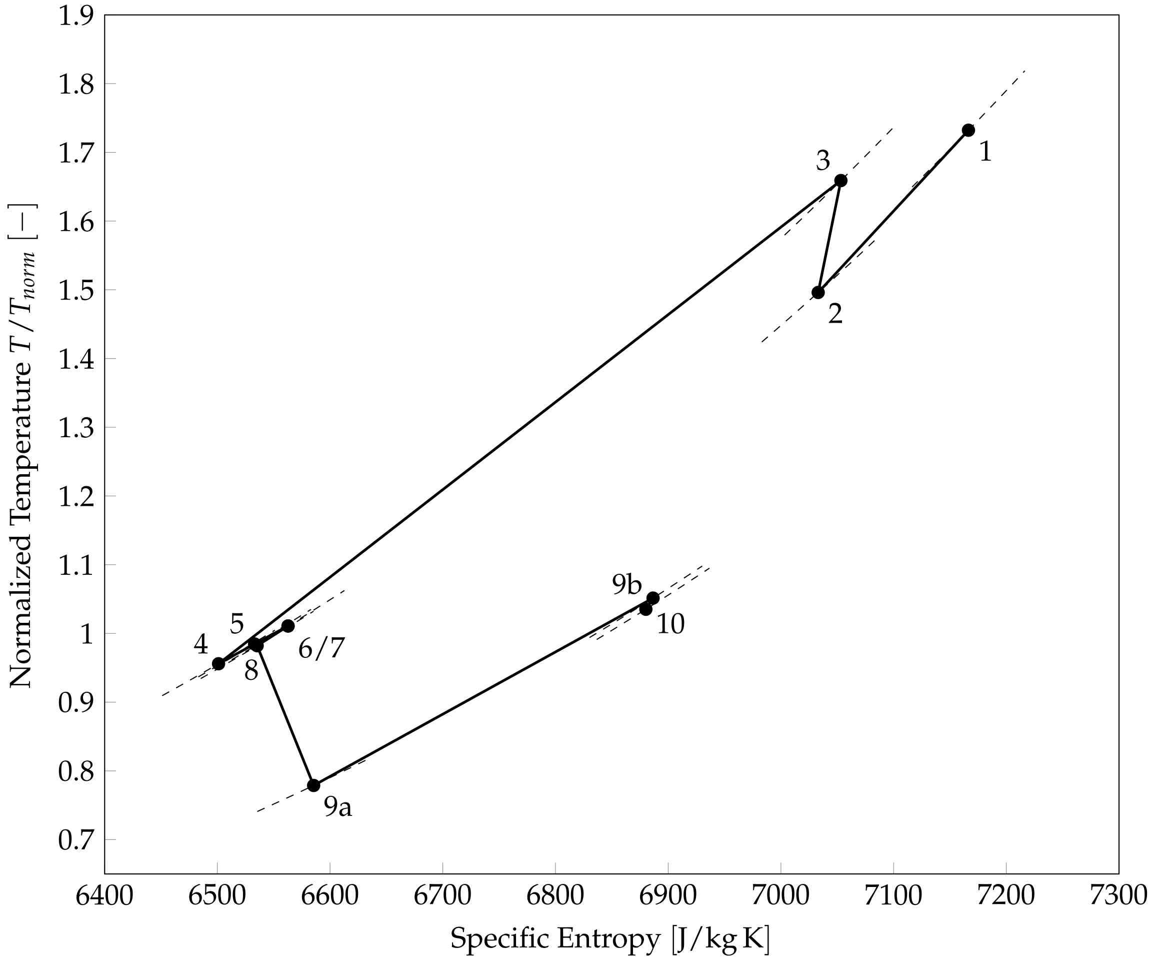

Figure 6.5: T-s diagram at cruise phase for the conventional bleed pack.

The T-s diagrams illustrate the thermodynamic cycles for the cruise and taxi phase and show the different operation conditions of the components. The bleed pack operates during cruise within a wider temperature and entropy range than during taxi.

Exergy Results

The results of the conventional exergy analysis for the taxi and cruise phase are listed in Table 6.3.

During taxi phase, the turbine produces the highest exergy destruction causing 42.2 % of the total exergy destruction share. The PHX follows with about one quarter and the MHX causes 16.6 % of the total exergy destruction. The remaining components have a share of less than 10 % each. The high value of the turbine comply with the large entropy increase shown in the T-s diagram of Figure 6.4. The exergetic efficiencies variy from 3 % for the MHX up to 88 % for the compressor. The ram air fan has the second highest exergy efficiency and cause only 1.5 % of the total exergy destruction. In general, all heat exchangers have low performances. The condenser works as a dissipative component, but has an exergy destruction share of 5.8 %. The results of the full flight mission analysis in

Table 6.3: Results of the exergy analysis of the bleed pack for taxi and cruise phases.

Component	Flight Phase: Taxi					
	$\dot{E}_{F,k}$ (kW)	$\dot{E}_{P,k}$ (kW)	$\dot{E}_{D,k}$ (kW)	ϵ_k (%)	y_k (%)	y_k^* (%)
turbine	54.159	34.787	19.372	64.2	35.8	42.2
compressor	27.096	23.832	3.265	88	12	7.1
PHX	19.832	8.613	11.219	43.4	56.6	24.5
MHX	7.833	0.237	7.596	3	97	16.6
reheater	0.968	0.218	0.75	22.5	77.5	1.6
condenser	0	0	2.645	0	0	5.8
fan	5.552	4.876	0.676	87.8	12.2	1.5
injection	0.006	0	0.006	0	100	0
extraction	0	0	0.33	0	0	0.7
TCV	0	0	0	0	0	0
dp	0	0	0	0	0	0
junction	0	0	0	0	0	0
System	59.595	0	45.859	0	77	100

Component	Flight Phase: Cruise					
	$\dot{E}_{F,k}$ (kW)	$\dot{E}_{P,k}$ (kW)	$\dot{E}_{D,k}$ (kW)	ϵ_k (%)	y_k (%)	y_k^* (%)
turbine	20.683	13.868	6.815	67	33	17.8
compressor	14.057	12.834	1.223	91.3	8.7	3.2
PHX	20.299	15.215	5.083	75	25	13.3
MHX	25.1	16.807	8.294	67	33	21.7
reheater	0.754	0.445	0.309	59	41	0.8
condenser	1.761	0.456	1.305	25.9	74.1	3.4
fan	0	0	0.798	0	0	2.1
injection	0	0	0	0	0	0
extraction	0	0	0	0	0	0
TCV	0	0	8.594	0	0	22.5
dp	0	0	0.046	0	0	0.1
junction	0	0	5.746	0	0	15
System	110.581	0	38.213	0	34.6	100

Figure 6.2 predicted already the poor performance for the MHX of 3 % exergy efficiency. The reheater works at 22.5 % exergetic efficiency, but has only a share of 1.6 % of the total exergy destruction. However, the PHX has low exergy efficiency of 43.5 % and cause 24.5 % of the total exergy destruction. The flows throught the temperature control valve and fan bypass valve (dP) are negligibly small and thus all values are zero for the taxi phase. In Section 4.1.4.2 the exergy balance on system was introduced and the bleed pack was identified as a dissipative component. Therefore, no exergy efficiency exists on system level. The total fuel exergy, the total exergy destruction, and the exergy destruction ratio

are listed in the results table. Concluding the bleed pack based on the taxi phase only, potential candidates for optimization would be the turbine, PHX, and MHX.

During cruise phase, the results of the exergy analysis show a different performance. The total exergy destruction decreased compared to the taxi phase by about 7.6 kW. The total fuel exergy almost doubled. Approximately 35 % of the total exergy destruction is caused by dissipative components (FAN, TCV, dP and JUN). This share can only be reduced by reducing the mass flow passing the components and optimizing the mixing conditions in the junction. Compared to the taxi phase, all productive components work at higher performances. The same three components as during taxi cause the major exergy destruction share, although the order changed. The exergy efficiency of the MHX has improved significantly. The turbine works at a slightly higher efficiency, but reduced its exergy destruction and the exergy destruction share by a factor of 2.5. The exergy efficiency of the compressor even increased up to 91.3 %. The PHX now works at 75 % and has a share of the total exergy destruction of 13.3 %. The REH and CON work at higher performance during cruise, although the exergy efficiency of the CON is still poor being 25.9 %. The exergy destruction ratio of the total system decreased to 34.6 %, but still does not have an exergetic product. Summarizing the cruise phase analysis, the same three components (MHX,TRB and PHX) are potential candidates for optimization, but with less empty space for improvement regarding the exergy efficiencies. Another important point is that about 35 % of exergy is destroyed within dissipative components. These losses can only be reduced by changing the performance conditions of the pack.

6.3.2 Electric Driven Vapor Cycle Pack

The thermodynamic cycles of the electric driven vapor cycle pack are shown in Figures 6.6 and 6.7. Both T-s diagrams are scaled to the same range. The temperature values on the ordinate are normalized. Compared to the cycles of the bleed air pack, the eVCP cycles differ significantly. The flow schematic of the eVCP was introduced in Figure 3.3. All numbers of the state points in the T-s diagrams refer to this figure.

The fresh air enters the pack at ambient conditions for both flight phases. The base compressor and pirmary heat exchanger are bypassed during ground conditions. The air is first conditioned within the ACM compressor $(3-4)$ and cooled inside the reheater $(4-5)$. Further cooling takes place in the MHX $(5-6)$ and the evaporator of the VaC $(6-7)$. The fresh air reaches the saturation point in the evaporator and the condensate is then extracted in the water extractor $(71-72)$. The dried air is heated in the reheater $(72-73)$ and expanded in the turbine $(73-74)$ before the fresh air is discharged to the mixing unit. For this particular taxi conditions, the eVCP operated in cooling mode. The ACM compressor works at almost isentropic conditions. Hardly any entropy is generated. The turbine, however, causes a larger entropy generation.

During cruise, the ambient air enters the pack at low temperature and low pressure. It is first compressed in the BCMP (1b-1c) and heated in the PHX $(1c-2)$. The ACM

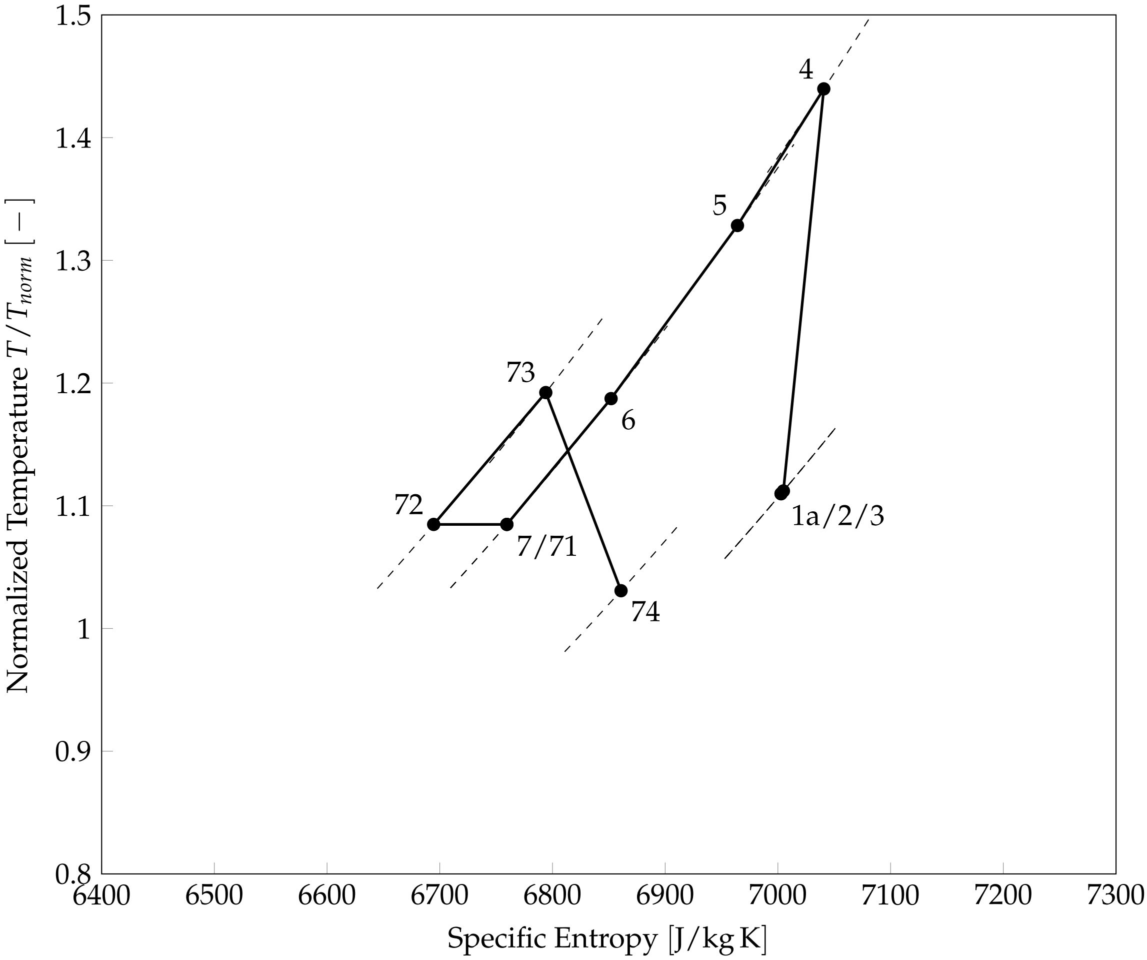

Figure 6.6: T-s diagram at taxi phase for the eVCP.

compressor increases the temperature and pressure level (3 − 4). The reheater (4 − 5) only causes a pressure drop what results in an entropy generation. The air is then cooled in the MHX (5 − 6) and VaC evaporator (6 − 7) before it is discharged to the mixing unit. The water separation loop (water extractor, reheater and turbine) is bypassed during cruise phase. Both compressors show again only little entropy generation.

Both thermodynamic cycles of the eVCP work at a smaller temperature and entropy range compared to the conventional bleed pack.

Exergy Results

Table 6.4 lists the results of the conventional exergy analysis for the eVCP architecture. Due to the large number of components, Table 6.4 contains only an extract with the main contributing components to the exergy analysis. The full table can be found in the appendix (Table C.2).

The main contributers to the total exergy destruction during taxi are the turbine (17.2 %) and the MHX (15.3 %) followed by the compressor, condenser and VaC compressor (all in the range 11.4 − 11.6 %). The reheater accounts for 9.4 %, the PHX for 7.3 % and the VaC

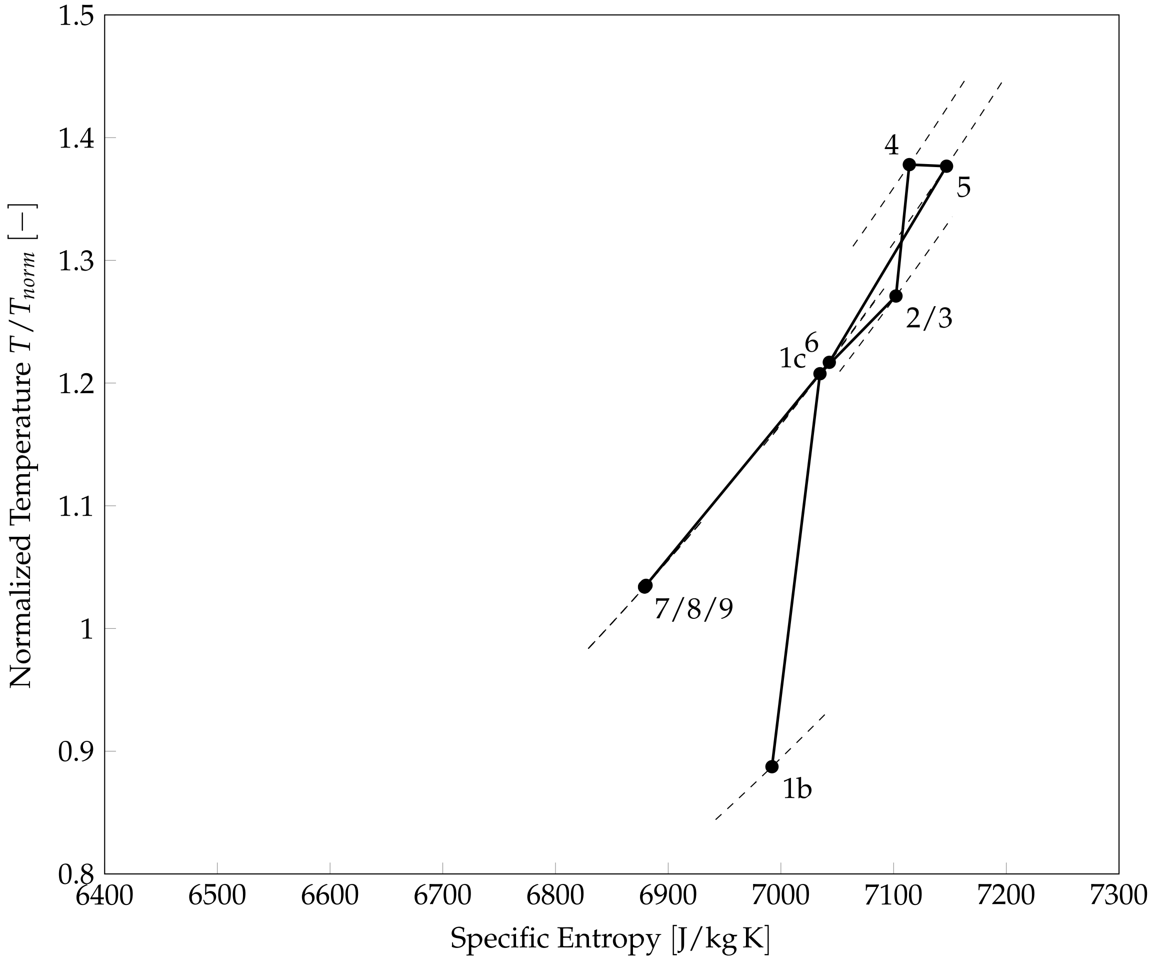

Figure 6.7: T-s diagram at cruise phase for the eVCP.

valve for 6.6 %. The remaining components have a share less than 5 % each for the taxi phase. Although the turbine accounts for the largest exergy destruction share, it works at an exergy efficiency of 80.1 %. Only the compressor and ram air fan have a higher exergetic efficiencies of more than 90 %. The vapor cycle compressor shows the lowest efficiency among the turbo components with 72.8 %. The heat exchangers in general show poor performances with the condenser having the highest efficiency with 39.9 %. The PHX work at only 1 % and the evaporator operates as a dissipative component during taxi. The base compressor and PHX are mainly bypassed during taxi and no pressure raise is provided by the compressor. The water separator is regarded as a dissipativ component in general, and the water injector operates in dissipative condition. Contrary to the conventionanl bleed pack, an exergetic product can be formulated for the eVCP on system level. During taxiing, the eVCP operates in the second case for the cooling mode (Table 4.7). That means that the fresh air enters the pack above the reference temperature and is cooled to a temperature lower than T_0. The exergetic efficiency on system level is 35.8 % during the taxi phase. Concerning optimization opportunities, one would start looking at the heat exchangers such as MHX, condenser and reheater. These three components account together for 36.1 %

Table 6.4: Results of the exergy analysis of the electric driven pack for taxi and cruise phases.

Component	Flight Phase: Taxi					
	$\dot{E}_{F,k}$ (kW)	$\dot{E}_{P,k}$ (kW)	$\dot{E}_{D,k}$ (kW)	ϵ_k (%)	y_k (%)	y_k^* (%)
MHX	7.922	2.276	5.646	28.7	71.3	15.3
evaporator	0	0	0.865	0	0	2.3
reheater	4.557	1.083	3.474	23.8	76.2	9.4
waterSeparator	0	0	0.244	0	0	0.7
waterInjector	0	0	0.84	0	0	2.3
fanRamAir	9.13	8.556	0.574	93.7	6.3	1.6
baseCompressor	0	0	0	0	0	0
turbine	31.986	25.635	6.35	80.1	19.9	17.2
PHX	2.716	0.028	2.688	1	99	7.3
compressor	45.544	41.346	4.198	90.8	9.2	11.4
condenser	6.996	2.791	4.205	39.9	60.1	11.4
VaCCMP	15.712	11.432	4.281	72.8	27.2	11.6
VaCsValve	0	0	2.427	0	0	6.6
System	70.582	25.273	36.946	35.8	52.3	100

Component	Flight Phase: Cruise					
	$\dot{E}_{F,k}$ (kW)	$\dot{E}_{P,k}$ (kW)	$\dot{E}_{D,k}$ (kW)	ϵ_k (%)	y_k (%)	y_k^* (%)
MHX	10.605	8.074	2.532	76.1	23.9	11
evaporator	7.402	4.547	2.855	61.4	38.6	12.4
reheater	1.658	0.048	1.609	2.9	97.1	7
waterSeparator	0	0	0	0	0	0
waterInjector	0	0	0	0	0	0
fanRamAir	0	0	0	0	0	0
baseCompressor	43.924	39.537	4.387	90	10	19
turbine	0	0	0	0	0	0
PHX	5.994	3.152	2.843	52.6	47.4	12.3
compressor	14.759	13.525	1.234	91.6	8.4	5.4
condenser	6.857	6.057	0.8	88.3	11.7	3.5
VaCCMP	2.796	2.297	0.498	82.2	17.8	2.2
VaCsValve	0.574	0.47	0.103	82	18	0.4
VenturiCompr	0	0	1.015	0	0	4.4
OzoneConv	0	0	1.085	0	0	4.7
PackVenturi	0	0	1.442	0	0	6.3
diffuser	0	0	2.431	0	0	10.5
System	61.479	32.357	23.045	52.6	37.5	100

of the total exergy destruction share and have high potential for increasing the exergetic efficiencies.

The cruise phase shows different performances for the system. The dissipative components account for a higher share of the total exergy destruction compared to the taxi

Figure 6.8: Ratios for unavoidable conditions for the conventional bleed pack.

Component	$\left(\frac{\dot{E}_D}{\dot{E}_P}\right)^{UN}$
turbine	0.254
compressor	0.010
PHX	0.145
MHX	0.45
reheater	0.283
condenser	1.463

phase. Regarding the productive components, the base compressor, PHX and evaporator cause the largest amount of exergy destruction with a share of 19 %, 12.3 % and 12.4 %. The MHX and reheater follow with 11 % and 7 %. During flight conditions, the water separation loop (71 − 74, Figure 3.3) and ram air fan are bypassed and thus do not impact the exergy analysis. The turbo components operate again at high exergetic efficiencies in the range of 82.2 % − 91.6 %. In general, the heat exchangers increased the exergetic performance significantly. Only the reheater works with poor performance at 2 % exergy efficiency. during flight conditions, only one side of the reheater is flown through as the other side is part of the water separation loop that is bypassed during cruise. The system balance shows an raise in exergetic efficiency of 16.8 % compared to taxi conditions. The total product exergy increased while the fuel exergy and exergy destruction decreased. The eVCP operates during cruise at the first case of the heating mode (Table 4.7). The total fuel exergy equals the electrical power supplied to the system. The results from the conventional exergy analysis represent in this case directly the energy conversion process from electrical power to conditioning of the fresh air flow. From an exergetic point of view, the evaporator and PHX are potential candidates for optimization.

6.4 Advanced Exergy Analysis

Within this thesis, the advanced exergy method is applied to the conventional bleed air driven pack. The exergy destruction of selected components is split into avoidable and unavoidable parts. The methodology for the splitting has been presented in Section 4.3.2.

The system model of the bleed pack was simulated for a full flight mission under the conditions of Section 6.2. The reference environment was set to ambient conditions. The simulation was performed six times for each component operating at its unavoidable conditions. The used efficiencies for the unavoidable conditions of each component are listed in Table 4.10. The unavoidable ratio $(\dot{E}_D/\dot{E}_P)^{UN}$ was calculated for each data point and the minimum was determined for the whole mission. The ratios for each component are listed in Table 6.8. For the application of the advanced exergy method only productive components are chosen. The fan works during cruise as a dissipative component and thus is not considered for the advanced analysis.

The ratios of the unavoidable conditions of Table 6.8 were then applied to the product exergy for the taxi and cruise phase following Equation 4.59. The results of the splitting of the exergy destruction into avoidable and unavoidable parts are displayed in Figure 6.9. Taxi and cruise phase are plotted next to each other. All components, except of the MHX show similar results for taxi and cruise phase. Approximately 50 % of the exergy destroyed within the turbine is avoidable during cruise phase and a little more during taxi. The unavoidable part of the destroyed exergy within compressor is similar during both flight phases. The percentage during cruise is higher as the total exergy destroyed is less during flight. The major part of the exergy destruction for PHX at taxiing is avoidable. During cruise it takes about 50 %. The MHX shows different results for taxi and cruise. During taxi, the unavoidable part is very low. However, in cruise conditions the major part of the exergy destruction is unavoidable. The results of the splitting for the MHX reflect the results from the mission based analysis (Figure 6.2) where the MHX operates at very low exergy efficiency during taxi and much higher efficiency during cruise. The avoidable part for the reheater takes almost the whole part of the exergy destruction during taxi and about half during cruise. For the condenser, the avoidable part has a higher share during taxi than during cruise.

The splitting into avoidable and unavoidable exergy destruction is an indication for the potential of optimization of the component. The results presented for the bleed air pack are extracts for two selected flight phases. The unavoidable parts determine the minimum possible amount of exergy destruction at the regarded phase compared to the best ratio of exergy destroyed to exergy of product at unavoidable conditions that the component achieved during the regarded flight mission. The results are therefore valid only for a specific flight mission.

With exception of the MHX at cruise phase, all components show a high potential for optimization. The graphic representation of Figure 6.9 directly indicates the best candidates for improvement. The turbine and PHX both cause the major share of exergy destruction during taxi and second most during cruise. The unavoidable parts each account for less than 50 % for taxi and cruise. A reduction of the destroyed exergy would have significant impact on the total exergy destruction on system level. The MHX causes the major share of destroyed exergy during cruise, but the avoidable part is small and thus the potential for improvement.

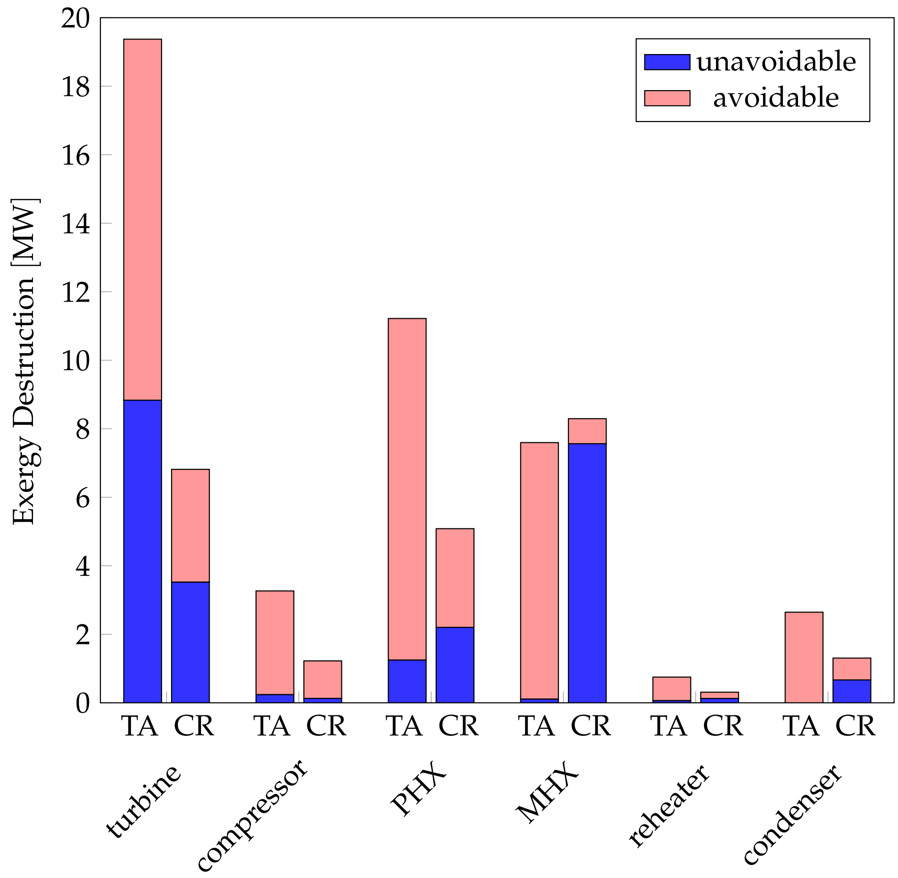

Figure 6.9: Results of the advanced exergy analysis for the bleed pack for taxi and cruise phases. The exergy destruction is split into its avoidable and unavoidable parts.

6.5 Exergoaeronautic Analysis

The exergoaeronautic methodology combines the traditional aircraft design parameters such as fuel weight penalties and extend it to the exergy of fuel consumption due to fuel weight penalties. Using Equation 4.56, the exergy of fuel consumption caused by weight, shaft power off-take, drag and bleed air extraction can be measured individually. The detailed approach has been presented in Section 4.2. Within this thesis, the exergoaeronautic approach is applied to both pack architectures for the cruise phase.

6.5.1 Conventional Bleed Air Driven Pack

In Section 2.3.3, an example application of the fuel weight penalties has been presented for the conventional bleed air pack. The considered cruise phase (see Table 6.1) slightly varies from the application example. The results for the regarded cruise case are illustrated in Figure 6.10. The major part of the additional fuel weight is caused by the bleed air extraction. The ram air accounts for slightly more fuel than the system weight. The individual weights of the components are displayed in the right part of the figure.

Figure 6.11 displays the results of the exergoaeronautic analysis for the bleed pack during cruise phase. The bleed pack is not supplied with any additional shaft power. The

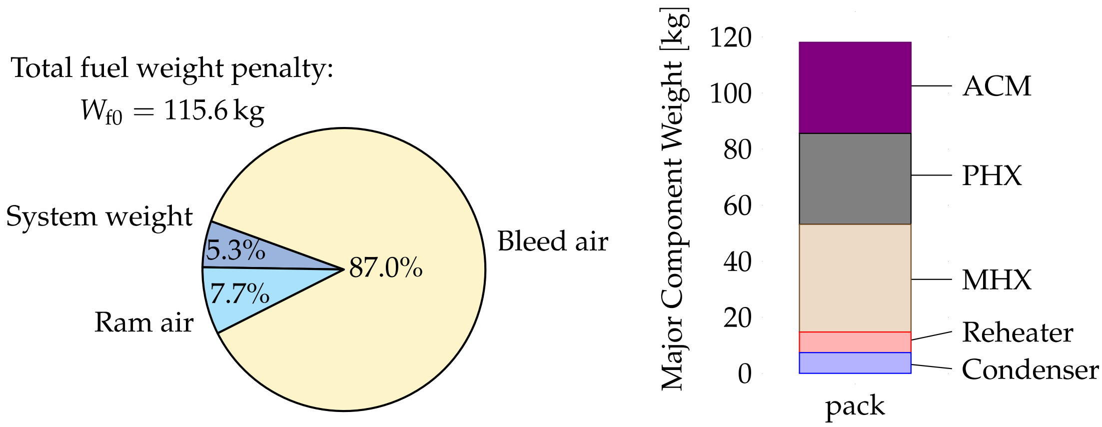

Figure 6.10: Distribution of fuel weight penalties during cruise phase and major component weights of the conventional bleed pack.

value for the exergy of fuel consumption due to shaft power off-take is therefore zero. The percentage share for weight, drag and bleed complies with the distribution of the fuel weight penalties in Figure 6.10. These results can now be combined with the results of the conventional exergy analysis.

The exergy flow of fuel consumption for bleed air constitutes the exergy flow that is needed to provide the bleed air mass flow at the pack inlet. The exergy of the entering bleed air expresses the fuel exergy of the pack system balance (see Equation 4.25). Table 6.5 lists the numbers of the exergy of fuel consumption due to bleed air split into further parts. Before the bleed air enters the pack it passes the engine bleed air system (EBAS) [13] where it loses 86.1 % of the exergy of fuel consumption. The remaining 13.9 % enter the bleed pack in form of bleed air which is assigned as fuel exergy within the system balance. The fuel exergy supplied to the pack balance is then divided into exergy of losses and

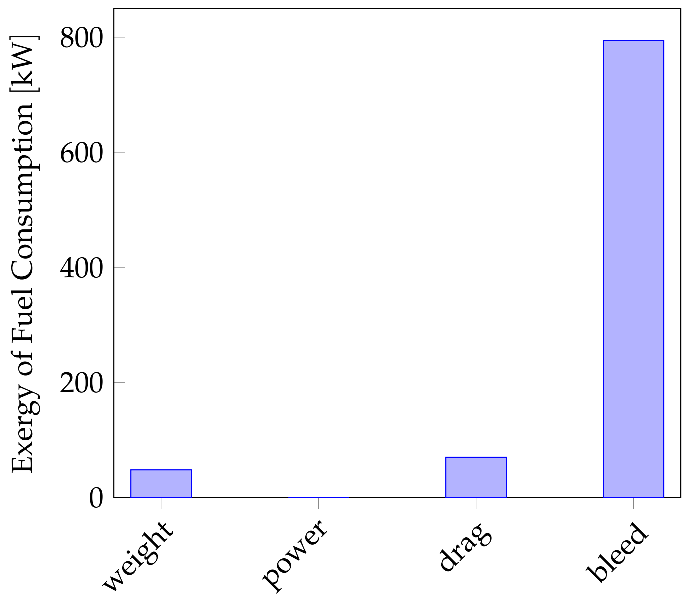

Figure 6.11: Exergy of fuel consumption during cruise for the conventional bleed pack.

exergy destruction. From an exergetic point of view, no product exergy can be identified for the conventional bleed pack. The losses are therefore listed separately into the exergy that is transferred to the ram air flow and the part that is stored within the exiting bleed air flow. The results show that 3.5 % of the exergy of fuel consumption is discharged to the ambient within the ram air. 5.6 % of $\dot{E}^{\mathrm{B}}_{\mathrm{FC}}$ leave the pack as conditioned bleed air ducted to the mixing unit. The remaining 4.8 % account for the exergy destruction within the pack due to irreversibilities.

Table 6.5: Exergy flow of the fuel consumption due to bleed air split into further parts.

$\dot{E}^{\mathrm{B}}_{\mathrm{FC}}$ (kW)		$\dot{E}^{\mathrm{B,\,loss}}_{\mathrm{FC}}$ (kW)		$\dot{E}^{\mathrm{B,\,pack}}_{\mathrm{FC}} = \dot{E}_{\mathrm{F,tot}}$ (kW)				
793.93	(100 %)	683.35	(86.1 %)	110.58	(13.9 %)	$\dot{E}_{\mathrm{D,\,tot}}$	38.21	(4.8 %)
						$\dot{E}_{\mathrm{L,\,ram}}$	27.64	(3.5 %)
						$\dot{E}_{\mathrm{L,\,bleed}}$	44.73	(5.6 %)

The exergy flow of fuel consumption due to bleed air off-take accounts for 87 % of the total exergy of fuel consumption induced by fuel weight penalties due to air conditioning. Combining this method with the conventional exergy analysis, the impact of the exergy destruction within the pack to the total exergy of fuel consumption can be measured. For a cruise mission time of 1.5 h, the exergy destruction due to thermodynamic irreversibilities accounts for 4.18 % of the total fuel required for the ECS.

6.5.2 Electric Driven Vapor Cycle Pack

Electric driven vapor cycle pack architectures are currently under development and will be used for future aircraft. Valid data concerning mass and component performance are barely or not available. The values of the results shall therefore be regarded as exemplary numbers. The application of the methodology is paramount for the example of the electric driven pack.

The electric driven vapor cycle pack is supplied with air from the ambient instead of bleed air. The turbo components are driven by electrical motors. The distribution of the different fuel weight penalties for the cruise phase in Figure 6.12 is more balanced. In this case, the ram air takes the largest share followed by the power off-take and fuel weight penalty for system weight. Although a great uncertainty is assumed, the amount of total fuel weight penalty for the eVCP decreased significantly compared to the bleed pack.

The power demanded from the turbo components and produced power by the turbine are plotted in Figure 6.13. The results are given in absolute values for clarity reasons. The different modes for taxi and cruise phase are illustrated. During taxi, the BCMP is bypassed and during cruise, the fan and TRB are bypassed. The CMP operates at different conditions during taxi and cruise. It demands for about 2.5 times higher power during taxi. In general, the power demand during taxi is higher than during cruise, even if the generated power from the turbine is supplied to the turbo components.

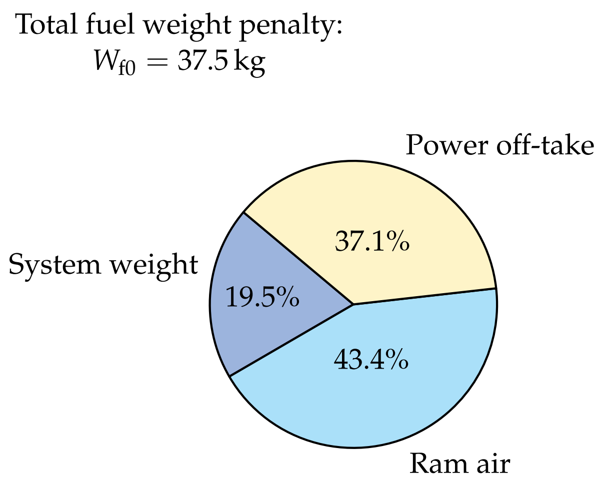

Figure 6.12: Distribution of fuel weight penalties for the electric driven vapor cycle pack at the cruise phase.

Figure 6.14 displays the results of the exergoaeronautic analysis for the eVCP during cruise phase. The electric pack is not supplied with bleed air. The value for the exergy of fuel consumption due to bleed air off-take is therefore zero. The percentage share for weight, drag and shaft power off-take complies with the distribution of the fuel weight penalties in Figure 6.12. These results can now be combined with the results of the conventional exergy analysis.

The exergy flow of fuel consumption for shaft power off-take constitutes the exergy flow that is needed to power the turbo components of the eVCP. The pack operates in heating mode at case 1 of Table 4.7 and the fuel exergy of the total system equals the power demanded by the turbo components. Table 6.6 shows the exergy of fuel consumption due

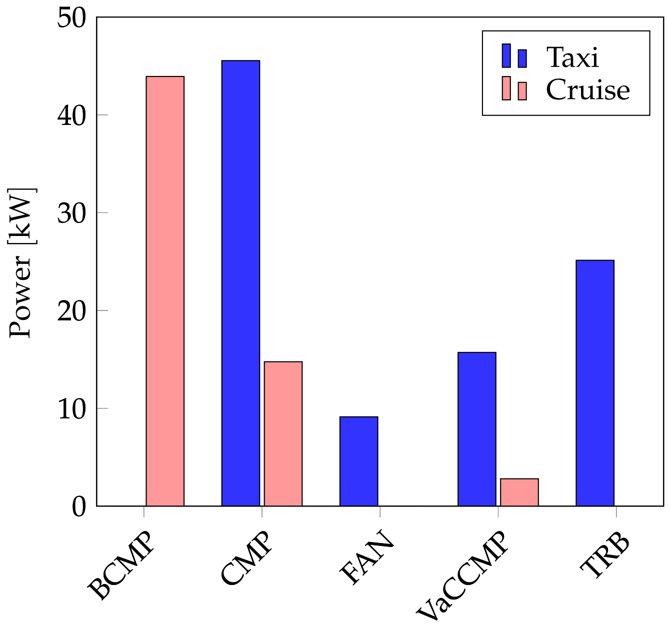

Figure 6.13: Electrical power consumption of turbo components for eVCP during taxi and cruise. (All values are given in absolute numbers)

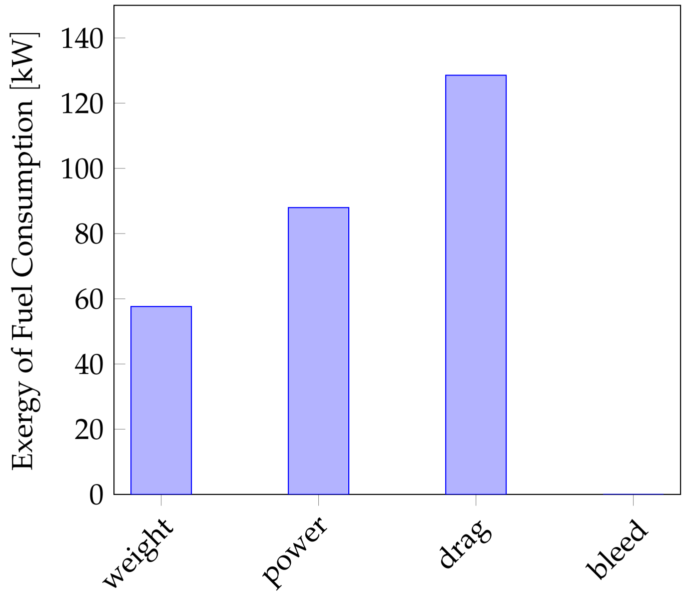

Figure 6.14: Exergy of fuel consumption during cruise for the electric driven vapor cycle pack.

Table 6.6: Exergy flow of fuel consumption due to shaft power off-take split into further parts.

$\dot{E}^{\mathrm{P}}_{\mathrm{FC}}$ (kW)	$\dot{E}^{\mathrm{P,\,loss}}_{\mathrm{FC}}$ (kW)	$\dot{E}^{\mathrm{P,\,pack}}_{\mathrm{FC}} = \dot{E}_{\mathrm{F,tot}}$ (kW)		
87.97 (100 %)	26.49 (30.1 %)	61.48 (69.9 %)	$\dot{E}_{\mathrm{D,\,tot}}$	23.05 (26.20 %)
			$\dot{E}_{\mathrm{L}}$	6.08 (6.91 %)
			$\dot{E}_{\mathrm{P}}$	32.36 (36.78 %)

to power off-take linked to the system balance of conventional exergy analysis. $\dot{E}^{\mathrm{P}}_{\mathrm{FC}}$ is split into the exergy of power that actually is supplied to the pack in form of fuel exergy and the losses $\dot{E}^{\mathrm{P,\,loss}}_{\mathrm{FC}}$ caused during the energy conversion process in the engine. 69.9 % of the exergy of fuel consumption remains as fuel exergy for the pack. This is a much higher percentage than the fuel exergy provided to the conventional bleed pack (13.9 %). The system balances further shows that 26.2 % is destroyed due to irreversibilities, 6.91 % discharged to the ambient with the ram air and 36.78 % finally account for an exergetic product. The product exergy includes the conditioning of the fresh air and the produced power of the turbine. Compared to the bleed pack, the eVCP shows a 6.5 times higher exergetic performance in terms of product exergy, respectively exergy of the leaving air of the bleed pack compared to the exergy of fuel consumption. The exergy destruction within the eVCP accounts for about one quarter. Taking the results of Table 6.4 into account, there is potential for reducing the share of the exergy destruction by improving the evaporator, PHX and MHX.

The exergoaeronautical methodology links the conventional exergy-based method and the fuel weight penalties due to air conditioning. This approach allows to measure the costs for the thermodynamic inefficiencies within the pack in terms of exergy of fuel consumption and evaluate the exergetic performance on aircraft level.

6.6 Combination of Exergy Methods

The final step is now the combination of the conventional exergy analysis, exergoaeronautic analysis and advanced exergy analysis. In the previous section, the link from the conventional exergy analysis to fuel consumption on aircraft level was made. The share of the total exergy destruction within the system to the exergy of fuel consumption was identified. Adding now the advanced exergy analysis, one can give a real assessment of the potential for optimization of the system.

The results of the advanced exergy analysis for the conventional bleed pack in Section 6.4 is combined with the results of the exergoaeronautic analysis in Table 6.5. The fuel exergy for the bleed air pack is stored within the bleed air. The exergy of fuel consumption due to bleed air off-take was calculated and broken down to the system balance of the pack.

Table 6.7 lists the results of the combination of the three exergy-based methods. This approach now gives real information about the potential for optimization. The first three columns are the results of the conventional exergy analysis. Further the ratios of the avoidable and unavoidable parts to the exergy destruction are written. The next column sets the avoidable part in relation to the total exergy destruction. The last three columns show the combination of the exergoaeronautic, conventional exergy analysis and advanced exergy analysis. The percentage shares in the last column identify the potential impact of component optimization on the total exergy of fuel consumption due to the environmental control system.

Table 6.7: Results of the conventional bleed air driven pack for the combination of conventional exergy, advanced exergy and exergoaeronautical analysis.

	Conventional Exergy Analysis			Advanced Exergy Analysis			Combination		
Component	$\dot{E}_{D,k}$ (kW)	ϵ_k (%)	y^*_k (%)	$\frac{\dot{E}^{AV}_{D,k}}{\dot{E}_{D,k}}$ (%)	$\frac{\dot{E}^{UN}_{D,k}}{\dot{E}_{D,k}}$ (%)	$\frac{\dot{E}^{AV}_{D,k}}{\dot{E}_{D,\,tot}}$ (%)	$\frac{\dot{E}_{D,k}}{\dot{E}^{B}_{FC}}$ (%)	$\frac{\dot{E}^{AV}_{D,k}}{\dot{E}^{B}_{FC}}$ (%)	$\frac{\dot{E}^{AV}_{D,k}}{\dot{E}_{FC}}$ (%)
turbine	6.815	67.00	17.80	48.33	51.67	8.62	0.86	0.41	0.36
compressor	1.223	91.30	3.20	89.53	10.47	2.87	0.15	0.14	0.12
PHX	5.083	75.00	13.30	56.68	43.32	7.54	0.64	0.36	0.32
MHX	8.294	67.00	21.70	8.82	91.18	1.91	1.04	0.09	0.08
reheater	0.309	59.00	0.80	59.26	40.74	0.48	0.04	0.02	0.02
condenser	1.305	25.90	3.40	48.88	51.12	1.67	0.16	0.08	0.07
system	38.213	0.00	100.00	23.09	76.91	23.09	4.81	1.11	0.97

Chapter 7

Conclusions & Outlook

Within this thesis, existing exergy-based methods were adapted to aircraft environmental control systems (ECS) and a new methodology was developed to combine exergy analysis with traditional aircraft design parameters. Further, the integration of exergy analysis into a model-based design environment was realized.

The requirements for the application of exergy analysis to aircraft ECS were derived from the particular boundary conditions for aircraft. Based on these findings, a formulation of the exergy balances following the fuel and product approach was developed on component and system level for a conventional bleed air driven pack (bleed pack) architecture and an electric driven vapor cycle pack (eVCP) architecture. A particular focus was put on the splitting of the exergy stream into thermal, mechanical and chemical parts. A formulation for the chemical exergy of moist air was developed with respect to any possible reference environment that allows both the working fluid and reference environment to be in unsaturated, saturated or fog region. A recommendation on how to define the reference environment was developed based on simulation case studies on exergy analysis for a full flight mission and the definition of exergy balances for the electric driven vapor cycle pack.

A methodology was developed to link fuel weight penalties due to air conditioning with the conventional exergy analysis. This allows the assessment of the exergetic performance of the ECS on aircraft level and to measure the impact on exergy of fuel consumption. The exergy of aviation fuel is described with available equations that consider the reference environment. Further, a methodology was developed for the splitting of the exergy destruction into avoidable and unavoidable parts. The advanced exergy analysis combined with the new methodology can not only locate the inefficiencies in the system components, but gives information about the real potential for optimization and the impact on aircraft level in terms of fuel consumption related to the environmental control system.

Within the frame of this thesis, an exergy library based on the object-oriented, equation-based modeling language Modelica was developed. This library provides the capability to integrate exergy analysis into thermo-fluid systems. Sensor models for typical components of an aircraft ECS contain the appropriate exergy balances and can be integrated into the component models of the thermo-fluid system. The exergy analysis is then performed during simulation for each component and on system level. The advantage of this approach is that the formulation of the exergy balances does not have to be provided for each component. The balances are calculated automatically taking into account the operation conditions of the individual component and the globally defined reference environment.

The developed methods were applied to both the bleed pack architecture and the eVCP architecture to show the applicability and the advantages of the obtainable results. The potential for reducing the exergy destructions of the individual component was identified and the impact of this improvement could be measured on aircraft level in terms of fuel consumption.

This thesis makes a valuable contribution to the adaption of exergy-based methods to aircraft environmental control system. Unfortunately, not all open questions could be answered. To close this thesis, a short outlook is given to name unsolved problems that could further improve the evaluation of aircraft ECS using exergy-based methods.

This thesis provides methods to link exergy analysis for ECS with fuel weight penalties on aircraft level and to identify which of the thermodynamic losses are avoidable or unavoidable. Unfortunately, the origin of these losses are not taken into account. Advanced exergy based analysis provides besides the identification of avoidable and unavoidable losses, methods which illustrate the interactions between the components. In view of the increasing complexity for future ECS architectures, interdependencies should be understood to support the design process and further improve the system efficiency. Splitting the exergy destruction into endogenous and exogenous parts can give such information. However, the application of this part of the advanced exergy analysis is not trivial for complex systems. Ideal conditions have to be defined for individual components and parts of the system. Currently, there are no methods available to realize such analyses for aircraft ECS in the frame of model-based environments and therefore this scientific problem remains unsolved.

Exergoeconomic and exergoenvironmental analyses combine the conventional exergy analysis with costs and environmental impact factors. The application of these methods to environmental control systems could provide valuable information to support improving the ECS in terms of operational and longterm costs as well as adding the aspect of sustainability to the design process.

There is one last remark. Exergy analysis is mostly applied from an academic point of view. The same applies for this thesis. Unfortunately, exergy-based methods are rarely present in industrial design processes, although it is seen as a powerful tool. There are several research groups around the world working on exergy-based methods for different fields of applications using different definitions and conventions. One first step could be to find a common standard and understanding of exergy analysis to support bringing exergy to the industry. The aircraft industry's trend towards more integrated design processes such as the model-based system engineering provides a great opportunity to establish the exergy analysis within the industry.

Bibliography

[1] ACARE. FlightPath 2050 Goals; 2017. Available from: http://www.acare4europe.org/sria/flightpath-2050-goals.

[2] Sielemann M, Giese T, Oehler B, Otter M. A flexible toolkit for the design of environmental control system architectures; 2007. Berlin. In: Proceedings of the First CEAS European Air and Space Conference.

[3] L Faleiro. Beyond the more electric aircraft. Aerospace America. 2005;p. 35–40.

[4] Lehle W, Sauterleute A. Konzeption und Entwicklung von Flugzeugklimatisierungsanlagen. Praxis-Seminar Luftfahrt, Hamburg; 01. Juni 2006.

[5] Schlabe D, Lienig J. Modellbasierte Entwicklung von Energiemanagement-Methoden für Flugzeug-Energiesysteme [Dissertation]. Technische Universität Dresden. Dresden; 2015. Available from: http://nbn-resolving.de/urn:nbn:de:bsz:14-qucosa-217893.

[6] Jones RI. The More Electric Aircraft: The past and the future? In: IEE Colloquium. Electrical Machines and Systems for the More Electric Aircraft. IEE; 1999. p. 1.

[7] Cutts SJ. A collaborative approach to the More Electric Aircraft. In: International Conference on Power Electronics Machines and Drives. IEE; 2002. p. 223–228.

[8] Rosero JA, Ortega JA, Aldabas E, Romeral L. Moving towards a more electric aircraft. IEEE Aerospace and Electronic Systems Magazine. 2007;22(3):3–9.

[9] Wheeler PW, Clare JC, Trentin A, Bozhko S. An overview of the more electrical aircraft. Proceedings of the Institution of Mechanical Engineers, Part G: Journal of Aerospace Engineering. 2013;227(4):578–585.

[10] Bals J, Hofer G, Pfeiffer A, Schallert C. Object-Oriented Inverse Modelling of Multi-Domain Aircraft Equipment Systems with Modelica. In: The Modelica Association, editor. Proceedings of the 3rd International Modelica Conference; 2003. p. 377–384.

[11] Schallert C, Pfeiffer A, Bals J. Generator Power Optimisation for a More-Electric Aircraft by Use of a Virtual Iron Bird; 2006. In: ICAS 2006 proceedings.

[12] Denti E, Schettini F, Di Rito G. A Tool for the Simulation of All-Electric Aircraft Systems. Aerotecnica Missili & Spazio. 2016;93(1-2):33–40. Available from: http://www.aerotecnica.eu/index.php/AMS/article/view/108.

[13] Pollok A. Modelling and Control of Aircraft Environmental Control Systems [Phd Thesis]. Politecnico di Milano; 2018. Available from: https://elib.dlr.de/119309/.

[14] Pellegrini LF, Gandolfi R, Da Silva GA, De Oliveira S. Exergy analysis as a tool for decision making in aircraft systems design. In: 45th AIAA Aerospace Sciences Meeting and Exhibit. vol. 23; 2007. p. 16485–16496.

[15] Muñoz J. Optimization Strategies for the Synthesis / Design of Highly Coupled, Highly Dynamic Energy Systems [Dissertation]. Blacksburg, VA; 2000.

[16] Bejan A, Tsatsaronis G, Moran MJ. Thermal design and optimization. A Wiley-Interscience publication. New York: Wiley; 1996. Available from: `http://www.loc.gov/catdir/description/wiley032/95012071.html`.

[17] Tipton R, Figliola RS, Ochterbeck JM. Thermal Optimization of the ECS on an Advanced Aircraft with an Emphasis on System Efficiency and Design Methodology; 1997. In: SAE Aerospace Power Systems Conference Proceedings.

[18] Bender D. Integration of exergy analysis into model-based design and evaluation of aircraft environmental control systems. Energy. 2017;137:739–751.

[19] Hunt EH, Reid DH, Space DR, Tilton FD. Commercial Airliner Environmental Control System: Engineering Aspects of Cabin Air Quality; 1995. Aerospace Medical Association annual meeting.

[20] Pollok A, Bender D, Kerling I, Zimmer D. Rapid development of an aircraft cabin temperature regulation concept; 2017. In: 12th International Modelica Conference 2017. Available from: `https://elib.dlr.de/118417/`.

[21] Sinnett M. 787 No-Bleed systems: saving fuel and enhancing operational efficiencies. AERO. 2007;(28).

[22] Schlabe D, Lienig J. Model-Based Thermal Management Functions for Aircraft Systems. SAE International400 Commonwealth Drive, Warrendale, PA, United States; 2014. SAE Aerospace Systems and Technology Conference.

[23] Sielemann M, Giese T, Oehler B, Gräber M. Optimization of an Unconventional Environmental Control System Architecture. SAE Int J Aerosp. 2011;4(2):1263–1275.

[24] Linnett K, Crabtree R. What's Next in Commercial Aircraft Environmental Control Systems?; 1993.

[25] The Modelica Association. The modelica language specification: Version 3.3. Online; 2013. Available from: `https://www.modelica.org/documents/ModelicaSpec33Revision1.pdf`.

[26] Limperich D, Braun M, Prölß K, Schmitz G. The Modelica Association, editor. System Simulation of Automative Refrigeration Cycles; 2005. Proceedings of the 4th International Modelica Conference.

[27] Alexander Pollok DZ. The Cryolib - Modelling Superconductors in Modelica; 2018. In: Proceedings of the 2nd Japanese Modelica Conference.

[28] Wetter M, Zuo W, Nouidui TS, Pang X. Modelica Buildings library. Journal of Building Performance Simulation. 2014;7(4):253–270.

[29] Zimmer D, Bender D, Pollok A. The Modelica Association, editor. Robust Modeling of Directed Thermofluid Flows in Complex Networks; 2018. In: Proceedings of the 2nd Japanese Modelica Conferences.

[30] Pfeiffer A. The Modelica Association, editor. Optimization library for interactive multi-criteria optimization tasks; 2012. In: Proceedings of the 9th International Modelica Conference.

[31] Bender D. DESA - Optimization of variable structure Modelica models using custom annotations. In: Casella F, Zimmer D, editors. Proceedings of the 7th International Workshop on Equation-Based Object-Oriented Modeling Languages and Tools - EOOLT '16. New York, New York, USA: ACM Press; 2016. p. 45–54.

[32] Wischhusen S, Lüdemann B, Schmitz G. The Modelica Association, editor. Economical Analysis of Complex Heating and Cooling Systems with the Simulation Tool HKSim; 2003. In: Proceedings of the 3rd International Modelica Conference.

[33] Zimmer D, Schlabe D. Implementation of a Modelica Library for Energy Management based on Economic Models. In: The Modelica Association, editor. Proceedings of the 9th International Modelica Conference; 2012. p. 133–142.

[34] Sanghi R, Pooyan J, Thamm A, Streblow R, Müller D. Dynamic Exergy Analysis - Part I: Modelica-Based Tool Development; 2014. Building Simulation and Optimization Conference.

[35] Transport, energy and CO2: Moving toward sustainability. Paris: OECD IEA; 2009. Available from: `http://site.ebrary.com/lib/alltitles/docDetail.action?docID=10355605`.

[36] Moorhouse DJ. Proposed System-Level Multidisciplinary Analysis Technique Based on Exergy Methods. Journal of aircraft. 2003;40(1):11–15.

[37] Figliola RS, Tipton R. An Exergy-Based Methodology for Decision-Based Design of Integrated Aircraft Thermal Systems. SAE International, 400 Commonwealth Drive, Warrendale, PA, United States; 2000. World Aviation Congress & Exposition.

[38] SAE International. SAE International, editor. Aircraft Fuel Weight Penalty Due to Air Conditioning; 2011.

[39] LONDON AL, SHAH RK. Costs of Irreversibilities in Heat Exchanger Design. Heat Transfer Engineering. 1983;4(2):59–73. Available from: `https://doi.org/10.1080/01457638108939603`.

[40] Sekulić DP, Herman CV. One approach to irreversibility minimization in compact crossflow heat exchanger design. International communications in heat and mass transfer. 1986;13(1):23–32.

[41] Poulikakos D, Johnson JM. Second law analysis of combined heat and mass transfer phenomena in external flow. Energy. 1989;14(2):67–73.

[42] Krane RJ. A Second Law analysis of the optimum design and operation of thermal energy storage systems. International Journal of Heat and Mass Transfer. 1987;30(1):43–57.

[43] Witte LC, Shamsundar N. A Thermodynamic Efficiency Concept for Heat Exchange Devices. Journal of Engineering for Power. 1983;105(1):199–203.

[44] Vargas JVC, Bejan A. Thermodynamic optimization of finned crossflow heat exchangers for aircraft environmental control systems. International Journal of Heat and Fluid Flow. 2001;22(6):657–665. Available from: `http://dx.doi.org/10.1016/S0142-727X(01)00129-1`.

[45] Vargas JVC, Bejan A. Integrative thermodynamic optimization of the environmental control system of an aircraft. International Journal of Heat and Mass Transfer. 2001;44(20):3907–3917. Available from: `http://dx.doi.org/10.1016/S0017-9310(01)00033-3`.

[46] Giese T, Oehler B, Sielemann M. A systematic approach to optimise conventional environmental control architectures; 2010. In: Deutscher Luft-und Raumfahrtkongress, Hamburg.

[47] Eurocontrol Experimental Centre EEC. User Manual for the Base of Aircraft Data (BADA): Revision 3.7; 2009.

[48] MTU Aero Engines GmbH. V2500 turbofan engine: The innovative power; n.d. Available from: `http://www.mtu.de/de/geschaeftsbereiche/zivil_neugeschaeft/Programme/v2500/brochure_v2500.pdf`.

[49] Dymola. Dassault Système; 2014. Available from: `http://www.3ds.com/products-services/catia/products/dymola`.

[50] Federal Aviation Administration FAA. 14 CFR Part 25; 2018.

[51] Pollok A, Bender D. Using multi-objective optimization to balance system-level model complexity. In: Proceedings of the 6th International Workshop on Equation-Based Object-Oriented Modeling Languages and Tools. ACM; 2014. p. 69–78.

[52] Pérez-Grande I, Leo TJ. Optimization of a commercial aircraft environmental control system. Applied Thermal Engineering. 2002;22(17):1885–1904. Available from: `http://dx.doi.org/10.1016/S1359-4311(02)00130-8`.

[53] Figliola RS, Tipton R, Li H. Exergy Approach to Decision-Based Design of Integrated Aircraft Thermal Systems. Journal of aircraft. 2003;40(1):49–55. Available from: `http://dx.doi.org/10.2514/2.3056`.

[54] Muñoz J, Spakovsky MRv. An Integrated Thermoeconomic Modeling and Optimization Strategy for Aircraft / Aerospace Energy System Design; 2000. Efficiency, Costs, Optimization, Simulation and Environmental Aspects of Energy Systems (ECOS).

[55] Muñoz J, Spakovsky Mv. The Application of Decomposition to the Large Scale Synthesis/Design Optimization of Aircraft Energy Systems. International Journal of Thermodynamics. 2001;4(2).

[56] Rancruel DF, Muñoz J, Spakovsky MRv. A Second Law Based Integrated Thermoeconomic Modeling and Optimization Strategy for Aircraft / Aerospace Energy System Synthesis and Design; 2001.

[57] Gandolfi R, Pellegrini LF, Silva G, de Oliveira Jr S. Aircraft air management systems trade-off study using exergy analysis as a design comparison tool; 2007. 19th International Congress of Mechanical Engineering.

[58] Gandolfi R, Pellegrini L, Silva G, Oliveira S. Exergy Analysis Applied to a Complete Flight Mission of Commercial Aircraft. 46th AIAA Aerospace Sciences Meeting and Exhibit. 2008;Available from: `http://dx.doi.org/10.2514/6.2008-153`.

[59] Gandolfi R, Pellegrini L, de Oliveira S. More Electric Aircraft Analysis Using Exergy As A Design Comparison Tool. 48th AIAA Aerospace Sciences Meeting Including the New Horizons Forum and Aerospace Exposition. 2010;Available from: `http://dx.doi.org/10.2514/6.2010-809`.

[60] Hayes D, Lone M, Whidborne JF, Camberos J, Coetzee E. Adopting exergy analysis for use in aerospace. Progress in Aerospace Sciences. 2017;93:73–94.

[61] Tsatsaronis G. Definitions and nomenclature in exergy analysis and exergoeconomics. Energy. 2007;32(4):249–253.

[62] Rosen MA, Dincer I. Effect of varying dead-state properties on energy and exergy analyses of thermal systems. International Journal of Thermal Sciences. 2004;43(2):121–133.

[63] Aljundi IH. Energy and exergy analysis of a steam power plant in Jordan. Applied Thermal Engineering. 2009;29(2-3):324–328.

[64] Acır A, Bilginsoy AK, Coşkun H. Investigation of varying dead state temperatures on energy and exergy efficiencies in thermal power plant. Journal of the Energy Institute. 2012;85(1):14–21.

[65] Sharma M, Singh O. Exergy analysis of the dual pressure HRSG for varying physical parameters. Applied Thermal Engineering. 2017;114:993–1001.

[66] Caliskan H, Tat ME, Hepbasli A. Performance assessment of an internal combustion engine at varying dead (reference) state temperatures. Applied Thermal Engineering. 2009;29(16):3431–3436.

[67] Baldi MG, Leoncini L. Effect of Reference State Characteristics on the Thermal Exergy Analysis of a Building. Energy Procedia. 2015;83:177–186.

[68] Etele J, Rosen MA. Sensitivity of exergy efficiencies of aerospace engines to reference environment selection. Exergy, An International Journal. 2001;1(2):91–99.

[69] Şöhret Y, Ekici S, Altuntaş Ö, Hepbasli A, Karakoç TH. Exergy as a useful tool for the performance assessment of aircraft gas turbine engines: A key review. Progress in Aerospace Sciences. 2016;83:57–69.

[70] Spakovsky MRv, Periannan V, Markell KC, Brewer K M . Virginis Tech, editor. The Use of Exergy and Decomposition Techniques in the Development of Generic Analysis and Optimization Methodologies Applicable to the Synthesis/Design of Aircraft/Aerospace Systems; 2006.

[71] Morosuk T, Tsatsaronis G. Strengths and Limitations of Advanced Exergetic Analyses. In: ASME 2013 International Mechanical Engineering Congress and Exposition; 2013. Available from: `http://proceedings.asmedigitalcollection.asme.org/proceeding.aspx?articleid=1858407`.

[72] Morosuk T, Tsatsaronis G. A new approach to the exergy analysis of absorption refrigeration machines. Energy. 2008;33(6):890–907.

[73] Morosuk T, Tsatsaronis G. How to Calculate the Parts of Exergy Destruction in an Advanced Exergetic Analysis. In: Ziębik A, Szmyd J, Kolenda Z, editors. ECOS 2008. Silesian University of Technology; 2008. p. 185–194.

[74] Tsatsaronis G, Morosuk T. Advanced thermodynamic (exergetic) analysis. Journal of Physics: Conference Series. 2012;395 012160. Available from: `http://dx.doi.org/10.1088/1742-6596/395/1/012160`.

[75] Wang L, Yang Y, Morosuk T, Tsatsaronis G. Advanced Thermodynamic Analysis and Evaluation of a Supercritical Power Plant. Energies. 2012;5(12):1850–1863. Available from: `http://dx.doi.org/10.3390/en5061850`.

[76] Morosuk T, Tsatsaronis G. Advanced exergetic evaluation of refrigeration machines using different working fluids. Energy. 2009;34(12):2248–2258. Available from: `http://dx.doi.org/10.1016/j.energy.2009.01.006`.

[77] Mosaffa AH, Garousi Farshi L, Infante Ferreira CA, Rosen MA. Advanced exergy analysis of an air conditioning system incorporating thermal energy storage. Energy. 2014;77:945–952.

[78] Tesch S, Morosuk T, Tsatsaronis G. Advanced exergy analysis applied to the process of regasification of LNG (liquefied natural gas) integrated into an air separation process. Energy. 2016;117:550–561.

[79] Morosuk T, Tesch S, Tsatsaronis G. In: Al-Megren HA, Altamimi RH, editors. Concepts for Regasification of LNG in Industrial Parks. InTech; 2017. .

[80] Balli O. Advanced exergy analyses to evaluate the performance of a military aircraft turbojet engine (TJE) with afterburner system: Splitting exergy destruction into unavoidable/avoidable and endogenous/exogenous. Applied Thermal Engineering. 2017;111:152–169.

[81] Balli O. Advanced exergy analyses of an aircraft turboprop engine (TPE). Energy. 2017;124:599–612.

[82] Tsatsaronis G, Winhold M. Exergoeconomic analysis and evaluation of energy-conversion plants—I. A new general methodology. Energy. 1985;10(1):69–80.

[83] Lazzaretto A, Tsatsaronis G. SPECO: A systematic and general methodology for calculating efficiencies and costs in thermal systems. Energy. 2006;31(8-9):1257–1289.

[84] Tsatsaronis G, Morosuk T. Exergy-based methods applied to the chain natural gas – LNG – natural gas; 2013. Proceedings of the 3rd International Exergy, Life Cycle Assessment, and Sustainability Workshop & Symposium (ELCAS3).

[85] Golle S, Hesse U, Klausner E, Klimpel F, Brunswig H, Raddatz M, inventors; Betriebsphasenabhängig steuerbare Flugzeugklimaanlage und Verfahren zum Betreiben einer derartigen Flugzeugklimaanlage. DE 10 2015 207 447 A1; 2016.

[86] Baehr HD, Kabelac S. Thermodynamik Grundlagen und technische Anwendungen: Mit zahlreichen Tabellen. 12th ed. Springer-Lehrbuch. Berlin, Heidelberg: Springer-Verlag Berlin Heidelberg; 2005. Available from: http://dx.doi.org/10.1007/b138786.

[87] Morosuk T, Tsatsaronis G. Energy Engineering I - Notes for the class; 2016.

[88] Tsatsaronis G, Cziesla F. Thermoeconomics. In: Encyclopedia of Physical Science and Technology. Elsevier; 2003. p. 659–680.

[89] Tsatsaronis G, Cziesla F . Encyclopedia of Life Support Systems, editor. Exergy Analysis of Simple Processes; 2004. Available from: www.eolss.net.

[90] Kotas TJ. The exergy method of thermal plant analysis. Reprint ed. with corr. and new app. g ed. Malabar, FL: Krieger Pub; 1995.

[91] Ahrendts J. Reference states. Energy. 1980;5(8-9):666–677.

[92] Szargut J, Morris DR, Steward FR. Exergy analysis of thermal, chemical and metallurgical processes. New York NY u.a.: Hemisphere Publishing Company; 1988.

[93] Bejan A, Siems DL. The need for exergy analysis and thermodynamic optimization in aircraft development. Exergy, An International Journal. 2001;1(1):14–24.

[94] Muñoz J, von Spakovsky MR. Decomposition in Energy System Synthesis/Design Optimization for Stationary and Aerospace Applications. Journal of aircraft. 2003;40(1):35–42.

[95] Roth B. The Role of Thermodynamic Work Potential in Aerospace Vehicle Design; 2003. XVI International Symposium of Air Breathing Engines (ISABE).

[96] Rancruel DF, von Spakovsky MR. Decomposition with Thermoeconomic Isolation Applied to the Optimal Synthesis/Design of an Advanced Tactical Aircraft System. International Journal of Thermodynamics. 2003;6(3):93–105.

[97] Coordinating Research Council S. Aviation Fuel Properties; 1983.

[98] Ahrendts J. Die Exergie chemisch reaktionsfähiger Systeme: Mit 18 Tafeln: Teilw. zugl.: Bochum, Univ., Diss., 1974. vol. 579 of VDI-Forschungsheft. Düsseldorf: VDI-Verl.; 1977.

[99] Edwards T, Maurice LQ. Surrogate Mixtures to Represent Complex Aviation and Rocket Fuels. Journal of Propulsion and Power. 2001;17(2):461–466.

[100] Huber ML, Lemmon EW, Bruno TJ. Surrogate Mixture Models for the Thermophysical Properties of Aviation Fuel Jet-A. Energy & Fuels. 2010;24(6):3565–3571.

[101] Clarke JM, Horlock JH. Availability and Propulsion. Journal of Mechanical Engineering Science. 1975;17(4):223–232.

[102] Haywood RW. A Critical Review of the Theorems of Thermodynamic Availability, with Concise Formulations. Journal of Mechanical Engineering Science. 1974;16(3):160–173.

[103] Rossini FD. Selected values of chemical thermodynamic properties. Circular of the National Bureau of Standards500. Washington: U.S. Govt. Print. Off; 1952.

[104] Rossini FD, Institute AP. Selected Values of Physical and Thermodynamic Properties of Hydrocarbons and Related Compounds: Comprising the Tables of the American Petroleum Institute. American Petroleum Institute Washington, DC. American Petroleum Institute; 1953. Available from: `https://books.google.de/books?id=7nsFAQAAIAAJ`.

[105] Taylor HS, Glasstone S. A Treatise on Physical Chemistry. Second edition. 1st ed. Van Nostrand; 1952.

[106] McBride BJ, Zehe MJ, Gordon S. NASA Glenn Coefficients for Calculating Thermodynamic Properties of Individual Species. Cleveland, Ohio; 2002. Available from: `https://www.grc.nasa.gov/WWW/CEAWeb/TP-2002-211556.pdf`.

[107] Royal Society, London. Quantities, units and symbols; 1971.

[108] Shafer L, Striebich R, Gomach J, Edwards T. Chemical Class Composition of Commercial Jet Fuels and Other Specialty Kerosene Fuels. American Institute of Aeronautics and Astronautics; 2006. 14th AIAA/AHI Space Planes and Hypersonic Systems and Technologies Conference.

[109] Gracia-Salcedo CM, McBride BJ, Brabbs TA. Experimental Verification of the Thermodynamic Properties of a Jet-A Fuel. Cleveland, Ohio; 1988. NASA Lewis Research Center.

[110] Faith LE, Ackerman GH, Henderson HT. Heat sink capability of jet A fuel - Heat transfer and coking studies. Cleveland, Ohio; 1971. Available from: `https://ntrs.nasa.gov/search.jsp?R=19710022006`.

[111] Gordon S, McBride BJ. Computer Program for Calculation of Complex Chemical Equilibrium Compositions, Rocket Performance, Incident and Reflected Shocks, and Chapman-Jouguet Detonations. Cleveland, Ohio; 1976. Available from: `https://ntrs.nasa.gov/search.jsp?R=19780009781&hterms=NASA+SP-273&qs=N%3D0%26Ntk%3DAll%26Ntt%3DNASA%2520SP-273%26Ntx%3Dmode%2520matchallpartial`.

[112] Tsatsaronis G, Park MH. On avoidable and unavoidable exergy destructions and investment costs in thermal systems. Energy Conversion and Management. 2002;43(9-12):1259–1270.

[113] Dardour H, Mazouz S, Bellagi A. Numerical Analysis of Plate Heat Exchanger Performance in Co-Current Fluid Flow Configuration. International Journal of Mathematical, Computational, Physical, Electrical and Computer Engineering, volume = 3. 2009;(3):213–217. Available from: `http://waset.org/Publications?p=27`.

[114] The Modelica Association. Modelica Libraries; 2018. Available from: `https://www.modelica.org/libraries`.

[115] Casella F, Otter M, Proelss K, Richter C, Tummescheit H. The Modelica Fluid and Media Library for Modeling of Incompressible and Compressible Thermo-Fluid Pipe Networks. In: 5th International Modelica Conference; 2006. p. 631–640. Available from: http://elib.dlr.de/47217/.

[116] Casella F, Otter M. Overview and Rationale for Modelica Stream Connectors; 2009. Available from: https://build.openmodelica.org/Documentation/Modelica%203.2.2/Resources/Documentation/Fluid/Stream-Connectors-Overview-Rationale.pdf.

[117] Idelčik IE. Handbook of hydraulic resistance. 3rd ed. Mumbai: Jaico Publ. House; 2008.

[118] Widhammer A. ASILib_AmbientConditions library: JTI – CleanSky WP 2.1.2 USE CASE: Development of a modular Energy System Simulation Tool Chain: Projektbericht, DLR; 2010.

[119] International Organization for Standardization. Standard Atmosphere; 1975.

[120] Hellerer M, Buse F. Compile-time dynamic and recursive data structures in Modelica. In: Zimmer D, Bachmann B, editors. Proceedings of the 8th International Workshop on Equation-Based Object-Oriented Modeling Languages and Tools - EOOLT '17. New York, New York, USA: ACM Press; 2017. p. 81–86.

[121] Wagner W, Kretzschmar HJ. International Steam Tables. Berlin, Heidelberg: Springer Berlin Heidelberg; 2008.

[122] Baehr HD, Tillner-Roth R. Thermodynamische Eigenschaften umweltverträglicher Kältemittel: Zustandsgleichungen und Tafeln für Ammoniak, R 22, R 134a, R 152a und R 123 ; [mit PC-Arbeitsgleichungen] = Thermodynamic properties of environmentally acceptable refrigerants. Berlin: Springer; 1995.

Appendix A
Media Models

Within this chapter the media models that have been used for the simulations with Modelica are presented here.

A.1 Moist Air

The main working fluid in aircraft environmental control systems is moist air. For all simulations in this thesis, the MoistAir medium model from the Modelica Standard Library [25] is used. The governing assumption of the full thermodynamic model are:

- the perfect gas law applies,
- water volume other than that of steam is neglected.

The model includes the fog region and temperatures below 0 °C. At the triple point temperature of water of 0.01 °C or 273.16 K and a relative humidity greater than 1, fog may be present as liquid and as ice resulting in a specific enthalpy somewhere between those of the two isotherms for solid and liquid fog, respectively. For numerical reasons a coexisting mixture of 50 % solid and 50 % liquid fog is assumed in the fog region at the triple point in this model.

The range of validity can be assumed from pressures below atmospheric conditions up to a few bars above atmospheric conditions. The thermodynamic model may be used for temperatures ranging from $190 - 647\,\mathrm{K}$. These ranges comply with the operation conditions of the ECS.

A.2 Water

The medium model that is used for water is derived from the IAPWS Industrial Formulation 1997 for the Thermodynamic Properties of Steam and Water [121]. The high precision water model calculate medium properties for water in liquid, gas and two phase regions and is valid in all regions.

A.3 Refrigerant

For the refrigerant in the vapor cycle of the electric driven vapor cycle pack, Tetrafluoroethane (R134a) was chosen. The fluid model is based on [122] and can be used within the following restrictions:

- Pressure range: $0.0039\,\mathrm{bar} \leq 700\,\mathrm{bar}$

- Temperature range: 169.85 K $\leq$ 455 K
- explicit for pressure and specific enthalpy

The library containing the model for the refrigerant medium is product of XRG Simulation GmbH.

Appendix B
Aircraft Specific Parameters

This chapter presents the equations used for calculating the aircraft specific data such as fuel consumption and aerodynamic parameters. The equations and data are all taken from the BADA models [47].

B.1 Fuel Consumption

The thrust specific fuel consumption for jet engines can be calculated with the following equation:

$$\eta = C_{\mathrm{f1}} \cdot \left(1 + \frac{V_{\mathrm{TAS}}}{C_{\mathrm{f2}}}\right) \qquad \text{in} \qquad \left[\frac{\mathrm{kg}}{\mathrm{min} \cdot \mathrm{kN}}\right] \tag{B.1}$$

with V_{TAS} being the true air speed [knots]. The conversion from η to SFC_{th} for the use in fuel weight penalties is done by:

$$SFC_{\mathrm{th}} = \frac{{}^{1}/_{0.45359237}}{{}^{1}/_{60} \cdot {}^{1}/_{4.4482216152605}} \cdot \eta \qquad \text{in} \qquad \left[\frac{\mathrm{lb}}{\mathrm{h} \cdot \mathrm{lbf}}\right] \tag{B.2}$$

B.2 Aerodynamic Drag

The lift-to-drag ratio is calculated from the lift and drag coefficients:

$$C_{\mathrm{L}} = \frac{2 \cdot m \cdot g}{\rho \cdot V_{\mathrm{TAS}}^2 \cdot S \cdot \cos\phi} \tag{B.3}$$

The drag coefficient is specified for normal conditions as a function of the lift coefficient C_{L}:

$$C_{\mathrm{D}} = C_{\mathrm{D0,\,CR}} + C_{\mathrm{D2,\,CR}} \cdot (C_{\mathrm{L}})^2 \tag{B.4}$$

This function is valid for all situations except approach and landing. The lift-to-drag ratio is then calculated by:

$$\frac{L}{D} = \frac{C_{\mathrm{L}}}{C_{\mathrm{D}}} \tag{B.5}$$

The values for the different coefficients are taken from a data sheet for an Airbus A320. The sheet is available in [47].

Appendix C
Results

C.1 Modeling & Simulation

Listing C.1: Generated text file with list of components with exergy sensors for eVCP.

```
Total Number of components containing exergy sensors = 30
Structure of vectors based on E_D:
[1]MHX
[2]Evaporator
[3]Reheater
[4]waterSeparator
[5]waterInjector
[6]fanRamAir
[7]BaseCompressor
[8]ACM_turbine
[9]PHX
[10]ACM_compressor
[11]Condenser
[12]VaCsTurboCompressor
[13]VaCsValve
[14]junction2
[15]junction13
[16]flowModelAirARamAir4
[17]flowModelAirARamAir1
[18]junction1
[19]Venturi_ACM_Compressor
[20]Ozone_Converter
[21]Pack_Venturi
[22]WaterExtractorAirFlowResistance
[23]AltitudeValveDuctAirFlowResistance
[24]Diffuser
[25]divPlenum
[26]junction4
[27]Base_Compresor_Check_Valve1
[28]junction5
[29]junction6
[30]Base_Compresor_Check_Valve
Full paths to exergy sensors:
eVCP_TaxiFL000.MHX.exergySensor
```

```
eVCP_TaxiFL000.Evaporator.exergySensor
eVCP_TaxiFL000.Reheater.exergySensor
eVCP_TaxiFL000.waterSeparator.exergySensor
eVCP_TaxiFL000.waterInjector.exergySensor
eVCP_TaxiFL000.fanRamAir.exergySensor
eVCP_TaxiFL000.BaseCompressor.exergySensor
eVCP_TaxiFL000.ACM_turbine.exergySensor
eVCP_TaxiFL000.PHX.exergySensor
eVCP_TaxiFL000.ACM_compressor.exergySensor
eVCP_TaxiFL000.Condenser.exergySensor
eVCP_TaxiFL000.VaCsTurboCompressor.exergySensor
eVCP_TaxiFL000.VaCsValve.exergySensor
eVCP_TaxiFL000.junction2.exergySensor
eVCP_TaxiFL000.junction13.exergySensor
eVCP_TaxiFL000.flowModelAirARamAir4.exergySensor
eVCP_TaxiFL000.flowModelAirARamAir1.exergySensor
eVCP_TaxiFL000.junction1.exergySensor
eVCP_TaxiFL000.Venturi_ACM_Compressor.exergySensor
eVCP_TaxiFL000.Ozone_Converter.exergySensor
eVCP_TaxiFL000.Pack_Venturi.exergySensor
eVCP_TaxiFL000.WaterExtractorAirFlowResistance.exergySensor
eVCP_TaxiFL000.AltitudeValveDuctAirFlowResistance.exergySensor
eVCP_TaxiFL000.Diffuser.exergySensor
eVCP_TaxiFL000.divPlenum.exergySensor
eVCP_TaxiFL000.junction4.exergySensor
eVCP_TaxiFL000.Base_Compresor_Check_Valve1.exergySensor
eVCP_TaxiFL000.junction5.exergySensor
eVCP_TaxiFL000.junction6.exergySensor
eVCP_TaxiFL000.Base_Compresor_Check_Valve.exergySensor
Total Number of fuel exergy sensors = 0
Structure of E_fuel vector:
Total Number of prod exergy sensors = 0
Structure of E_prod vector:
Total Number of loss exergy sensors = 2
Structure of E_loss vector:
[1]eVCP_TaxiFL000.exergySensor_Loss_ramInlet
[2]eVCP_TaxiFL000.exergySensor_Loss_ramOutlet
```

C.2 Conventional Exergy Analysis

C.2.1 Bleed Pack

Table C.1: Thermodynamic data of bleed pack for taxi and cruise phase. Temperature and pressure are normalized.

	Working Fluid	$\dot{m}$, [kg/s]		p/p_{ref}, [−]		T/T_{ref}, [−]		$\dot{E}_{t,i}$, [kW]	
#	Flight Cases	TA	CR	TA	CR	TA	CR	TA	CR
0	Air	0.5	0.5	2.49	1.8	1.73	1.73	58.057	110.577
1	Air	0.5	0.5	2.43	1.7	1.24	1.5	39.522	91.809
2	Air	0.5	0.31	2.43	1.7	1.24	1.5	39.522	57.01
3	Air	0.5	0.31	3.74	2.29	1.44	1.66	63.354	69.844
4	Air	0.5	0.31	3.69	2.26	1.18	0.96	56.672	46.55
5	Air	0.5	0.31	3.65	2.24	1.16	0.98	55.903	46.839
6	Air	0.5	0.31	3.61	2.22	1.13	1.01	55.007	47.073
7	Air	0.49	0.31	3.61	2.22	1.13	1.01	54.674	47.073
8	Air	0.49	0.31	3.6	2.2	1.17	0.98	54.693	46.474
9a	Air	0.49	0.31	1.03	0.82	0.97	0.78	2.673	25.807
9b	Air	0.49	0.5	1.03	0.82	0.97	1.05	2.673	46.266
10	Air	0.49	0.5	1.01	0.8	1.01	1.04	0.924	44.728
11	Air	1.41	0.48	1.01	0.24	1.11	0.89	-0.452	3.311
12	Air	1.42	0.48	1.01	0.24	1.11	0.89	-0.122	3.311
13	Air	1.42	0.48	0.99	0.22	1.18	1.34	-1.037	18.312
14	Air	1.42	0.44	0.98	0.21	1.35	1.59	6.28	31.997
15	Air	1.42	0.44	1.01	0.21	1.37	1.59	11.516	31.36
31	Power	0	0	0	0	0	0	-5.552	0.206
32	Power	0	0	0	0	0	0	-27.096	-14.057
33	Power	0	0	0	0	0	0	32.649	13.851
21	Air	0	0.19	2.43	1.7	1.24	1.5	0	34.799
22	Air	0	0.19	1.03	0.82	1.24	1.5	0	26.205
71	Water	0.0069	0	1.01	0.24	1.13	1.01	0.002	0

C.2.2 eVCP

Table C.2: Results of exergy analysis of electric driven pack for taxi phase.

Component	Flight Phase: Taxi					
	$\dot{E}_{F,k}$ (kW)	$\dot{E}_{P,k}$ (kW)	$\dot{E}_{D,k}$ (kW)	ϵ_k (%)	y_k (%)	y_k^* (%)
MHX	7.922	2.276	5.646	28.7	71.3	15.3
evaporator	0	0	0.865	0	0	2.3
reheater	4.557	1.083	3.474	23.8	76.2	9.4
waterSeparator	0	0	0.244	0	0	0.7
waterInjector	0	0	0.84	0	0	2.3
fanRamAir	9.13	8.556	0.574	93.7	6.3	1.6
baseCompressor	0	0	0	0	0	0
turbine	31.986	25.635	6.35	80.1	19.9	17.2
PHX	2.716	0.028	2.688	1	99	7.3
compressor	45.544	41.346	4.198	90.8	9.2	11.4
condenser	6.996	2.791	4.205	39.9	60.1	11.4
VaCCMP	15.712	11.432	4.281	72.8	27.2	11.6
VaCsValve	0	0	2.427	0	0	6.6
junction2	0	0	0	0	0	0
junction13	0	0	0	0	0	0
AltitudeValve	0	0	0.007	0	0	0
BCMPResist	0	0	0	0	0	0
junction1	0	0	0	0	0	0
VenturiCompr	0	0	0.278	0	0	0.8
OzoneConv	0	0	0.281	0	0	0.8
PackVenturi	0	0	0.289	0	0	0.8
WEResistance	0	0	0.258	0	0	0.7
AltValveDuct	0	0	0	0	0	0
diffuser	0	0	0.024	0	0	0.1
divPlenum	0	0	0.003	0	0	0
junction4	0	0	0	0	0	0
FanCheckValve	0	0	0	0	0	0
junction5	0	0	0	0	0	0
junction6	0	0	0.012	0	0	0
BCMPCheckVlv	0	0	0.001	0	0	0
System	70.582	25.273	36.946	35.8	52.3	100

Table C.3: Results of exergy analysis of electric driven pack for cruise phase.

Component	Flight Phase: Cruise					
	$\dot{E}_{F,k}$ (kW)	$\dot{E}_{P,k}$ (kW)	$\dot{E}_{D,k}$ (kW)	ϵ_k (%)	y_k (%)	y_k^* (%)
MHX	10.605	8.074	2.532	76.1	23.9	11
evaporator	7.402	4.547	2.855	61.4	38.6	12.4
reheater	1.658	0.048	1.609	2.9	97.1	7
waterSeparator	0	0	0	0	0	0
waterInjector	0	0	0	0	0	0
fanRamAir	0	0	0	0	0	0
baseCompressor	43.924	39.537	4.387	90	10	19
turbine	0	0	0	0	0	0
PHX	5.994	3.152	2.843	52.6	47.4	12.3
compressor	14.759	13.525	1.234	91.6	8.4	5.4
condenser	6.857	6.057	0.8	88.3	11.7	3.5
VaCCMP	2.796	2.297	0.498	82.2	17.8	2.2
VaCsValve	0.574	0.47	0.103	82	18	0.4
junction2	0	0	0	0	0	0
junction13	0	0	0.007	0	0	0
AltitudeValve	0	0	0.001	0	0	0
BCMPResist	0	0	0.202	0	0	0.9
VenturiCompr	0	0	1.015	0	0	4.4
OzoneConv	0	0	1.085	0	0	4.7
PackVenturi	0	0	1.442	0	0	6.3
WEResistance	0	0	0	0	0	0
AltValveDuct	0	0	0	0	0	0
diffuser	0	0	2.431	0	0	10.5
divPlenum	0	0	0	0	0	0
junction4	0	0	0	0	0	0
FanCheckValve	0	0	0	0	0	0
junction5	0	0	0	0	0	0
System	61.479	32.357	23.045	52.6	37.5	100